Anatomical and Quantitative Structural MRI Studies in Parkinsonian Disorders

Othman Mohamad Alaa Abdulwahab Al Helli

A thesis submitted to University College London for
the degree of Doctor of Philosophy at
Department of Brain Repair and Rehabilitation
Institute of Neurology, University College London
Queen Square, London, United Kingdom WC1N 3BG

September 2016

Declaration

I, Othman Mohamad Alaa Abdulwahab Al Helli, confirm that the work presented in this thesis is my own. Where information has been derived from other sources, I confirm that this has been indicated in the thesis.

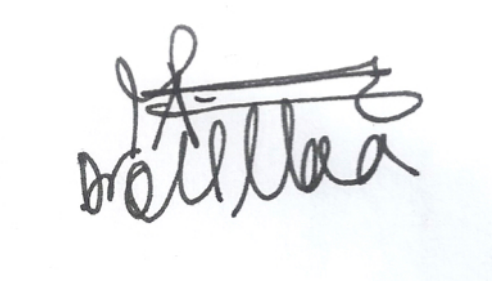

Abstract

The primary aim of this work is to investigate the value of quantitative magnetic resonance imaging (qMRI) metrics in patients with Parkinson's disease (PD), progressive supranuclear palsy (PSP) and multi-system atrophy (MSA), and to investigate the potential role of these metrics in the diagnostic work-up of patients with Parkinsonian disorders.

Chapter one discusses imaging theories and the clinical context of Parkinsonian disorders, summarizing their clinical features, imaging aspects, and the limitations of current imaging modalities.

Chapter two is a methodological study of the imaging anatomy of the subthalamic nucleus (STN), a key structure in the pathogenesis of the disorders. Pre-operative stereotactic 1.5-T MR images—for patients with PD that underwent STN deep brain stimulation (DBS)—were studied. The distance between the anterior border of the mamillothalamic tract and the STN anteromedial border has shown to have minimal variation. This may help with more accurate localization of the STN on MRI for the work presented later in this thesis.

Chapter three is a case study in which 1.5-T post-operative images, as well as 9.4-T post-mortem MR images (of a patient who had had STN DBS), were studied. It is demonstrated that lead artifact location on postoperative MRI corresponded well with anatomical location on post-mortem high-field imaging and histological examination. It helps in understanding the complex anatomy of the STN and its environs on MRI and histology.

Using a 3-T MRI protocol, chapters four through six study fifty-nine subjects with PD, PSP, and MSA and control subjects at study-entry and at 6-16 month intervals thereafter using a region-of-interest (ROI) based method. They report T2 and T2* relaxation times in three key basal ganglia structures: the subthalamic nucleus (STN), the red nucleus (RN) and the substantia nigra (SN).

T2 relaxation times are reduced in the STN ROIs of the PSP group when are compared to those from the control and the PD ones ($p< 0.05$). There is a significant correlation between age and T2 times in the control group ($p <0.05$). T2* and T2 relaxation times of the RN in the PD group are reduced ($p <0.05$) when are compared to those in the control group. In the SN of patients with PD and PSP, T2* times are reduced. There are no significant differences noticed in the longitudinal section of the work.

The findings of the present studies suggest that T2 and T2* times of the STN, RN and SN may help in differentiating different Parkinsonian disorders from each other by measuring T2 and T2* times of the STN, RN and SN. qMRI may compensate for the lack of sensitivity and specificity offered by structural MRI when studying Parkinsonian disorders and may have the potential to provide insights into their pathophysiology.

Acknowledgements

I would like to thank my supervisors—Dr David Thomas, Dr John Thornton and Prof Tarek Yousry—for their constant encouragement and careful reading, and for giving me the opportunity to undertake this research in the first place. I would also like to extend my gratitude to Dr Enrico De Vita for his help with normalizing the data using SPM, and to Dr Luke Massey and the movement disorders consultants at Queen Square for their invaluable aid in referring subjects to this study — and then for recruiting subjects as well as assessing them for their clinimetric scores. I would also like to thank Ms Lisa Strycharczuk for scanning patients, and acknowledge Prof Allan Hackshaw for his statistical advice and guidance.

To Mr. Ludvic Zrinzo (consultant neurosurgeon at the National Hospital for Neurology and Neurosurgery, Queen Square, London) I wish to extend my appreciation for the necessary guidance while collecting the data in chapter two, and to Nick Brett of Medtronics™ for providing the Stealth machine.

Shukran and gratitude to my wonderful wife and the love of my life, Eiona, and our future baby, and to my mother and sisters in Baghdad.

Finally and to the patients and their families that participated in this study, I remain indebted and sincerely hope that your contributions will make a substantial impact on the diagnosis and treatment of Parkinsonian disorders. I was continuously humbled and honored by your commitment to help broaden this scientific field.

Publications Associated with this Thesis

1. Al Helli, O., L. Massey, E. De Vita, J. Thornton, and T. Yousry. "The Substantia Nigra in Parkinsonian Disorders: A Multimodal MRI Assessment at 3T [Abstract]." Movement Disorders 28, no. Suppl. 1 (2013): 106.

2. Al Helli, O., L. Massey, M. Hariz, T. Foltynie, D. Thomas, T. Yousry, J. Holton, and L. Zrinzo. " MRI-Guided Deep Brain Stimulation of the Subthalamic Nucleus: Correlation of Postoperative 1.5T MRI with Post-Mortem 9.4T MRI and Histopathology [Abstract]." Stereotactic and Functional Neurosurgery 90, no. Suppl. 1 (2012): 1-202.

3. Massey, L.A., M.A. Miranda, L. Zrinzo, O. Al-Helli, H.G. Parkes, J.S. Thornton, P.W. So, M.J. White, C. Mancini, C. Strand, et al. "High Resolution Mr Anatomy of the Subthalamic Nucleus: Imaging at 9.4T with Histological Validation." *NeuroImage* 59, no. 1 (2012): 2035-44.

4. Al Helli, O., L. Zrinzo, and T. Yousry. "The Mamillothalamic Tract: A New Landmark for Targeting the Subthalamic Nucleus During Deep Brain Stimulation." *British Journal of Neurosurgery* 24, no. 2 (2010): 108-47.

Table of Contents

List of Figures

List of Tables

Abbreviations

1H	Hydrogen Nuclei
B0	External Magnetic Field
ADC	Apparent Diffusion Coefficient
APD	Atypical Parkinsonian Disorders
AC-PC	Anterior commissure – posterior commissure
CI	Confidence Interval
CT	Computed Tomography
DTI	Diffusion-Tensor Imaging
DWI	Diffusion-Weighting Imaging
FA	Fractional Anisotropy
FSE	Fast Spin Echo
GRE	Gradient-Recalled Echo
ION	Institute of Neurology
IPD	Typical or Idiopathic Parkinson's Disease
MNI	Montreal Neurology Institute
MRI	Magnetic Resonance Imaging
MTT	Mamillothalamic Tract
MSA	Multi-System Atrophy
PD	Parkinson's Disease
PET	Positron Emission Tomography
PSP	Progressive Supranuclear Palsy
RN	Red Nucleus
ROI	Region of Interest
SD	Standard Deviation
SE	Spin Echo
SNR	Signal to Noise Ratio
SN	Substantia Nigra
STN	Subthalamic Nucleus
T1	Longitudinal Relaxation Time
T1-W	T1-Weighted
T2	Transverse Relaxation Time
T2*	T2 Star (Loss of Phase Due to Inhomogeneity within the Magnetic Field)
T2-W	T2-Weighted
TE	Echo Time
TR	Repetition Time

CHAPTER ONE—Background and Aims—An introduction to the clinical context of Parkinsonian disorders and the imaging theory underpinning high-field quantitative MRI

1.1 Clinical Context

Parkinsonian disorders form a group of neurological diseases, characterized by slowness of movement, tremor at rest and on posture, and extrapyramidal rigidity.[1-3]

They are divided into two spectrums: typical or idiopathic Parkinson's disease (IPD)—which is the most common movement disorder—and atypical Parkinsonian disorders (APD). Post-mortem studies have shown that 20-25% of patients initially diagnosed with IPD actually had APD.[4-7]

Typical or idiopathic Parkinson's disease (IPD) is pathologically characterized by Lewy body degeneration that mainly targets the substantia nigra (SN), then by extra-pyramidal signs and symptoms of asymmetrical rest tremor, lead-pipe rigidity and slowed movements, voice changes and dementia.[8 9]

Parkinsonism is considered atypical when the clinical syndrome evolves rapidly and responds poorly or transiently to Levodopa therapies. APD can have other associated features. Structural damage within this group of disorders is more extensive and multi-systemic than with IPD, which might also explain the poor therapeutic responses and unfavorable prognoses associated with APD.[5 10 11] The most common types of APD are progressive supranuclear palsy (PSP) and multi-system atrophy (MSA) (Table 1).

Accurately diagnosing a Parkinsonian disorder is paramount due to the substantial differences in treatments[12 13] as well as the natural history of the various disease processes and their final outcomes.[14] Even with strictly applied criterion, clinical diagnoses remains far from ideal.[7 15] Table 1 summarizes the clinical features of IPD, PSP and MSA.

	IPD	PSP	MSA
Tremor	Asymmetrical; post 4–8 Hz, rest 3–5 Hz; arms and legs, jaw, eyelids; latency to onset	Uncommon	Asymmetrical; post 4–8 Hz, rest 3–5 Hz; arms or legs; latency
Rigidity	Asymmetrical; limb	Symmetrical; axial >limb	Asymmetrical; limb
Finger Movements	Progressive slowing with decreasing amplitude	Spared early	Progressive slowing with decreased amplitude
Facies	Early loss of expression and blinking. Late blepharoclonus	Lid retraction; staring; eye opening apraxia	Early loss of expression; facial dyskinesias
Dysautonomia	Early impotence, late orthostatic hypotension, bladder, constipation	Early impotence, bladder, orthostatic hypotension rare	Early orthostatic hypotension, bladder, impotence, constipation
Bulbar	Late dysarthria; hypophonia	Early dysarthria, dysphagia	Early dysarthria, dysphagia; night stridor
Gait and posture	Late falls; retropulsion; festination, flexed posture	Early falls, retrocollis	Early falls, flexed posture; antecollis ++
Eye movements	Hypometric	Eye deviation to optokinetic nystagmus, supranuclear gaze palsy	Nystagmus, hypometric
Ataxia	None	Rare	Frequent
Apraxia	None	End stage limb; eye opening	None

Table 1: Clinical discriminators of Parkinsonian disorders (modified from Brook's 2002)

Progressive supranuclear palsy (PSP)—or Steele-Richardson-Olszewski syndrome—is a multi-system syndrome that is akinetically-rigid. It affects the neck and the trunk, and the limbs where ataxia can be seen at later stages of the disease. It can also present with a wide variety of eye, cognitive or motor related symptoms, and affects the following areas: the pallidum; the SN; peri-aqueductal grey matter; oculomotor, vestibular and cerebellar dentate nuclei; the cerebellar colliculi; the cortex of superior frontal areas.[16-18]

Within its broad spectrum, multiple system atrophy (MSA) includes striatonigral necrosis, olivopontocerebellar atrophy and isolated autonomic failures. Most MSA patients present with asymmetric akinetic-rigid syndrome. Others present with the following: limb ataxia; gait disturbance, with falls; bulbar involvements; urinary symptoms; significant orthostatic

hypotension. Argyllophllic neuronal and glial cytoplasmic inclusions that stain positive for alpha synuclein are considered pathognomic.[10 19 20]

Clinimetric scales are bedside tests that score and objectively quantify clinical syndromes and their severity, as well as likely responses to treatment and follow-up. The unified Parkinson's disease rating scale (UPDRS) was developed in 1987 and is now commonly used by clinicians and researchers to assess PD signs and symptoms. It is composed of four sections: assessing mentation and mood (UPDRS I); activities of daily living (symptoms, UPDRS 2); motor function (signs, UPDRS 3); complications of dopaminergic medications (UPDRS 4).[21 22] Again, the higher the score, the worse the symptoms.

The commonly used Hoehn and Yahr scale (H&Y) is a simple and descriptive staging scale that helps estimate clinical PD functions, combined with functional deficits or disabilities and objective signs or impairments.[21 23] The higher the Y&H score, the worse the symptoms. A frontal assessment battery (FAB) can also be used to assess the functions of the frontal lobe. With advanced Parkinsonian disorders like PSP, the frontal lobe can also be affected. With FAB, the lower the score, the worse the clinical status.

Currently, definitive diagnoses are based on the characteristic anatomical distribution of neuronal degeneration and subsequent gliosis. With PSP, the neuropathological hallmarks are predominant neuronal apoptoses and gliotic reactions in either the globus pallidus (GP) or SN. With MSA, changes tend to be mainly in the putamen (Pu) or SN[18]—noting that the SN is predominantly affected with IPD. Detecting such changes *in vivo* would have a major impact on the diagnostic accuracy of Parkinsonian disorders and their management.

Anatomically accurate imaging is the key to measuring chemical and pathological changes of the relatively small structures involved in the degenerative processes of Parkinsonian disorders, and it is therefore paramount to accurately localize these structures and obtained measures that reflect pathological changes.

Two MRI features can be exploited, (a) the anatomical distribution of abnormalities and (b) the pathological differences of these same areas. For patients presenting for the first time with a Parkinsonian symptom, an MRI is used to exclude secondary or symptomatic diseases like basal ganglia tumours, haemorrhages, small vessel diseases and calcifications, all of which have been associated with Parkinsonism.

For a patient previously presenting to a movement disorder clinic with a Parkinsonian symptom, standard MRI protocols include T2-weighted spin-echo (SE) imaging (T2WI) and fluid attenuation inversion recovery (FLAIR) sequences. With some patients, FLAIR sequences have the ability to show structural or anatomical changes. Patchy losses or volume losses of the nigral signal may be seen with PD. With PSP, mid-brain atrophy and the dilatation of the third ventricle have been described. With MSA, qualitative changes tend to be diffuse, whereas in the putamen there is a low posterior T2WI signal, and a lateral or slit-like hyperintensity. In the pons, an increased tegmental signal and the "hot-cross bun" sign. In the cerebellum, lost volume. All have been described with variable sensitivities and specificities. MRI–based volumetry has shown selective volume loss in the striatal and infra-tentorial structures, which is secondary to degeneration in patients with PSP and MSA when compared to PD and neurological control subjects.

A recent study[24] revealed that radiological assessments—conventionally qualitative MRI—is accurate only 16 in 22 times (72.7%) for pathologically confirmed PSP cases, and 10 in 13 times (76.9%) for pathologically confirmed MSA cases. In addition, studies have shown that the MRI was less sensitive than clinical diagnoses of PSP. The low diagnostic sensitivity of clinical assessments and conventional MRIs and macroscopic examinations at post-mortem, all indicate the need for an imaging technique that is sensitive to microstructural abnormalities but without regional volume loss.

Iron is the most abundant transitional metal in the body; in some parts of the brain there are higher concentrations than in the liver. The most concentrated areas of iron in the brain are the globus pallidus, the red nucleus, the SN, putamen, and caudate nucleus, all of which are associated with Parkinsonian disorders. Iron is needed for brain development, proper function, and helps transport electrons and generates hydroxyl radicals. An overabundance of iron and iron toxicity can lead to oxidative stress, especially when iron amounts exceed the detoxification capacity of the cellular system.

1.2 Principles of Quantitative MRI (qMRI) and Spatial Normalization

The MRI relies on the magnetic properties of atomic nuclei to build a spatial representation of human tissue. Human tissues are saturated with hydrogen atoms (^{1}H), each with one proton making imaging the most commonly used MRI procedure. In order to detect the signal from a ^{1}H nuclei, a radio frequency (RF) must be applied in the form of an oscillating magnetic

field (B1). This RF energy causes the nuclei to rotate away from its equilibrium orientation—parallel to the external magnetic field (B0)—and shift more toward the x-y plane.

The "flip angle" is the angle through which the rotation has occurred, away from the z-axis. An 180^{o} RF pulse rotates the orientation of the spin, making it anti-parallel to the B0. The process of return—of the nuclei to its equilibrium state (parallel to B0) after an RF impulse—is called "relaxation." Relaxation is considered the outcome of three processes: the longitudinal relaxation (T1), the transverse relaxation (T2), and the influence of magnetic field inhomogeneities.

T2 decay, or spin-spin relaxation, controls the irreversible decrease of the x-y component of the net magnetism. The spin-spin relaxation time (T2) is the time needed for transverse magnetization to drop below 37% of its original value, in the absence of magnetic field inhomogeneities. Another time constant, T2*, describes transverse magnetization decay, which is the outcome of both B0 inhomogeneities and T2 relaxation. In order to obtain a pure T2 signal, rather a dependent T2* signal, a spin-echo (SE) sequence is used that incorporates both 90^{o} and 180^{o} pulses.

A qualitative or structural MRI is based on selective time repetitions (TR) and time echoes (TE), leading to image contrasts that are based on the relative mass of different tissues. TR is defined as the time between two consecutive 90^{o} RF pulses, and thus determines the T1 relaxation contrast. A long TE and a long TR will allow full longitudinal relaxation and significant T2 signal decay, leading to the production of a T2-weighted image (T2WI).

These T2WI images are often used exclusively to provide qualitative diagnostic information and it is relatively straightforward to extend the principle of the T2WI to produce *quantitative* T_2 maps that yield more information. This can be achieved by generating images using different values for *TE*. A quantitative T_2 map can be used to define a normal range of T_2 values, or used as a statistical comparison again the norm in a clinical study of a diseased population, for example.

Quantitative MR imaging (qMRI) involves metrics. This type of image can be used to measure differences or changes following pathological or physiological processes. With qMRI, the outcome is a parametric "map" that can be calculated from one or more images taken from the same region of tissue. An example would be to collect two images with differing T2 weightings: by solving the mono-exponential T2 decay equation, using two images for each

pixel, a third image matrix or T2 map can be formed. This technique differs from conventional T2WI approaches in the sense that individual pixels are given a numerical value—i.e. T2 value at each pixel—rather than representing a relative signal intensity contrast.

As previously stated, T2 is the characteristic time constant for transverse magnetization or spin-spin relaxation in the absence of B0 inhomogeneity. T2* is the characteristic time constant that describes the decay of transverse magnetization, taking into account both the effect of inhomogeneity in the static magnetic field and the intrinsic spin-spin (T2) relaxation of the tissue: the former resulting in a rapid loss of phase coherence, and proportionally a decrease of the MRI signal.[5] Though T2* is potentially sensitive to iron-induced magnetic susceptibility variations, its maps are commonly associated with considerable artefacting, making the T2 a relatively more reproducible measure.

T2*-weighted gradient echo (GRE) is conventionally included in clinical MRI examinations for micro-bleed and calcification detection. Quantitative T2* mappings have other applications where sensitivity to iron concentrations between neighboring structures might be important.[25] Iron tissue concentrations have been reported as elevated in the SN—for PD, PSP and MSA—compared to neurological controls with different topographic distributions: the iron tends to be more concentrated in the posterolateral SN for PD, and in the anteromedial tiers for PSP and normal ageing.[26-31] Using a GRE sequence to measure T2* at 3 Tesla (T), it is plausible to differentiate PD from the controls.[25 32-34]

Since T2* decay incorporates T2 decay plus field inhomogeneity decay, T2* is always shorter than T2 in tissue. The effects of the inhomogeneous[5] B0 field can be eradicated by detecting the peak of the spin-echo. T2* will characterize the existence of strong tissue magnetic susceptibly effects as considerably smaller than T2.[35] The quality and to a certain extent the accuracy of T2 relaxation maps are determined by the quantity and value of the TE used to define the T2 decay curve. As an alternative it is feasible to employ a dual-echo sequence that measures only two time-points—using the newly freed time within each TR period to collect more data from more slices and therefore increase the available anatomical coverage. In principle, the greater the quantity of echo-points the better T2 will be measured, with two points being the minimum to define an exponential function. Typically, up to 32 echoes are used to measure T2.[35 36]

Co-registration is the method of realigning images and combining information. It commonly maximizes the data from two images and creates a direct anatomical correspondence

between them, thus facilitating the identification of specific local structures through co-localization. This can be achieved by matching templates like the MNI (Montreal Neurology Institute) space.

An MRI image can be generally registered to a corresponding template that conforms to the same anatomical space using a 12-parameter affine transformation. An affine transformation is a linear transformation followed by a translation a.*x*+b. A simple *rigid body* transformation is generally insufficient and accounts for the remaining issues within a scaling parameter.

By matching each subject to a standard template such as the MNI space, spatial normalization creates a one-to-one correspondence between the brains of different subjects, thus yielding the following advantages: averaging of measures across subjects; determination of findings, generically over individuals; identification of commonalities and differences between subject groups. Another advantage is the possibility of identifying activation sites according to their Euclidian coordinates within a standard space, which mainly concerns mapping a single subject's brain image into a standard space, whereby the brain of a subject is transformed to match the brain of another subject or template. Standard templates also make the results from different studies comparable, aligning them to a standard space like the MNI; they also increase statistical power, and allow for the generalization of findings to a given population.

Spatial normalization in packages such as the SPM (http://www.fil.ion.ucl.ac.uk/spm) requires two steps. The first is linear registration using a 12-parameter affine transformation that accounts for differences in head shape and position. The second is nonlinear registration or warping which accounts for smaller scale anatomical differences. Registration determines the parameters describing a transformation; transformation alters one of the images according to a given set of determined parameters.

The limitations of normalization come when attempting exact structural matches between subjects, due to inter-individual anatomical differences. Where anatomical areas can be exactly matched there is no functional guarantee that homologous regions will be matched as well because individuals may vary in their structure-function relationships. These relationship and the resulting limitations are not fully understood.[1 3 37]

1.3 Key Structures in Parkinsonian Disorders

1.3.1 The Subthalamic Nucleus

Jules Bernard Luys, the Nineteenth Century French neuroscientist and artist, first described the subthalamic nucleus (STN) in 1865, which is also referred to as the *Luys body* or the *corpus Luysii.* It then took another 60-years for Luys' finding to gain clinical significance, which has been well elucidated by the Queen Square neurologist James Purdon-Martin. Luys considered that the pathogenesis of the hemichorea depends on involvement of the dorsal part of the body. The twentieth century saw further discoveries regarding the importance of the subthalamic nucleus.

The STN is a bilateral almond—a disc or oval-shaped grey matter—a collection located within the subthalamus and partially within the diencephalon—between the thalamus and the mesencephalon and around the central area of the human brain. It lies *ventral* to the zona incerta and *dorsomedial* to the substantia nigra and cerebral peduncles. It contains more than 500,000 neurons, most of which are Golgi type I excitatory neurons, projecting to the GP, SN and neostriatum.

The subthalamic nucleus is related to the posterior limb of the internal capsule on its anterolateral border; to the fields of Forel and the hypothalamus on its less-defined medial border; to the substantia nigra, anteroinferiorly and anterolaterally. The zona incerta and lenticular fasciculus are dorsally located, especially superiorly and medially. To the standard anatomic axes, it has oblique orientations of 20-degrees to the horizontal plane (AC-PC), 35-degrees to the sagittal plane, and 55-degrees to the frontal plane.

Direct evidence from histopathological studies suggest that the STN suffers changes during PSP, corticobasal degeneration and post-encephalitic Parkinsonism. It is severely affected at the end stage of PSP; where up to 85% of neuronal loss occurs, suggesting that prolonged disease increases neuronal loss. In advanced PD, indirect evidence from MRI studies suggest a probable increase in iron deposition within the STN. Iron concentrations are known to increase within areas of the brain that undergo degeneration.[4 38 39]

With PSP and during normal controls, the STN is at least half-size due to uniform neuronal loss, whereas in PD the STN does not appear to show any structural change,[8 37] though indirect evidence from MRI studies do suggest increased iron deposition within the STN during PD. The STN is a key structure in the surgical treatment of PD, being a target for subthalamotomy[11 40] and deep brain stimulation.[16 19 21]

A correlation between the non-motor symptoms of PD and the T2 of the anterior (limbic) STN has been suggested,[19 37] where it was found that STN T2* times were lower in PD than those of controls: it was hypothesized that these findings were due to shortened T2 because of increased iron deposition. Perl's stain confirms that the associative and limbic portions of the STN, the anteromedial STN, have more iron than the T2 hypointense dorsolateral portion.[21 41]

Since the advent of the MRI in the 1980s there have been numerous attempts to image the STN, and challenges encountered to identify the nucleus via MRI could be related to the following:

(1) Size: In in-vitro studies, the mean volume of the STN was 106 mm^3, range 87-126 mm^3, maximum width 12 mm, maximum depth 3.2 mm, maximum height 6.6 mm.[21 42] A more recent *in vivo* study reported the mean volume to be 60 mm^3, range 31-72 mm^3, with marked individual variability of up to 100%.[36 43] The small size of the nucleus makes it particularly difficult to visualize when using low-resolution imaging.

(2) Orientation: The inclination angles of the anteroposterior axis on the axial plane is 20-degrees, on the sagittal plane 35-degrees, and on the coronal plane 55-degrees.[37 40 43 44] These oblique orientations make the visualization process difficult for sectional imaging. Some have argued that it is easier to visualize the nucleus on the coronal plane than in any other plane,[38 39 45] however the axial plane is probably most effective because it shows more of the nucleus by virtue of being parallel to its longest axis.[37 43 46 47] With coronal images, and with some patients, the ventral or anterior border can merge into the substantia nigra.[40 48]

(3) Shape: When reconstructed in 3-dimensions (3D),[21 49] the STN appears to have irregular shape: similar to a biconvex lens-shaped structure, with the anteroposterior or ventrodorsal axis as the longest anteriorly the STN is larger and thicker than it is posteriorly.[37 50]

(4) Intensity: The composition of the subthalamic nucleus is heterogeneous and signals returned are similarly variable: seen as a region of T2-weighted hypointensity, the neighboring substantia nigra also returns a hypointense signal. When viewing axial T2-weighted images, the border between these two iron-rich neuronal collections is not clear.[41 51 52] In addition, the anterior portion of the nucleus tends to be hypointense because of elevated iron concentrations, when compared to the more isointense

posterior portion seen via T2WI images.[42 53] The reason for the differential iron density is yet to be determined.

(5) Variability: Inter-individual variations of the exact position of the STN are evident when comparing Inter-individual coordinates with atlas-derived coordinates.[43 54] In addition, other studies have reported variability of the subthalamic nucleus at different ages: variability of size, shape and orientation. Exact stereotactic localizing of the nucleus differs between individuals[39 40 43 44] and again changes with age. It has been hypothesized that these changes might be related to age-related physiological neuronal loss.[45 48]

Functional neurosurgeons and neuroradiologists commonly use two methods to identify and localize the STN on MR imaging. These methods are based on (a) the geometric relationship between the nucleus and other well-defined structures that are clearly visualized and near-by that act as landmarks from which imaginary lines can be drawn in the direction of the STN, and on (b) standardized atlases of anatomic data or functional data.

(a) Landmarks:

(i) The mid-commissural point (MCP):[40 43 46 47] the centre point on the anterior commissure-posterior commissure (AC-PC) line: two points in the midsagittal plane with the shortest intraventricular distance between the commissures.[44 48] The STN is usually located 2 mm behind the MCP, 4 mm ventral to the AC-PC plane, 12 mm lateral to the midsagittal plane.

(ii) The red nucleus (RN): a line drawn from the anterior border of the RN on the axial section, that shows the latter at its maximal transverse diameter, will hit the centre of the ipsilateral STN.[49 55 40 43 44 50]

(iii) Mamillothalamic tract:[51 52 56] with limited inter-individual variation, the distance between the anteroposterior coordinates of the tract and the anteromedial border of the nucleus in normal subjects.

(iv) Supramammillary commissure: the top of the commissure is directly lateral the STN and is 12 mm from the AC-PC line.[40 53]

(v) The mammillo-posterior commissure line: a line connecting the mammillary body and the posterior commissure; lies in the same plane as the STN; along the antero-posterior axis of the midbrain.[54 57]

(vi) The internal capsule: the STN can be seen more medially from the axial plane as a dent in the internal capsule outline; "dent internal capsule sign."

(vii) Internal auditory canal: in the coronal plane, in a section perpendicular to the AC-PC plane, and at the level of the internal auditory meatus, the STN looks like Sukeroku's makeup to the side of his eye;[39 58] the "Sukeroku sign."

(b) Atlases:

(i) Schaltenbrand and Wahren[48 58-61]: The most commonly used atlas by functional neurosurgeons,[40 62] it is used mainly as a guide to identify the boundaries of the STN against surrounding structures. Based on this atlas, the AC-PC distance is fixed at 21 mm; the coordinates are 13 mm along the x-axis, 3.75 mm along the y-axis, and 2.5mm along z-axis (13, 3.75, 2.5)[44 63]; the coordinates are 12 mm lateral, 3 mm posterior, and 3 mm inferior to the midcommissural point (12, 3, 3).[55 64 65] Because the atlas is based on four cadavers that did not have a documented history of PD, it is not surprising that several studies[40 43 66] have found significant differences between atlas coordinates and coordinates measured via direct MRI visualizations, showing significant AC-PC distances.

(ii) Talairach and Tournoux: The Talairach and Tournoux atlas[56 63 67] is a probabilistic atlas of human neuroanatomy based on one brain. It has been shown that the STN appears to be smaller, and situated more posteriorly and laterally, on MR images compared to atlases.[40 64]

A study[57 68] reviewed twelve publications of atlas-based coordinates against MRI-based coordinates and found shared conclusions: MRI-based coordinates are more accurate for STN localization than atlas-based equivalents mainly because of considerable inter-individual variability.

1.3.2 The Red Nucleus (RN)

Despite being known and recognized in the anatomy literature for a long time before 1907, it was only in 1907 that the RN was attentively studied by Hatschek.[58 69] He summarized

his conclusions saying that the RN of mammals consisted of two parts: a nucleus ruber-magnocellularis and a nucleus parvicellularis. The former is strongly developed in lower mammals, less so among apes, and rudimentary in man. The latter, on the other hand, is less developed in lower mammals, increases considerably among apes, and finds its highest development in man. The nucleus ruber-magnocellularis is the nucleus of origin of "von Monakow's bundle" or the rubrospinal tract. Further studies of the RN and its connections followed.[58-61 70]

The human RN form a pair of globular structures located in the midbrain.[63 71] The RN is predominantly a collection of grey matter in the anterior (rostral) mesencephalic tegmentum, close to the SN. It is considered a part of the extrapyramidal motor system, though data on the activation of the human parvocellular RN during tactile discrimination tasks also links it with a sensory structure.[31 64 65 72] It is not a uniform structure, composed of smaller and posteriorly located magnocellular, and larger and anteriorly located parvicellular subnuclei. The latter is further subdivided into three medullary lamellae: the pars oralis, the pars dorsomedialis and the pars caudalis.[66 73]

The RN is a pink, ovoid, mass of grey-matter, that is approximately 5 mm in diameter and laying dorsomedial to the SN. The RN of humans is particularly pronounced compared to other animals. A rich capillary bed, as well as ferric-iron pigments in its multipolar neurons, cause the pronounced tint. Rostrally, the RN is poorly demarcated, blending into the reticular formation and the caudal interstitial nucleus. It is traversed and surrounded by fascicles of nerve fibers, many of which are from the oculomotor nucleus.[64 74]

The RN is part of the extrapyramidal system, and its injury predominantly gives rise to motor syndromes. There is no direct histopathological evidence suggesting that the RN is involved in PD and MSA.[12 23 73 75 76] Even with PSP, where it suffers neuronal loss and neurofibrillary degeneration,[30 31 72] the involvement of the RN in PSP is considered to be variable and moderate with no macroscopic changes[31 63]. Indirect evidence from neuroimaging studies of the RN in Parkinsonian disorders may suggest involvement. It has been argued that iron content in the RN of patients with PD is higher than in healthy subjects, especially for patients suffering from dyskinesia.[57 73] This conclusion was based on noticing that R2* (the reciprocal of T2*, and an in vivo MRI marker of iron) was lower in the RN of PD patients, and that RN R2* values correlated with off-drug UPDRS-motor scores.[73 76] A comparable finding was suggested in another study: in patients with PSP, the ex vivo assessment of iron revealed its burden to be 15% in the control group, compared to 29% in the PSP cohort.[74 77]

The high iron content of the RN is partially responsible for low T2 signal intensities.[69 74 78] On axial T2WI, it could be seen as a uniformly round, T2-hypointense structure, located posteromedial to the SN in the upper tegmentum of the midbrain.[73 79] Its dimensions are approximately 5 mm anteroposterior x 5 mm mediolateral x 6 mm superoinferior (5 x 5 x 6 mm).[30 73 76 80]

Iron in brain tissue may have three effects: a shift in the local resonance frequency, the result of iron-induced magnetic susceptibility; a decrease in effective T2 relaxation times, due to the molecular diffusion through the susceptibility induced gradient; a local line broadening (T2* decrease), due to the voxel gradient. The latter contrast mechanism was exploited in a high-resolution gradient-echo MR study showing that it may be possible to detect the internal anatomy of a healthy RN by detecting the medullary lamellae.[63 77 81 82]

1.3.3 The Substantia Nigra

The substantia nigra (SN), a heterogeneous collection of grey matter with regional input and output variations, can be affected differently—different patterns and different pathological processes—as is the case in the physiological ageing process. In PD, neuronal loss is severe in its caudal and ventrolateral parts, affecting neuromelanin containing neurons and dopaminergic cells. With normal ageing, the most severely affected region is the anteromedial tiers.[30 83].

The SN is a mesencephalic motor nuclear complex, lying posteriorly and deeply to the crus cerebri, and anteriorly to the midbrain tegmentum.[2 10 57] It runs from the level of the mammillary bodies and along the ventral pontine nuclei, and through the whole of the midbrain from the medial to the lateral crural sulcus and from the pons to the subthalamic region.[76 84] Its bulk lies inferolateral to the red nucleus (RN).[77 85] Of the mesencephalon, it has the largest cell-mass. It lies between the tegmentum and the cerebral peduncle, with its most rostral part extending into the diencephalon, closely approaching the GP. The parabrachial pigmented nucleus forms a thin sheet of grey matter between the RN and SN.[84 86]

The SN is semilunar in axial section, concave dorsally, thicker medially, and runs from lateral to medial. It divides the cerebral peduncles into the dorsal and ventral regions, the tegmentum and crus cerebri respectively. It is subdivided into (i) dorsal pars compacta (SNc) and (ii) ventral pars reticularis (SNr). However, the SNr extends between SNc subnuclei, pars diffusa. The SN's location and its borders cannot be accurately identified on the basis of T2WI imagery,

nor with sequences like STIR, nor with proton-density weighted-imaging.[78 87] Despite these limitations, T2WI is routinely used to investigate patients that present with movement disorders.

The dopaminergic SN is affected in PD, PSP and MSA.[79 88] Involvement is topographically different: with normal ageing, the most severely affected region is the medial anterior and posterior tiers; with PD, the loss is greatest in the lateral anterior tier or ventrolateral tier; with MSA, the loss is marked in the posterior tier.[30 42 80]

Defining the MRI anatomy of the SN has always been challenging but earlier studies have helped define the SN: the relative hyperintensity of the SN on T2WI puts it between crus cerebri and the red nucleus (RN). However, studies comparing histologic sections against post mortem T2WI have shown that the SN is a poorly defined hyper-intense structure in the midbrain, anterior to the relatively hypointense cerebral peduncles, and not clearly separated from a cluster of pigmented neurons (the parabrachial pigmented nucleus) and white matter tracts (nigrostriatal tracts).[43 77 81 82]

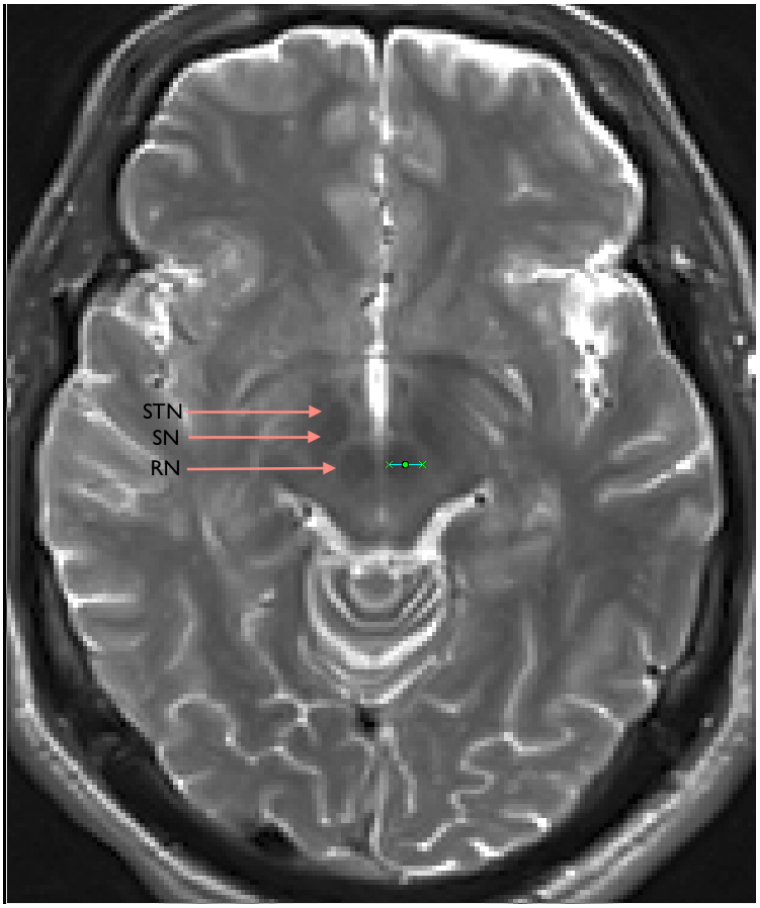

Figure 1: The STN, RN and SN on axial MRI image at the maximum transverse RN diameter.

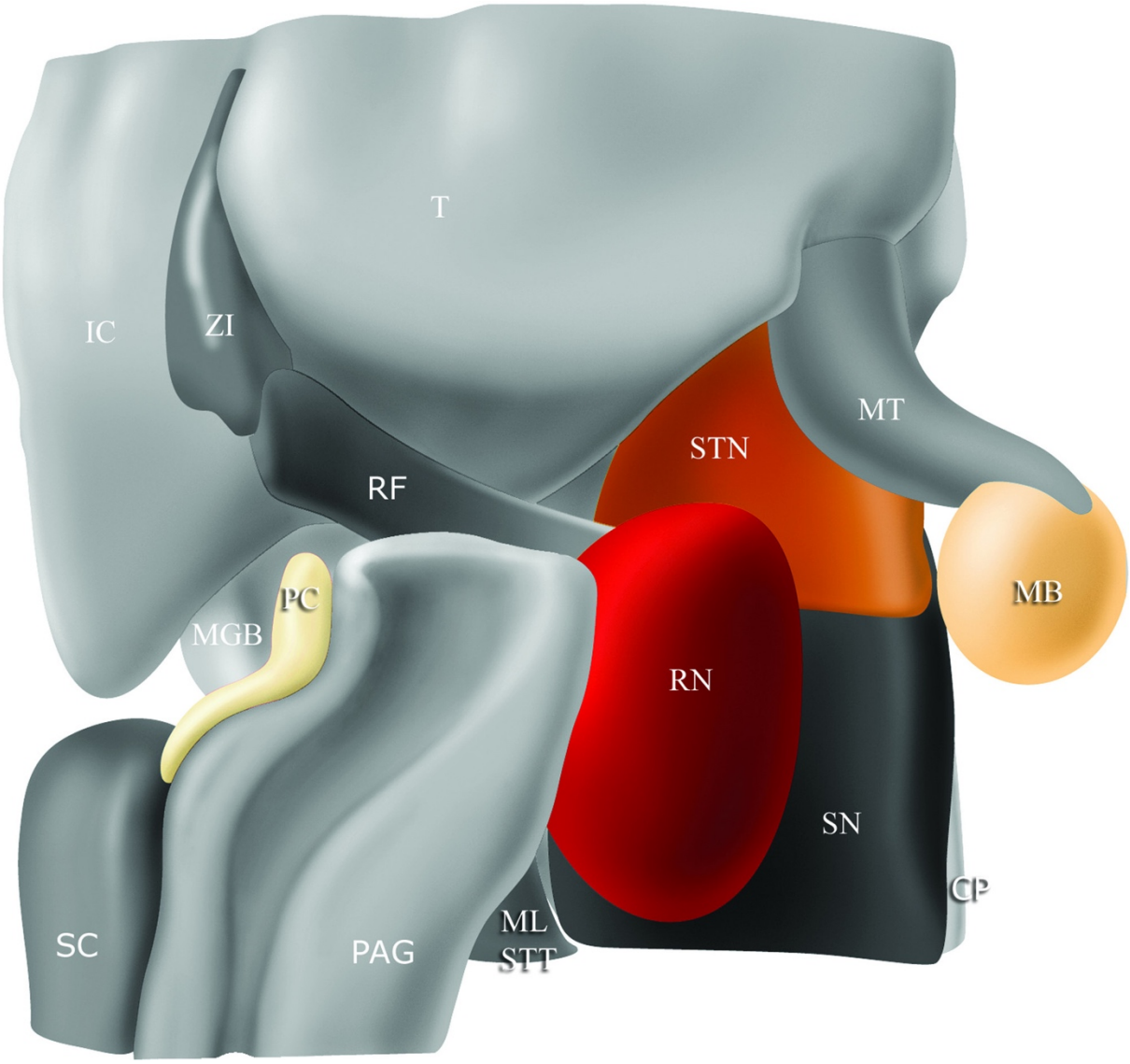

Figure 2: 3D computer reconstruction showing the anatomical relationship between the STN, RN and SN, adapted from Rijkers et al 2007. The three structures could be identified at the same axial plane.

1.4 Aims

This work involved three experiments.

The first pair of experiments was anatomical studies with the aim of better understanding the complex anatomy of the STN.

The first experimental work was to determine if the mamillothalamic tract (MTT) could be used as a reliable internal fiducial marker to find the position of the subthalamic nucleus (STN) in individual patients with Parkinson's disease (PD). If found, this marker might increase the identification and localization accuracies of the STN, which is a small and heterogeneous structure.

The second piece of research was a case study of a patient with Parkinson's disease who had undergone STN deep brain stimulation (DBS). The aim of that work was to assess the anatomical accuracy of lead placement, after MRI-guided and MRI-verified STN DBS, using post mortem histology and high-field MRI at 9.4T.

The main aim of the third experimental work, or the bulk of this thesis, was to determine the achievability of using T2 and T2* times obtained at 3-Tesla of the STN, RN and the SN to help discriminate among Parkinson's disease (PD), progressive supranuclear palsy (PSP), multi-system atrophy (MSA), and control subjects with no neurological disease.

The main research question was: Do differences in 3T MRI indices (T2, T2*) in key basal ganglia structures—the STN, RN and SN—enable improved differentiation between patients presenting with Parkinsonian symptoms?

Secondary questions were*:* Do MRI measurements correlate with clinical measures of disease severity and clinical outcomes?; is clinical progression of disease reflected in progression of MRI measurements?; Does the duration of a clinical disease correlate to MRI indices?

Summary

Parkinsonian disorders are a group of neurological diseases that share clinical signs and symptoms and yet differ in their underlying pathogeneses, pathologies, treatments and prognoses. Accurate diagnoses of Parkinsonian disorders are paramount.

The group can be divided into (Typical) idiopathic Parkinson's disease (PD) and atypical Parkinsonian disorders (APD), of which PSP and MSA are the most common. Post-mortem studies have shown that 20-25% of patients initially diagnosed with PD would eventually be diagnosed with APD.

Definite diagnosis is currently based upon the characteristic anatomical distribution of neuronal degeneration and subsequent gliosis. Selective distribution of pathological changes is the hallmark of any degenerative disorder, and Parkinsonian disorders are no exception.

Many MRI methods have been proposed to address the aim of detecting pathological changes *in vivo*, and their anatomical distribution and their variations, among PD, PSP and MSA patients. However, conventional qualitative MRI is accurate only 16 in 22 times (72.7%) for pathologically confirmed PSP cases, and 10 in 13 times (76.9%) for pathologically confirmed MSA cases.

Quantitative MR imaging (qMRI) is simply used to measure the differences or changes that result from pathological or physiological processes. T2 and T2* relaxation times are affected by iron concentrations, which tend to increase in the neurodegenerative process.

The STN is a bilateral almond-shaped grey matter that is collected and located within the subthalamus and around the central area of the human brain. With PSP and during normal controls, the STN is at least half-size, though indirect evidence from MRI studies does suggest increased iron deposition within the STN during PD. Moreover, the STN is a key structure in the surgical treatment of PD. Defining STN anatomy via MRI has proved challenging due to its small size and heterogeneity.

The human RN are a pair of globular structures located in the midbrain. The RN are part of the extrapyramidal system. There is no direct evidence for its involvement in Parkinsonian disorders, though indirect evidence suggests otherwise. R2* (an in vivo MRI marker of iron) was lower in the RN of PD patients; RN R2* values correlated with off-drug UPDRS-motor scores.[73] [76]

The substantia nigra (SN) is the largest grey matter collection in the midbrain. It can be affected differently, by different patterns and different pathological processes. Pathological studies have suggested that the SN is affected in PD and PSP. Defining its borders via MRI has proved challenging due its complexity and heterogeneity.

The aim of this work was to determine the achievability of using T2 and T2* times obtained at 3-Tesla, to discriminate Parkinson's disease (PD) from progressive supranuclear palsy (PSP), multi-system atrophy (MSA), and control subjects with no neurological diseases.

CHAPTER TWO—Methodological Study—The mamillothalamic tract as a landmark to localize the subthalamic nucleus on MRI

2.1 Introduction

Deep brain stimulation (DBS) of the subthalamic nucleus (STN) is widely used in the surgical management of advanced Parkinson's disease where medical treatment has failed to deliver effective symptom control.[85 89] In addition, the STN is involved and important in progressive supranuclear palsy (PSP) where it suffers apoptosis and atrophy,[85 86] and in hemiballism where the clinical significance of the STN was first realized.[87 88]

The mamillothalamic tract (MTT) is a structure that can be well visualized and located on 1.5-T MRI, lying in close proximity to the STN (Figure 3). A group[51] studied the brains of 16 healthy volunteers imaged with 3-T MRI and observed a strong correlation between the y-coordinates of the MTT's centre and the STN's anteromedial border, concluding that the MTT could be a good landmark for STN localization during DBS. Another study[52] reported the alignment of the MTT with the anteromedial border of the ipsilateral STN.

Yamada et al used MRI to image the MTT and demonstrated that the vast majority of paired MTTs were symmetric in size and location, and that the signal intensity was always isointense to other normal white matter tracts. The axial plane is optimal for its visualization, due to its fibers which are predominantly course and in a craniocaudal fashion.[89]

The aim of this study was to examine a possible role of the MTT when identifying the position and borders of the STN by assessing the spatial relationship between the two structures on preoperative axial MR images in patients with Parkinson's disease who underwent MRI-guided and MRI-verified DBS procedures of their STNs. In this work I will be looking at boundaries and distance from the MTT to give an area where the STN lies. This may provide a better way to identify the STN for surgical procedures, and measurements of the STN, discussed later in this thesis.

2.2 Subjects and Methods

This study was an observational retrospective imaging research study, performed with patients with Parkinson's disease who had undergone MRI-guided and MRI-verified STN DBS procedures.[85]

Patients fitted with a Leksell frame, mounted on the head, were scanned in a 1.5T Echo-Speed LX GE machine using axial T2WI (TE 95 ms, TR 3000 ms, echo length 9, band width 20.8 kHz, FOV 25 cm, matrix 256 x 256) and with 20 contiguous 2 mm sections centered on the AP-PC line, pre- and postoperatively.[88 90-95]

By scrolling the images up and down, the desired axial slice demonstrating the red nucleus at its maximum-transverse diameter was identified (Figure 3). Both the STN and the MTT were visualized at the level of the maximum-rubral diameter, 3-5 mm below the AC-PC plane. All measurements were taken on that one slice. 37 patients were studied, of which analysable data, with no artefacts degrading quality, were available from 24.

Using Microsoft Excel, x-, y- and z-coordinates were recorded for the following structures into a spreadsheet: AC, PC, centre-of-the-right MTT, anteromedial border-of-the-right STN (as per best visualization), centre-of-the-left MTT, anteromedial border-of-the-left STN (as per best visualization) and the diameter of the third ventricle at the mid-commissural point (the mid-point between the anterior and posterior commissures).

Statistical analyses were performed using SPSS Statistics 17.0 for Microsoft Windows, including: the Pearson correlation; the one-sample, paired, t-test, comparing the x- and z-coordinates of each STN with its ipsilateral MTT. The threshold for statistical significance was a p-value less than 0.05.

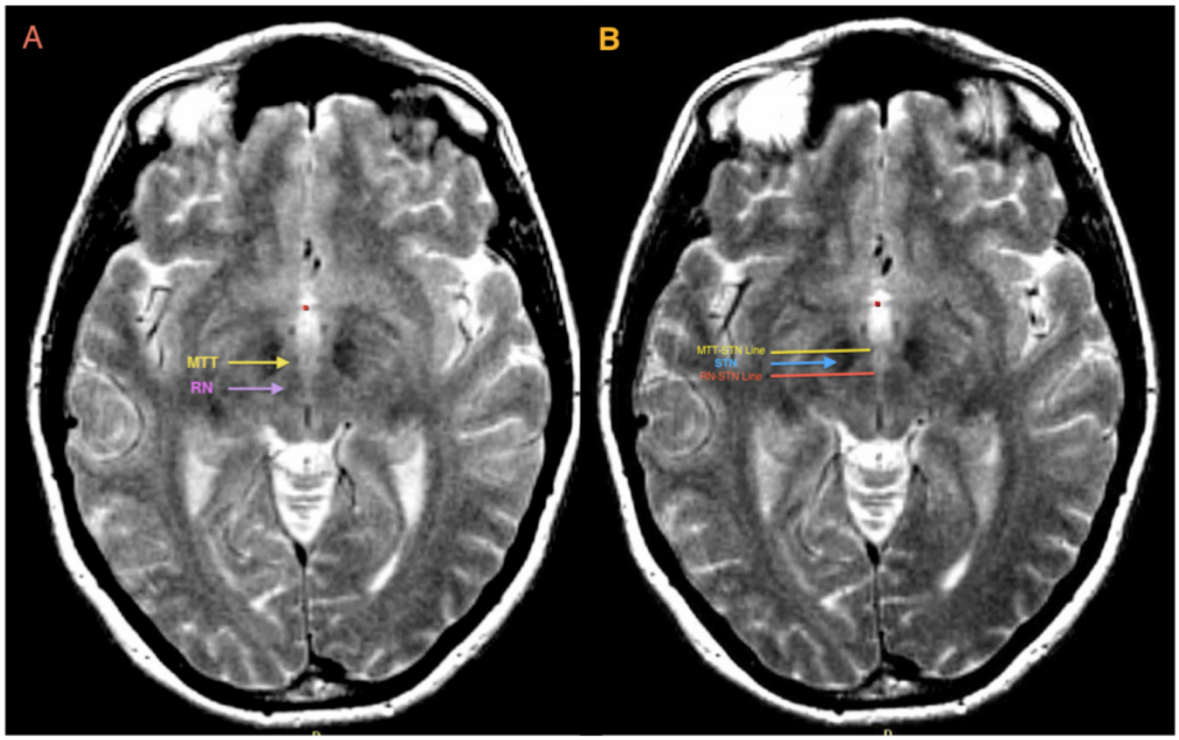

Figure 3: A 1.5-T T2-weighted axial MR image at the level of maximum transverse rubral width. MTT: the mamillothalamic tract. RN: the red nucleus. STN: the subthalamic nucleus. The MTT-STN Line is an imaginary line drawn from the centre of the MTT, parallel to the x-axis and at the same y-coordinate abutting the anteromedial border of the STN. The RN-STN Line is an imaginary line drawn from the anterior border of the RN, parallel to the x-axis and at the same y-coordinate hitting the centre of the ipsilateral STN (Bejjani's Method).

2.3 Results

Data was collected from 24 scans. The mean anterior commissure – posterior commissure (AC-PC) distance was 24.3 mm (SD 1.3 mm; range 22.4 to 26.5 mm, $p < 0.05$).

On the right, the mean (SD) distance, from the STN anteromedial border to the centre of the ipsilateral MTT, was -4.35 mm (0.13 mm), with 95% CI, -4.31 to -4.41 mm, along the x-axis, and 0.01 mm (0.11 mm) with 95% CI, -0.04 mm to 0.07 mm, along the z-axis. The Pearson correlation coefficient (r) — between an x-coordinate on the right MTT and that of the right STN — was 0.966 ($p < 0.05$).

On the left, the mean (SD) distance, from the STN anteromedial border to the centre of the ipsilateral MTT, was 4.34 mm (0.06 mm) with 95% CI, 4.31 mm to 4.37mm, along the x-axis, and 0.09 mm (0.1 mm) with 95% CI, 0.05 mm to 0.13 mm, along the z-axis. The Pearson correlation coefficient (r) — between an x-coordinate on the left MTT and that of the left STN — was 0.992 ($p < 0.05$) (Table 2).

Along the y-axis, the mean (SD) distance, from the STN anteromedial border to the centre of the ipsilateral MT, was invariably 0.0 mm on both sides. All measurements were thoroughly subjected to quality control by a functional and experienced neurosurgeon (Mr L Zrinzo).

Distance from the tract to the nucleus	Mean (mm)	Std. Deviation (mm)	95% Confidence Interval (mm)	
RMTTX-RSTNX	-4.35	0.13	-4.41	-4.3
RMTTZ-RSTNZ	0.01	0.13	-0.04	0.07
LMTTX-LSTNX	4.34	0.06	4.31	4.37
LMTTZ-LSTNZ	0.09	0.1	0.05	0.13

Table 2: The distance between the nucleus and the tract on either side. RMTTX: x-coordinate of right MTT; RSTNX: x-coordinate of right STN; RMTTZ: z-coordinate of right MTT; RSTNZ: z-coordinate of right STN; LMTTX: x-coordinate of left MTT; LSTNX: x-coordinate of left STN; LMTTZ: z-coordinate of left MTT; LSTNZ: z-coordinate of left STN.

2.4 Discussion

The spatial, anatomical relationship between the STN and the MTT was studied using stereotactic T2-weighted 1.5-T MRI from 24 patients who underwent effective MRI-guided STN DBS.

The MTT was found to have minimal variability (variable distance) along the x-axis from the ipsilateral STN. The mean distance between the tract and the nucleus, along the x-axis, was 4.3 mm, with narrow 95% CI, 4.3 mm to 4.4 mm. Knowing the distance—from an easily visualized MTT, to a poorly visualized STN—may help to localize and target the nucleus.

Since the distance between the MTT and the STN was found to be invariably 0.0 mm along the y-axis, and very close to 0.0 mm along the z-axis, an imaginary line could be drawn from the centre of the MTT and running parallel to the x-axis, abutting the anteromedial border of the ipsilateral STN in almost all cases. Other studies evaluating the spatial relations of the two structures have made similar conclusions.[51 52 96 97]

Direct visualization and identification of STN borders should be the gold standard, the best approach for accurately localizing the nucleus anatomically within individual patients. Note that whenever resources are limited and imaging quality is suboptimal—resulting in difficult identification of the nucleus—landmarks closer than the AC and the PC may be more helpful. The mamillothalamic tract, therefore, may function as a valuable landmark to target poorly visualized STNs, in combination with other landmarks already in use, such as the red nucleus.

The MTT may act as a reliable landmark when drawing regions of interests (ROI) of the STN, to get quantitative MRI indices of the STN, as discussed later in this thesis.

2.5 Conclusions

The MTT was demonstrated to be clearly visible on stereotactic axial T2-weighted 1.5-T MR images. The distance between the STN anteromedial border and the centre of the MTT on the x-axis show little inter-subjective variation. Direct visualization should always be sought when targeting the STN during DBS procedures: the MTT may be a stable and reliable landmark for accurate localizations of the STN during DBS procedures, as well as when drawing ROI to get MRI metrics.

Summary

The main objective of this work was to determine if the mamillothalamic tract (MTT) can be used as a reliable and internal fiducial marker for the position of the subthalamic nucleus (STN) and thus improve accurate localizations of the STN on MRI.

It is an observational imaging study, within which pre-operative stereotactic T2-weighted Magnetic Resonance (MR) images were studied from patients with Parkinson's disease (PD) that were undergoing STN DBS. Lateral and the anteroposterior (A-P) distances, between the anteromedial border of each STN and the centre of the ipsilateral MTT, were measured on the axial section showing the red nucleus (RN) at its maximal-transverse diameter. Accurate measurements from 24 patients or 48 nuclei were obtained.

The mean distance from the STN anteromedial border to the centre of ipsilateral MTT, along the x-axis, was 4.4 mm (SD 0.13 mm) on the right side and 4.3 mm (SD 0.06 mm) on the left side. The distance between the MTT and its STN anteromedial border, on axial stereotactic MR images, showed little variation. The MTT may, therefore, be used as an anatomical landmark to help localize the STN on MRI, and this relationship can further be exploited to help place the ROI when assessing MRI metrics of the STN, as discussed later in this thesis.

CHAPTER THREE—Case Study—Correlations of clinical data with post mortem 9.4-T MRI and histopathology in deep brain stimulation of the subthalamic nucleus

3.1 Introduction

When medical management fails to improve quality of life, patients with Parkinson's disease can undergo deep brain stimulation (DBS) of the subthalamic nucleus (STN). Stereotactic MR imaging is now used to plan surgical targeting and to verify the lead location after implantation.[85 91 98 99]

This study features the outcome of a single patient who underwent bilateral STN DBS using an MRI-guided surgical technique, analyzed with post-mortem high-field MRI at 9.4-T as well as with histopathological studies.

The present study sought to evaluate the anatomical accuracy of MRI-guided STN DBS without microelectrode recording. The anatomical relationship of each electrode to the corresponding nucleus was explored by high-field MRI at 9.4-T that were confirmed by histological examination.

3.2 Subject and Methods

Idiopathic Parkinson's disease was diagnosed in a 52-year-old male builder that was right-hand dominant. When medical therapy proved ineffective, bilateral STN DBS was performed at age 67-years — 15-years after the onset of his symptoms. MRI-guided targeting and visualization of the STN on T2-weighted imagery, as well as macro-electrode stimulation under local anesthesia, were performed.[43 85 100]

Prior to frame removal, a post-operative stereotactic MRI (Table 3) is acquired to document the lead location. In this particular instance, the patient became very dyskinetic and agitated, with head movements during the post-implant MRI, and the image had to be terminated before completion of the scanning protocol. The frame was removed and agitation resolved after a few hours without residual sequelae. The T2-weighted MRI was obtained on the second postoperative day.

Imaging	Magnet Strength	Sequence	TR (ms)	TE (ms)	FOV	Slice Thickness (mm)	Gap (mm)	Plane
In vivo **(stereotactic)**	1.5T	T2	3,500	90.9	250 x 250	2 mm	0	AC-PC
		T2	3,500	90.9	250 x 250	3 mm	0	Coronal
Ex vivo	9.4T	T2 (FSEMS)	5000	40	120 x 120	0.5	0	AC-PC
		T2 (FSE3D)	5000	40	120 x 120		0	Coronal

Table 3: MRI Protocols employed to image the subject before surgery and after death.

Regular outpatient follow-up and formal UPDRS scores were obtained preoperatively and at one, three and five years after the procedure (Table 4) Preoperative L-dopa challenge resulted in a 47 % improvement in UPDRS motor scores. STN DBS continued to provide motor benefit 5-years after surgery. A 31% improvement from baseline was observed at three- and five-year follow-up when the patient was on-stimulation and off-medication.

Status	Medication	DBS	Score
Pre-op	Off	-	58
Pre-op	On	-	31
3 years	Off	Off	48
3 years	Off	On	40
3 years	On	On	36
5 years	Off	Off	53
5 years	Off	On	40
5 years	On	On	26

Table 4: UPDRS (part 3) scores pre-operatively (pre-op) (February 2008) and at three (March 2011) and five years (February 2013) post-DBS

The patient died at 74 years of age from pneumonia. The brain was donated to the Queen Square Brain Bank, where donation is made under ethically approved protocols and tissue is stored under a license from the Human Tissue Authority (HTA). Approval for this study was obtained from the local research ethics committee.

The brain was removed with DBS leads *in situ* and fixed in 10% formalin. The DBS leads were subsequently removed and a tissue block comprising brainstem and diencephalon was cut parallel to the AC-PC line to include the electrode tracks, the subthalamic nuclei and mesencephalon. The resulting tissue block was immersed in perfluoropolyether (Fomblin^{TM}, Solvay Selexis); this attenuates air-tissue interface MRI magnetic susceptibility artifacts, and the lack of MR-visible protons renders it invisible to ^{1}H MR sequences. The brain block was then imaged using a Varian 9.4T MR scanner with a transmit-receive quadrature volume radiofrequency (RF) coil (inner diameter = 150mm).

The MRI protocol included (Table 3):

(1) 2D, T2-weighted fast spin-echo sequence, optimized for the best possible spatial resolution (0.234 x 0.234 x 0.234 mm3) and STN contrast. Slice orientation was parallel to the AC-PC plane (TE= 40 ms, TR=5000 ms, averages=4).

(2) 3D, fast spin-echo sequence, nominal orientation: coronal (TE=40 ms, TR=5000 ms, averages=1).

Total imaging time: 7-hours.

Images viewed and processed using ImageJ software (https://imagej.nih.gov/ij/).

Following MRI, the brain block was cut into 3 mm slices, parallel to the AC-PC plane. The remainder of the brain was cut along the coronal plane; blocks were selected for histological analysis to establish diagnosis. All tissue-blocks that were selected for histology were processed into paraffin wax, then tissue sections 7-micron thick were stained using conventional methods: haematoxylin and eosin; Luxol fast blue/cresyl violet; Perl's stain for iron. Immunohistochemistry tests were performed using standard avidin-biotin techniques, utilizing the following antibodies: tau (1:600, AT8, Autogen Bioclear, Calne, UK); glial fibrillary acidic protein (GFAP, 1:1000, Dako, Ely, UK); amyloid β (Aβ, 1:100, Dako); α-synuclein (1:50, Novacastra, Newcastle, UK) and CD68 (1:50, Dako).

3.3 Findings

Findings: Imaging

At 1.5T, no abnormalities were detected on the stereotactic localizer sequence, obtained before the first perioperative MRI examination was terminated. However, a non-stereotactic scan obtained on the second postoperative day revealed T2 hyper-intensity—which is suggestive of edema—around the electrodes tracks and around the tip of the electrode track, which appeared to be located in the medial aspect of the STN on either side (Figure 4).

The 9.4T MR images showed the electrode tracks level to the subthalamic nuclei (Figure 5 and Figure 7). A signal, compatible with a hemosiderin ring, was visualized throughout their length, surrounding the track defects. Both DBS leads were seen to traverse the internal capsule, terminating in the region of the STN bilaterally (Figure 5). The left electrode track appeared to be toward the medial aspect of the STN, adjacent to the STN border with the zona incerta. On the

right-side, the track appeared to be embedded within the subthalamic nucleus (Figure 5 and Figure 7).

Findings: Histopathology

A microscopic examination of the tissue clearly showed the electrode tracks surrounded by lymphocytes, gliosis, microglia and macrophages, as well as a small number of multinucleate giant cells. The tracks were lined by collagen throughout their lengths; adjacent, Perl's positive iron-containing pigments. The electrode tracks extended to the level of the subthalamic nucleus bilaterally, and at this level were of a similar diameter, consisting of a small collagenous scar with surrounding gliosis and Perl-positive pigments. The left track terminated and abutted the medial border of the subthalamic nucleus, while the right track terminated within the subthalamic nucleus and close to the medial border (Figure 5). Histological examinations confirmed the clinical diagnosis of idiopathic Parkinson's disease, and additionally showed a cortical Lewy body pathology of the neocortical type (Figure 6).[101]

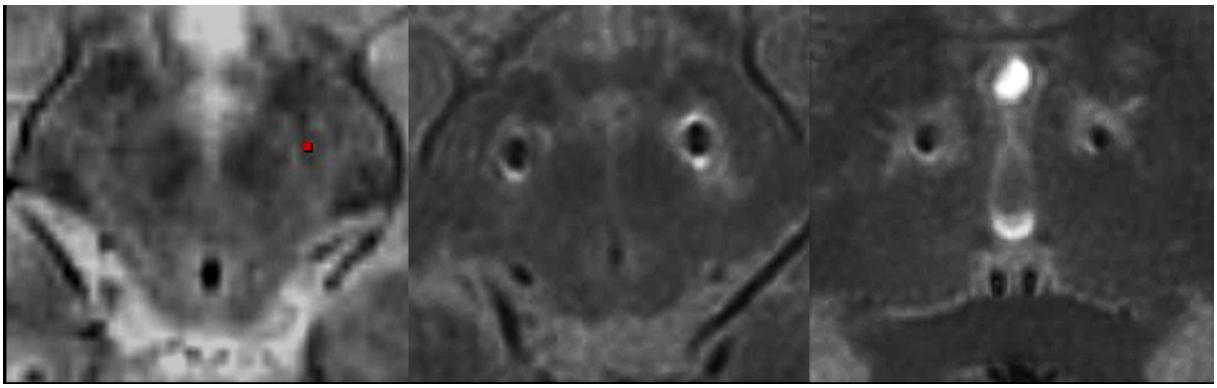

Figure 4: Axial MR images at the level of the STN (left and centre) and the level of the anterior commissure (right). Left: preoperative stereotactic image shows the STN (red dot on the left STN). Center and Right: two-day postoperative images showing DBS electrodes within the STN region, and T2 hyper-intensity (suggesting oedema) surrounding the leads down to their tips.

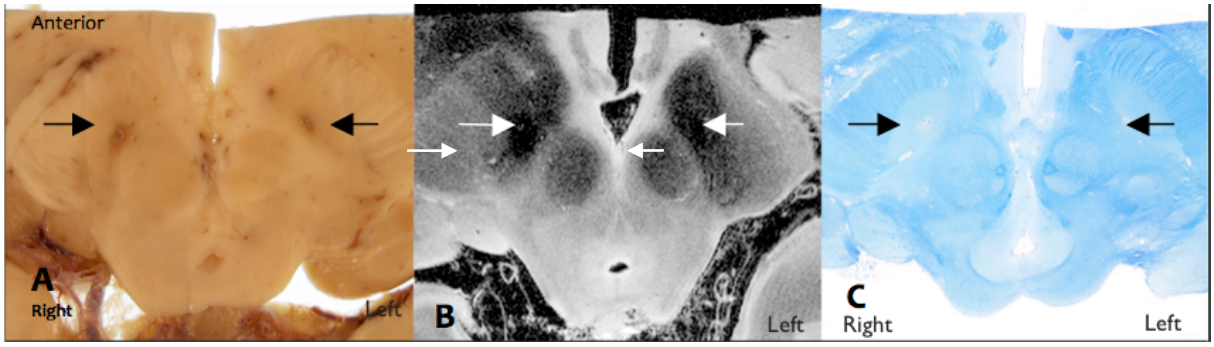

Figure 5: Comparison of post-mortem gross section (A) at the level of the STN, with 9.4T T2-weighted image (B) and histological section using LFB/CV method (C) at the same level. The subthalamic nuclei are clearly visualised in all three modalities (arrows). The left electrode defect is more medially located than the right. No gross pathological or signal changes can be seen within the nuclei or their environs.

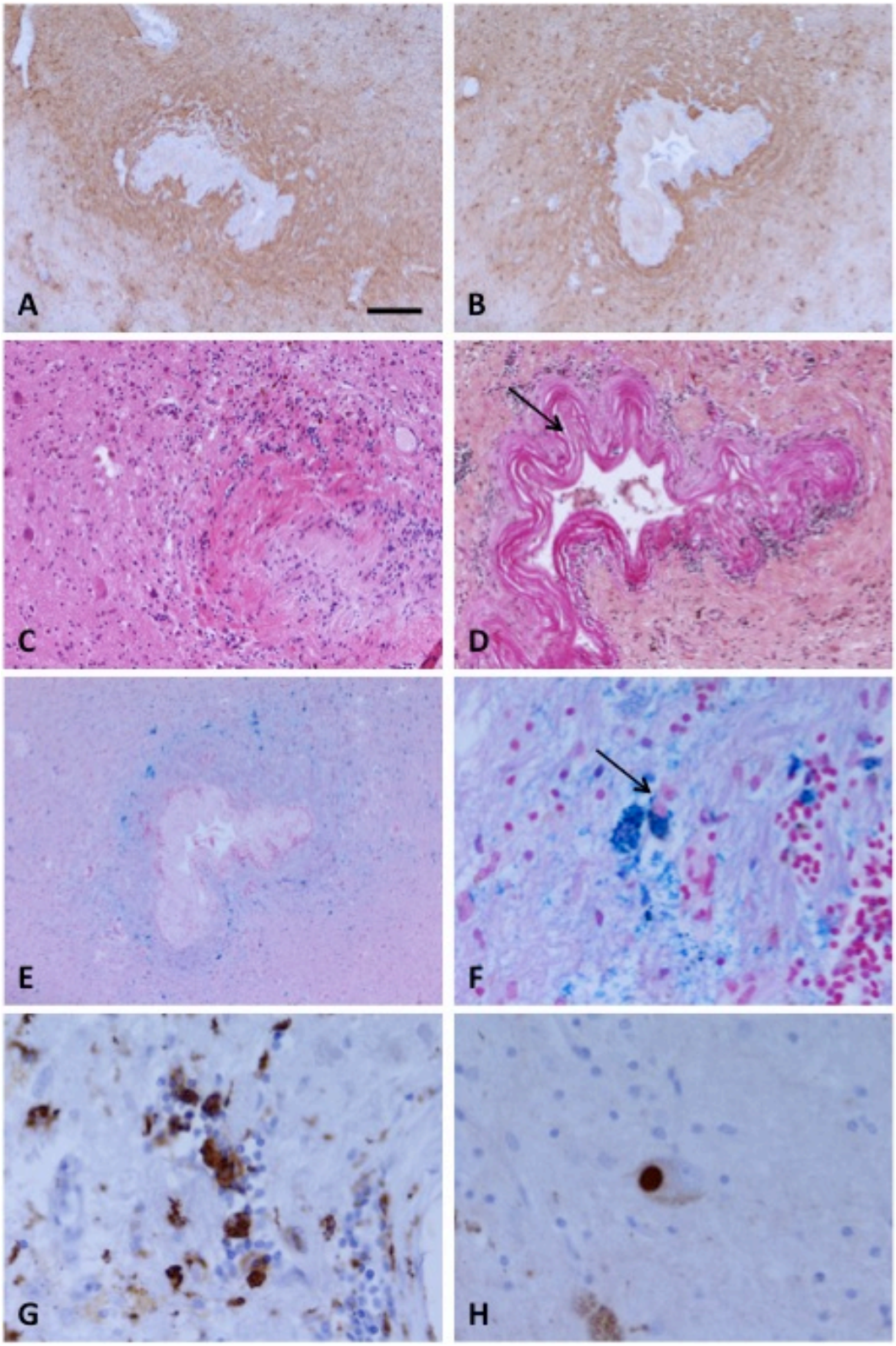

Figure 6: At the level of the subthalamic nuclei the electrode tracks were surrounded by fibrillary gliosis, demonstrated using GFAP immunohistochemistry (A: left, B: right). Around each track, haemosiderin pigments was deposited; there was a mild lymphocytic infiltrate (C: haematoxylin and eosin). Each track was lined by a collagen (D: arrow, Van Gieson). E and F: surrounding haemosiderin depositions, in the neutrophil and the macrophages (F, arrow), demonstrated by Perl's stain.

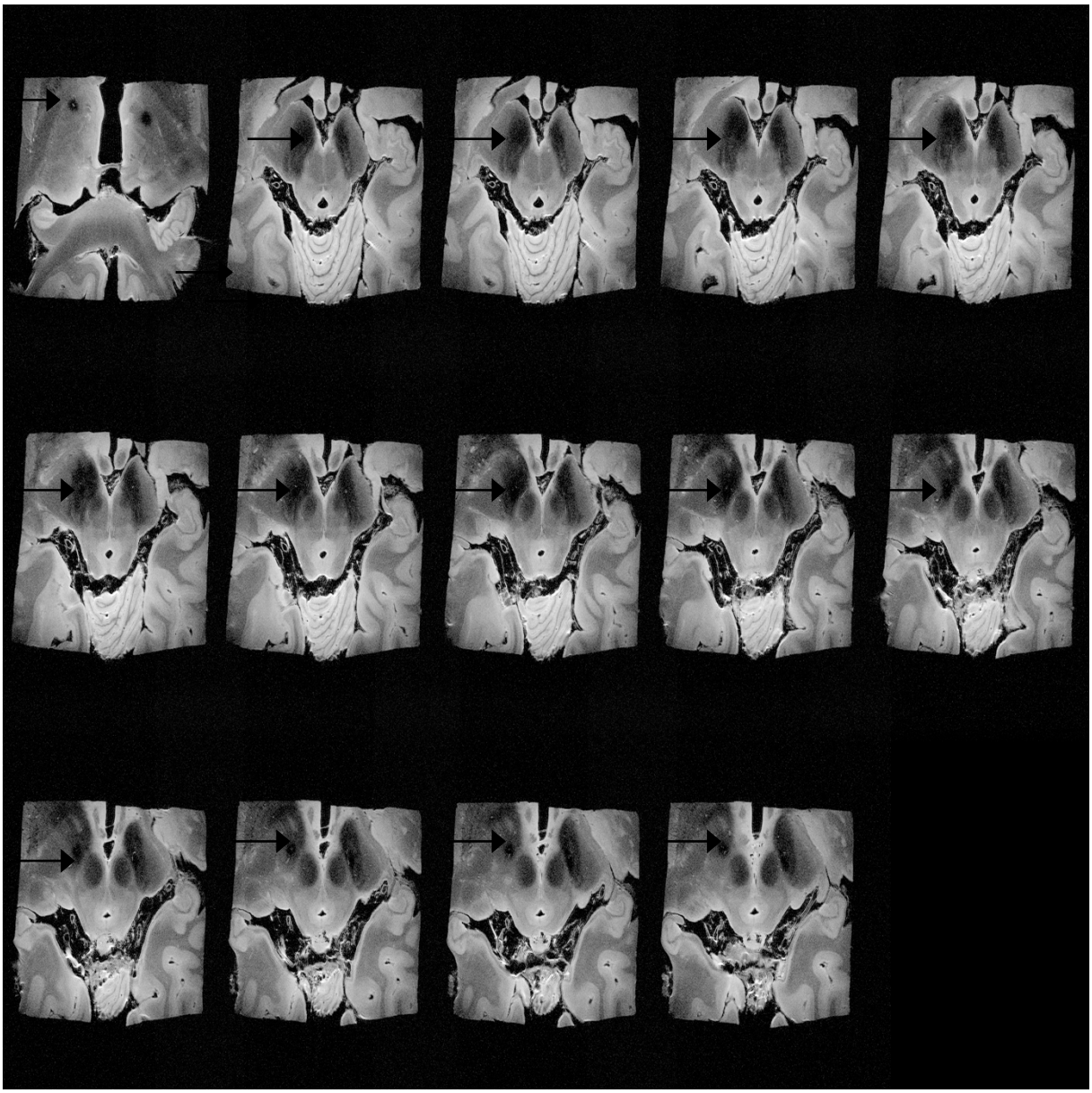

Figure 7: Serial axial T2-weighted FSE MR images at 9.4T, showing the electrode tracks running down to the STN on either side (right track into the STN is labeled with a black arrow). The top left slice is at the level of the third ventricle, while the remaining slices follow the course of the tract into the STN. The STN can be seen as a hypointense structure, medial to the substantia nigra. Slice orientation was parallel to the AC-PC plane (TE= 40 ms, TR=5000 ms, averages=4).

3.4 Discussion

This study features a clinical follow-up, *in vivo* MRI and post mortem high resolution MRI and histopathological analysis for a patient who had 72-months of continuous MRI-guided STN DBS, prescribed for medically refractory idiopathic Parkinson's disease.

Consulting the literature, few studies have described neuroparenchymal reactions to STN DBS-lead implantation and STN DBS stimulation.[21 90-95 102 103] In this instance, the surgical technique applied was MRI-guided.

MRI-guided DBS helps target the STN accurately; best practices have been to err toward the medial border and away from the internal capsule. This strategy minimizes current-leakage into the capsule, which might limit the stimulation amplitude. Moreover, medial current-leakage tends to stimulate the medial zona incerta, which might be an effective target for DBS in PD.[10 96 97] Nevertheless, serial follow-ups of large cohorts are needed to establish the best sub-region of the subthalamic area for targeting, noting that this must include speech and cognitive performances as well as motor improvements.

72-months is one of the longest periods of continuous subthalamic stimulation, with histopathological analyses, reported in the published literature.[6 90-95]

In the postoperative MRI, T2 hyper-intensity was seen along the track to the STN, suggesting edema. In contrast, the same area was seen as T2-weighted hypo-intense on PM imagery, suggesting haemosiderin deposition — which was later confirmed via histological analysis. One explanation is micro-trauma to the surrounding parenchyma, with excessive head motion, during the MR scan.

Other PM studies have not demonstrated significant pathological changes adjacent to the DBS lead.[91 93 98] Similarly, and with this patient, the only histological changes noted were a lining of collagen surrounded by mild and chronic inflammation, as well as reactive gliosis and iron depositions. The formation of a fibrous capsule consisting of collagen is an extremely rare and unusual tissue reaction to find following DBS implantation, and was referenced only once in the previous literature.[93 100] These minor pathological changes adjacent to the electrodes do not suggest that chronic stimulation leads to tissue damage because the neuronal population of the STN appears to be well preserved.

Previously, high-resolution or field MRI have been used to study the anatomy and signal characteristics of the STN.[21 54 104-106] In this work, the STN is seen excellently along the axial

plane as an almond-shaped, T2-weighted, hypointense structure. The high spatial resolution (88 microns) that can be obtained from scanning specimens at 9.4T MRI magnet—sometimes called Magnetic Resonance Microscopy or MRM[80 102 103]—may allow nondestructive examination of valuable specimens as well as direct comparison with histological data—additionally, possible applications in disease and in vivo. These resolutions allow for validation, verification and understanding of the histological basis for MRI signal changes of the peri-track tissues as well as the STN. Such an approach has been used by other researchers and has helped understand MRI changes.[21 102 103 107] The main advantages of high magnetic-field MRI are increased signal-to-noise ratio (SNR) and the ability to image in orthogonal planes with multiple averages without the need to destroy tissue, enabling a significant increase in spatial resolution while reducing partial volume effects. Moreover, and in this study, correlations with histopathology were particularly useful to help verify the precise location of electrodes.

3.5 Conclusions

This study presents post-mortem high-field MRI and histological analysis of the brain from a patient who underwent chronic bilateral DBS of the STN for a period of 72-months. Findings support the results of other post mortem studies and validate the use of MRI-guided approaches to STN targeting, and further suggest that high frequency stimulation does not cause neuroparenchymal tissue damage.

Summary

Deep brain stimulation (DBS) of the subthalamic nucleus (STN) using an MRI-guided and MRI-verified technique without microelectrode recording, is an effective and safe surgical treatment for patients with Parkinson's disease (PD).

The objective of this study was to assess the anatomical accuracy of lead placement after MRI-guided and MRI-verified STN DBS using post mortem histology and high-field MRI at 9.4T, thus giving a better understanding of the anatomy of the STN, needed for the work discussed later in this thesis.

Using 9.4T MRI and histology, we conducted post mortem analyses of a patient's brain that had undergone MRI-guided and MRI-verified STN DBS for PD. After death, the brain was retrieved and a block—that included the electrode tracks down to the mesencephalon—was examined using high-field MRI at 9.4T as well as examined using histological analysis.

High-field MRI images, and their corresponding histological examinations, showed that each electrode track ended within the intended target area, and that DBS did not cause significant neuroparenchymal tissue damage. This study supports the anatomical accuracy of MRI-guided and MRI-verified methods of STN DBS and helps to understand the anatomy of the STN, its environs on MRI, and thus supports subsequent work presented in this thesis.

CHAPTER FOUR—Quantitative 3T MRI in Parkinsonism—Subjects and Methods—Description of methods for patient recruitment, clinical assessment, image acquisition and image analysis

4.1: A: Aims

The aim of this work was to determine the achievability of using T2 and T2* times, obtained at 3-Tesla, of the STN, RN and the SN, and to discriminate among Parkinson's disease (PD), progressive supranuclear palsy (PSP) and multi-system atrophy (MSA), as well as control subjects with no neurological diseases.

The primary research question for this work was: do differences in 3T MRI indices, of T2 and T2* times, within key basal ganglia structures like the STN, RN and SN, enable improved differentiation between patients that present with Parkinsonian symptoms?

Patients with clinical diagnoses of PD, PSP and MSA were recruited from Movement Disorders Outpatient Clinics organized through the National Hospital for Neurology and Neurosurgery. Patients were recruited by advertising in patient support group newsletters (PSP Association, PD Society), and the age and gender-matched control subjects were recruited in a similar fashion.

B: Patients Recruitment

Inclusion criteria for patients saw the fulfillment of the clinical diagnostic criteria for PSP, PD and MSA.[10 52] The control subjects were age- and gender-matched with no symptoms or signs of neurological disease nor abnormal MRI findings. Exclusion criteria included presence of other neurological diagnoses, standard contraindications for MRI scanning: implants like pacemakers, coronary stents, artificial heart valves or other cardiac implant, aneurysm clips or coils, shunts or valves, neurostimulator implants or other implants, metallic implants from spinal surgeries, metallic implants from accidental exposure; pregnancy or the possibility thereof; a Mental State Examination (MSE) score below 21/30; incompetency to give informed consent to participate. Additionally, certain patients were excluded from the study because they were physically unable to have an MRI scan ; this was decided on an individual basis, taking into consideration the lifestyle of the patient, as well as their opinions and advice from other researchers.

Initial patient recruitment to completion of scanning took a total of 24-months. All subjects provided informed consent to participate, in accordance with the Declaration of Helsinki; the study was approved by the Research Ethics Committee, National Hospital for Neurology and Neurosurgery.

Informed consent was obtained from all participants and documented on a standardized consent form. Participants were informed that withdrawal from the study would not affect their medical treatment in any way and that on-going participation remained voluntary. Consent was granted to publish the results in scientific journals and at scientific meetings.

Subjects fulfilled the clinical research criteria for PD,[6 51] PSP[108 109] and MSA,[51 110] or acted as a neurological controls, i.e. with no symptoms nor signs of neurological diseases. Clinimetric assessments at baseline included validated scales such as the Hoehn & Yahr score (Y&H),[43 105] the unified Parkinson disease rating scale (UPDRS) with all of its subcomponents (I, II & III),[92 96] and the mini-mental state examination (MSE). Clinical assessments took place either on the day of imaging or at the earliest available subsequent date depending on the availability of clinical rooms. Disease duration was defined from the date of the onset of symptoms to the date of examination. The effect size was calculated as the difference between the control group and the disease group, divided by the standard deviation but not nil.

Regarding the sample size and statistical power, analogous studies using 1.5-T published with between 8 and 30 patients per diagnostic group. For the measures we investigated we had a paucity of data at 3T; but to give a comparable example, here are sample size calculations for a study based on data from DWI at 1.5T:[8 97] the sample size needed to detect a significant difference in the middle cerebellar peduncle rADC, between MSA and controls, with 7 participants per arm, and a power of 80% and β of 5%. Using magnetization transfer imaging data at 1.5T,[4 72] the sample size needed to establish a significant MTR difference in the substantia nigra, between PSP and controls, with 3 participants per arm, and a power of 80% and β of 5%.

4.2 Image Acquisition

Imaging was performed using a 3-Tesla (T) scanner and the manufacture's 32-channle head coil: manufacturer, Siemens, Erlangen, Germany; scanner, Siemens Magnetom TrioTim; software, level B17. During scanning, all participants were comfortably positioned and their heads fixated within the head coil using special cushions.

The imaging protocol acquired the following:

(1) Parameters for T2* multiple-gradient recalled echo sequence: TR 100 ms; TE 3, 8.18, 13.36, 18.54, 23.72, 28.9, 34.08, 45.00, 50.18, 60.00, 70.00, 79.00 ms; field-of-view, 220 mm x 220 mm; slice thickness, 3.0 mm; voxel size, 0.9 x 0.9 x 3.0 mm; number of slices, 60; sequence dimension, 3D.

(2) Parameters for 3-TE T2 sequence: TR 4,500 ms; TE 12 ms, 62 ms, 111 ms; field-of-view, 240 mm x 240 mm; slice thickness, 3.0 mm; voxel size, 1.0 x 0.9 x 3.0 mm; number of slices, 46 (providing close to whole-brain coverage); sequence dimension, 2D.

(3) Parameters for 32-TE CPMG multi-echo sequence: TR 3,000 ms, TE 13.2, 26.4, 39.6, 52.8, 66, 79.2, 92.4, 105.6, 118, 132,145.2, 158.4, 171.6, 184.8, 198, 211.2, 224.4, 237.6, 250.8, 264, 277.2, 290.4, 303.6, 316.8, 330, 343.2, 356.4, 369.6, 382.8, 396, 409.2, 422.4 ms; field-of-view, 200 mm x 200 mm; slice thickness, 3.0 mm; voxel size, 0.8 x 0.8 x 3.0 mm; number of slices, 6 (covering solely the mesencephalon); sequence dimension, 2D.

Total scanning time: 25-minutes.

Patients were invited for a repeat scan on the day of their next clinical visit; clinimetric scores were also re-assessed at that time.

All acquired imaging data was systemically examined for artifacts.

The image quality for each sequence of raw data was assessed against a six-point scale: 5, no artifacts; 4, minimal artifacts; 3, moderate artifacts; 2, significant artifacts; 1, massive artifacts; 0, no image data or not evaluable.[19 107] Assessments were performed by myself and rechecked by Prof TA Yousry, Neuroradiologist, and by Dr E De Vita, MRI Physicist. Scores were tallied into a digital spreadsheet (Microsoft Excel).

4.3 Image Analysis

Java-based imaging software Jim 6.0™ (Xinapse™ Systems Limited) running on a Sun™ Solaris workstation was used to calculate the quantitative MRI measures from the source images. The investigator was blinded to the clinical diagnosis. Initial calculations were in the source image native space. The Jim 6.0 “image fitting” tool performed non-linear, least-square regressions called “fittings” on a series of images that represented a variable at the same position: i.e. for the echo times in a set of multi-echo acquisition scans, “fitting” was used to estimate the

transverse relaxation time, on a voxel-by-voxel basis. The "fitting" tool worked through every pixel for a given set of input images and then altered the appropriate formula to produce a set of output images: one for each of the fit variables, containing pixel-by-pixel estimations for each.

T2* Maps

T2* were calculated by fitting to an assumed and single exponential T2* decay, $y=M0\times\exp(-TE/T2^*)$, which required two fit-variables (M0 and T2).[111] The input images were four, with different TEs: four odd TEs (3.0, 13.4, 23.7, 34.1 ms) producing four odd TE T2* times, or four even TEs (8.18, 18.5, 28.9, 45 ms) producing four even TE T2* times.

T2 Maps

T2 was estimated by fitting to a single exponential function, $y=M0\times\exp(-TE/T2)$, where the independent variable was TE, and the two fit-variables were M0—the estimated signal at TE=0, corresponding to the equilibrium transverse magnetization—and T2—the required transverse relaxation time constant. Prior to the final T2 map generation, initial exploratory analyses were performed interactively on the region of interest (ROI), with the software providing a graphical view of the ROI-data fit, which allowed for an interactive assessment of the regional-fit quality. For both the 3-TE and 32-TE data sequences, the first TE images were excluded from the analyses to ensure a uniform stimulated-echo coherence baseline. For 3-TE T2 data calculations, the two TE points for analysis were therefore 62 and 111 ms.

For 32-TE data and their T2 calculations, the initial TE point (13.2 ms) was discarded and a non-linear fit was applied to the remaining 31 image-volumes with the remaining TEs combined into one file — the additional TEs values were 26.4, 39.6, 52.8, 66, 79.2, 92.4, 105.6, 118.8, 132, 145.2, 158.4, 171.6, 184.8, 198, 211.2, 224.4, 237.6, 250.8, 264, 277.2, 290.4, 303.6, 316.8, 330, 343.2, 356.4, 369.6, 382.8, 396, 409.2, and 422.4 ms. A mono-exponential fit function was used, this time in the form $y=M0\times\exp(-TE/T2)+\text{baseline}$, and this time using three fit-variables (M0, T2, and baseline).

Co-registration and Spatial Normalisation

For this study, a colleague and MRI Physicist with experience in SPM co-registration, Dr E De Vita, normalized the T2 and T2* data into a standard space using SPM software, first co-registering the individual T1-volumes into an MNI space, and then applying the resultant transformations to T2 and T2* source-data and to parameter maps, thus also normalizing these

into the MNI space. 26 cases (18 cross-sectional and 8 longitudinal) failed the automatic SPM co-registration, and for these manual intervention was required; using the "SPM Graphics" function, reorientation was performed manually until the crosshair position became 0.0, 0.0, 0.0 for the centre of each image.

4.4 Drawing Regions of Interest (ROI)

Regions of interest (ROIs) were defined on T2-weighted images with TE 62 ms, normalized with linear and nonlinear registration to the MNI space as described.

STN

The following steps were employed to define the STN's ROI:

(1) Slice identification of the image selection: the working plane[8 52 86] was first defined, in order to minimize the plan-replan as well as the inter-examiner variance in the ROI localization procedure. Criteria for slice selection were:

(a) For each subject, we selected the slice located 4 mm under the AC-PC plane because (i) this slice is close to the Schaltenbrand LXXVII H.v -4.5 mm and because (ii) the STN and the MTT could be visualized for all patients on this slice (Figure 8).[8 51]

(b) This slice shows the maximal transverse rubral diameter (6 mm at slice 42 and 7 mm at slice 41). The maximum diameter was defined as the largest distance measured from a visible boundary point—at the demarcation between hypointense signal of the RN and the surrounding WM—to exactly the opposite point of the RN.[72 108]

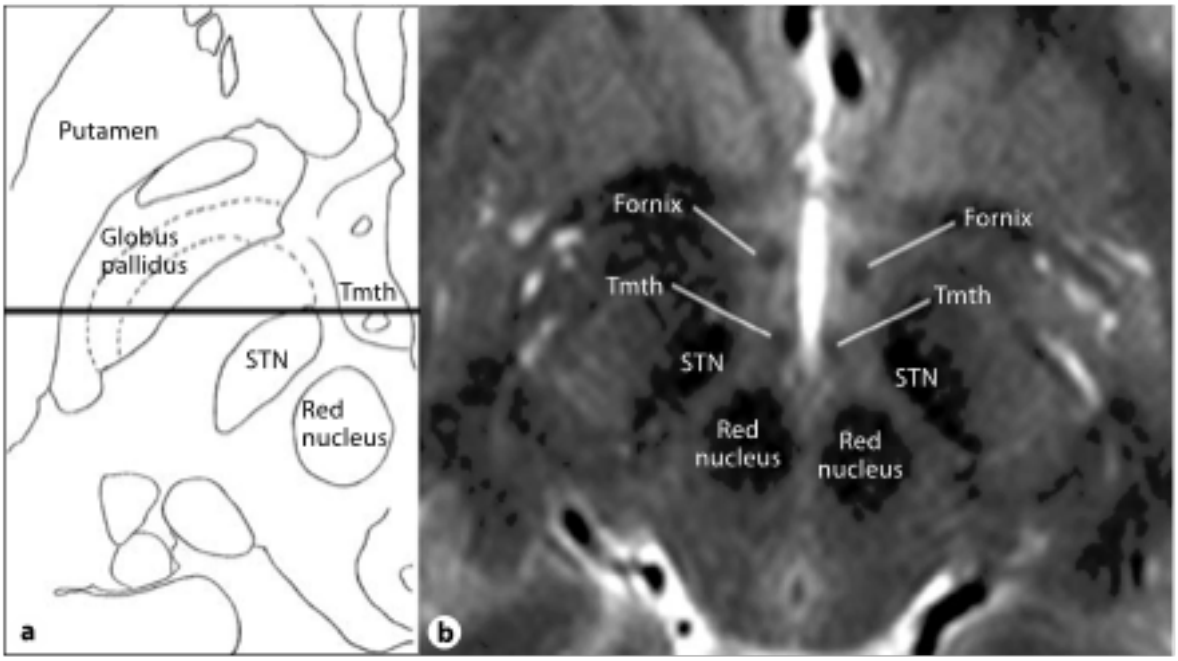

Figure 8: Anatomical relationship between the MTT (labeled as Tmth as per the Latin nomenclature used in the S&W atlas)) and the STN, adapted from S&W Atlas.

(2) The MTT-STN line was defined as a line drawn from the anterior border of the mamillothalamic tract (MTT) running medially and parallel to the x-axis of the lateral aspect of the STN.

(3) The RN-STN line was defined as a line drawn from the anterior border of the red nucleus (RN) running medially and parallel to the x-axis of the lateral aspect of the STN.

(4) Creating ROIs: the STN could be seen as a T2WI hypointense structure that was lateral and dorsal to the red nuclei .[8 43] Within the STN, a circular ROI with a radius of 1.25 mm and surface area of 4.91 mm^2 was drawn in the area between the two lines. The distance between the two lines was 3.5mm. However, 1.25 mm rather than 1.75 mm radius was chosen as a reasonable compromise between them, ensuring maximum coverage of the STN and ensuring minimum volume contamination with neighboring structures, considering that 2 mm is the smallest dimension of the nucleus. The accuracy of the drawn ROI was re-assessed by Prof TA Yousry, Neuroradiologist.

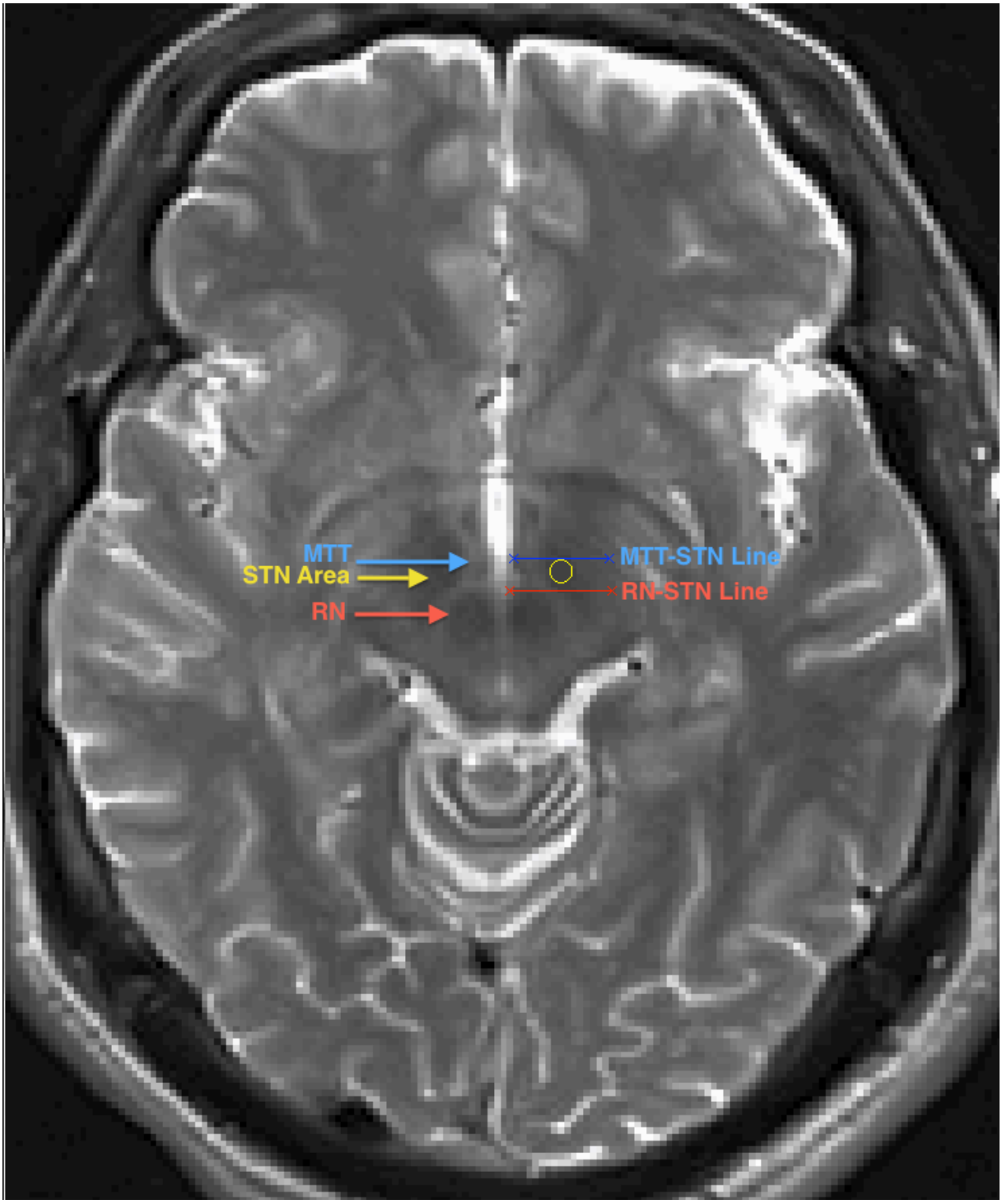

Figure 9: Our method to localize the STN ROI, which was identified as between two imaginary lines drawn from the MTT and the RN at the level of the maximum transverse RN diameter.

Red Nucleus (RN) ROIs

The steps employed to define RN ROIs were as follows:

(1) To minimize the plan-replan and inter-examiner variance for the ROI localization procedure, we first defined the working plane.[52] Criteria for slice selection were: the slice where the maximal transverse rubral diameter (6 mm at slice 42 and 7 mm at slice 41) was selected.[4 19 108] The maximum diameter was defined as the largest distance, measured from a visible boundary point—at the demarcation between hypointense signal of the RN and the surrounding WM—to exactly the opposite point of the RN.

(2) A circular ROI was drawn using the software function with a radius of 2.3 mm, a diameter of 4.6 mm, and a surface area covering 16.62 mm^2. A standard reference that states the typical size of the RN was used in consultation with Prof TA Yousry, an experienced neuroradiologist. Care was taken to avoid contact with the surrounding peri-rubral white matter capsule (Figure).

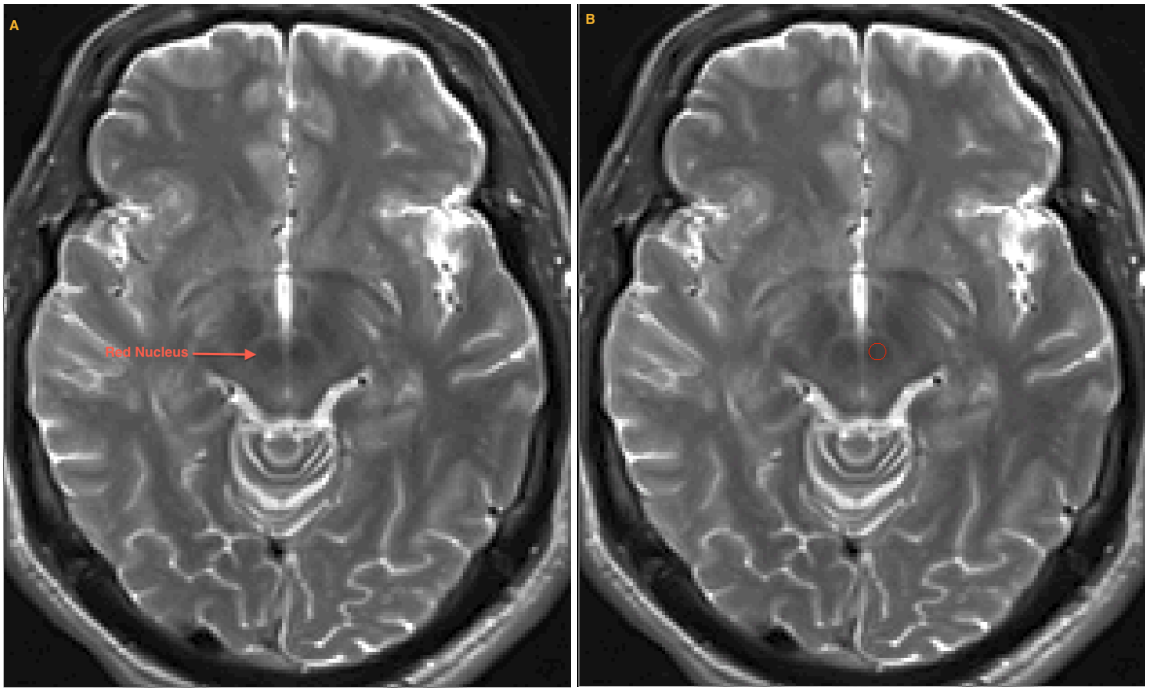

Figure 10: Axial slice where RN ROI was drawn (A and B). It is the axial section where the RN could be seen at its maximum transverse diameter.

Substantia Nigra (SN)

Steps employed to define the SN ROI were (Figure):

On the T2WI, the slice showing the red nucleus (RN) at its maximum transverse diameter was identified. We then moved inferiorly because much of the SN is inferior to the red nucleus. On that slice, the substantia nigra was always visible and the inferior pole of the red nucleus was faintly seen. The mid-level of the mammillary bodies were used as reproducible confirmatory landmarks. ROIs were placed lateral to a line, connecting lateral and medial crural sulci (inter-crural lines) (Figure). We placed the first ROI (round-shaped, 2 mm in diameter, 12.5 mm^2) in the rostral (most anterior/medial) part of the SN, while ensuring we stayed within the structure and avoided the hyper-intensive signal that is returned from the neighboring CSF. The middle ROI was placed lateral and posterior to the first circle, such that the two circles did not overlap. The caudal (most posterior/lateral) ROI was placed lateral and posterior to the middle circle, such that the two circles did not overlap, and did not overlap with each other or with the adjacent CSF spaces.

ROIs drawn on normalized T2-weighted images were imported onto their corresponding co-registered map (Figure , Figure and Figure).

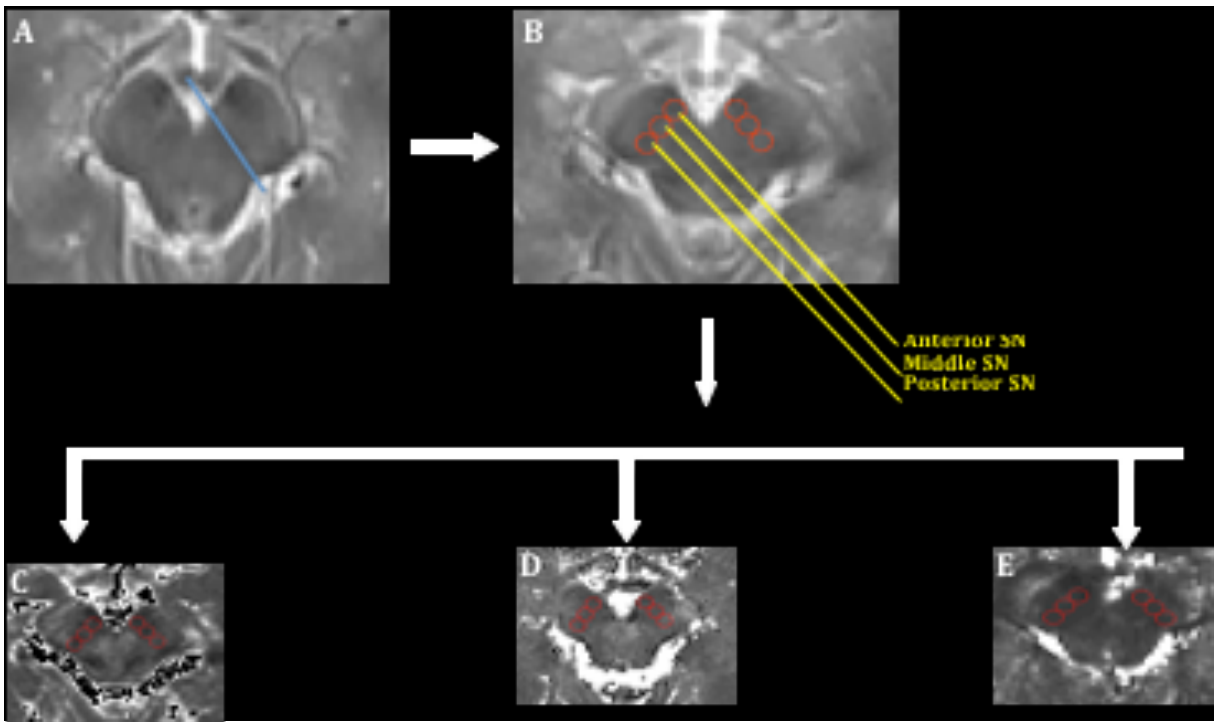

Figure 11: Procedure used to draw ROI in the SN. The SN was identified as being just lateral to an imaginary line drawn between the medial and lateral crural sulci (A). (see text for further explanation). Three circular ROIs were drawn representing the anterior, middle and posterior regions of the SN (Martin 2012) (B). ROIs were imported from T2 images onto T2* and T2 maps (C, D, E).

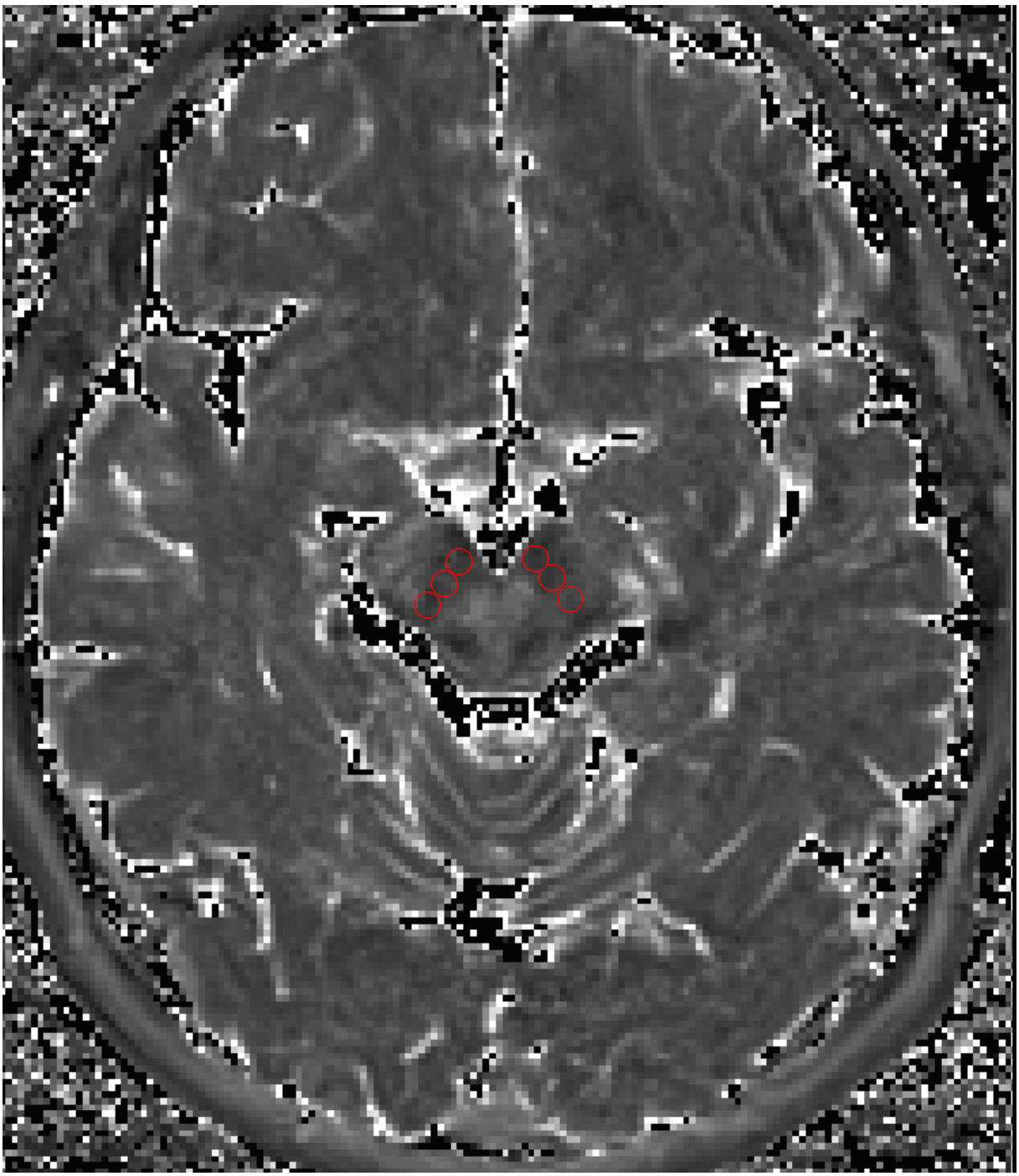

Figure 12: 2-TE T2 map with the SN ROIs imported and placed.

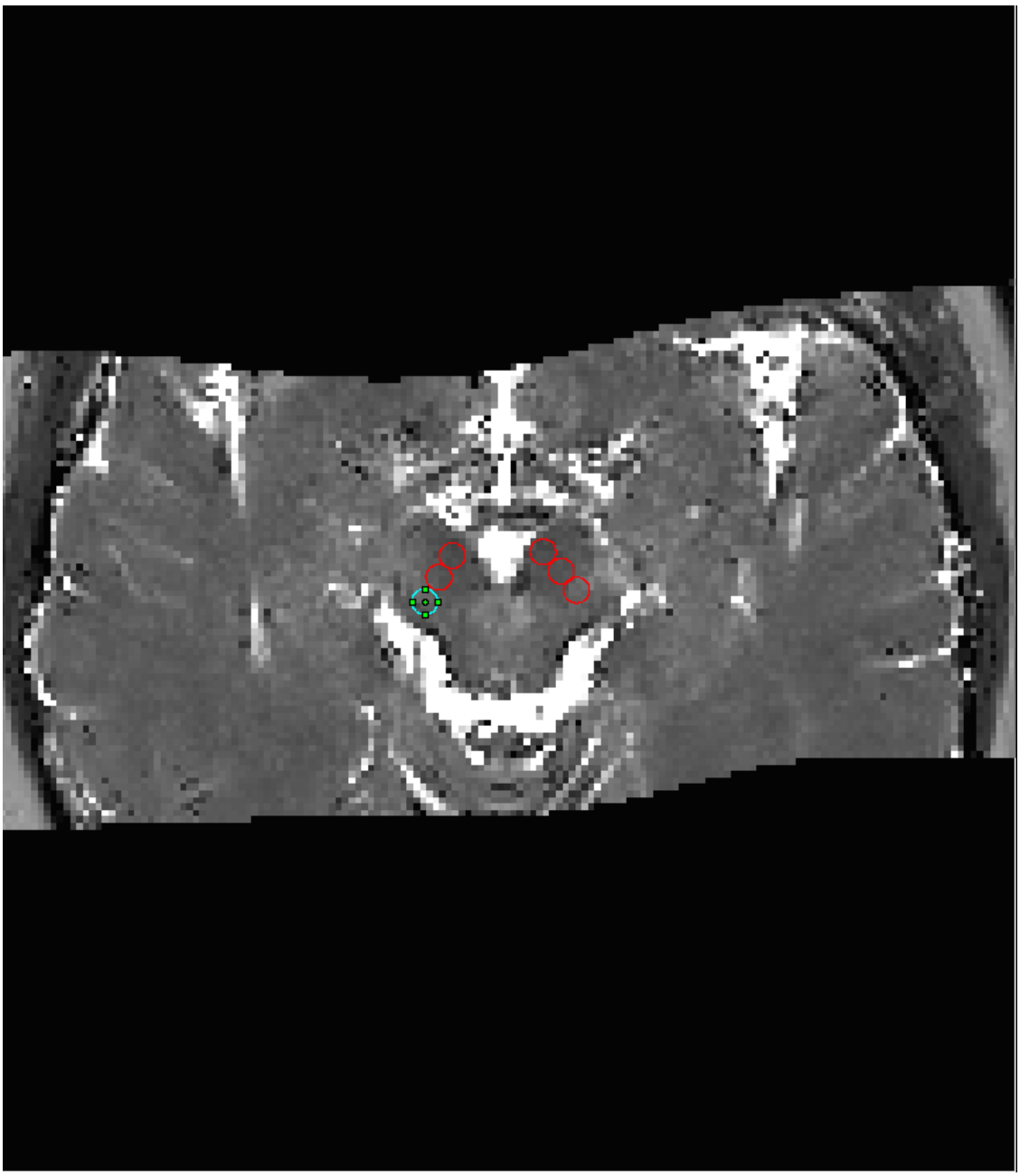

Figure 13: 31-TE T2 map with the SN ROI imported and placed. It was not clear why the margins of images were not linear for this limited field of view scans after the performing the registration process. However, it did not appear to have any effect on the areas of interest being relatively far from the margins.

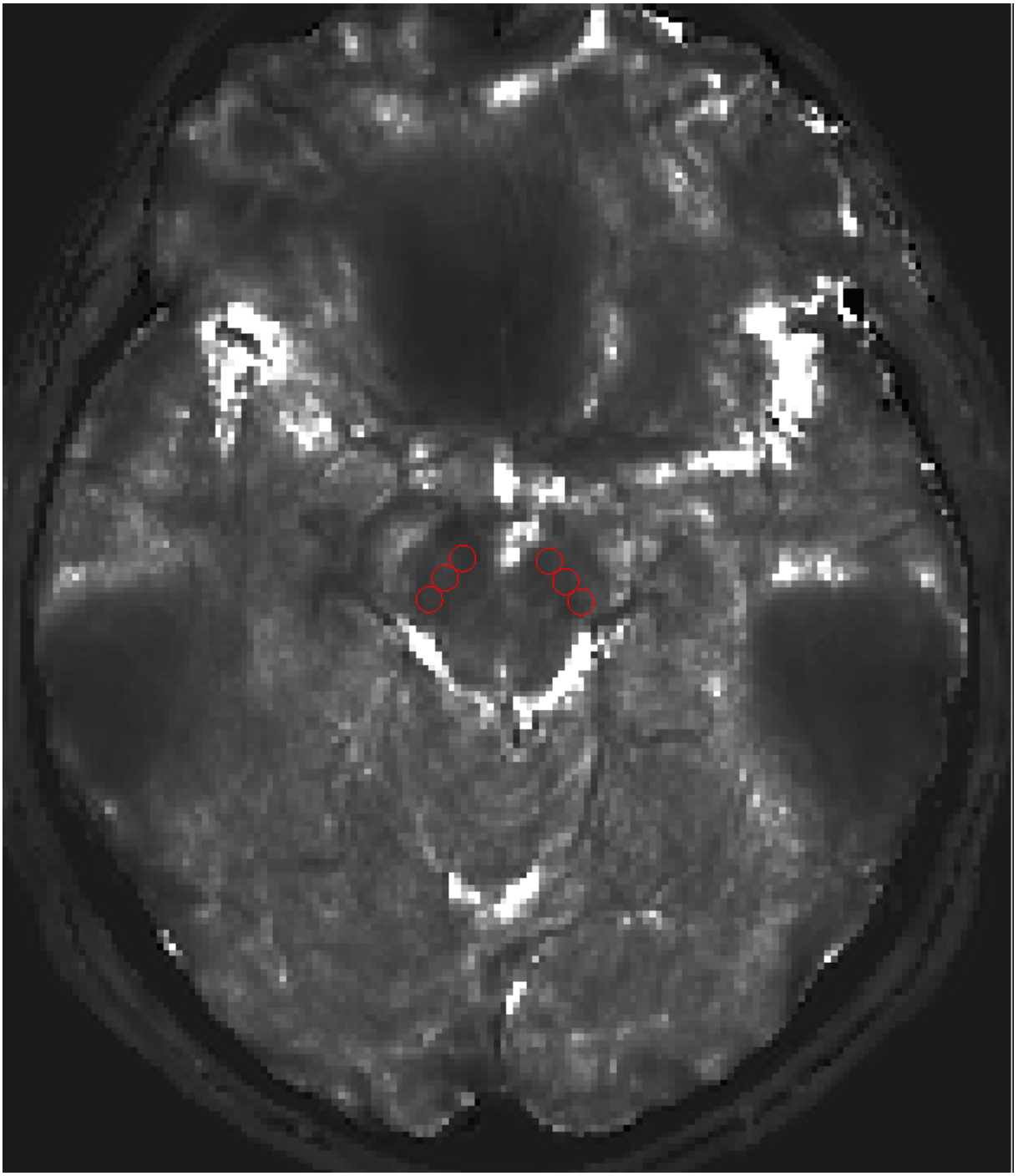

Figure 14: T2* map with the SN ROIs imported and placed.

4.5 Statistical Analysis

T2 values for each ROI (right ROI, left ROI and the mean of both sides) were recorded in a digital spreadsheet (Microsoft Word), and careful control was exercised at each step to ensure the quality of the images, maps and ROI locations.

The PD, PSP, MSA, and the control group demographics, were compared using ANOVA and Bonferroni-corrected post-hoc comparisons. The data was first examined for statistical normality using frequencies, comparing median and mean values to determine skewness, and then examining skewness values using SPSS. Regional qMRI values were compared among the three patient groups and against the control group using ANOVA, and when this was significant post-hoc comparisons were performed. After controlling for important confounders like disease duration, relationships between values and clinimetric scores and ages were examined using the Pearson correlation and regression analysis. A two-way analysis of co-variance (ANCOVA) was used to compare groups controlled for gender and age. Repeated-measures of ANOVA were used to examine longitudinal data. All statistical tests were performed using a two-tailed test and a 0.05 level of significance or 95% CIs. The Bonferroni correction for multiple comparisons was applied to the p-values. Statistical analyses were performed using the SPSS® software version 20.0 (SPSS Incorporated, Chicago, Illinois) for Macintosh computers.

CHAPTER FIVE—Quantitative 3T MRI in Parkinsonism—Results—T2* and T2 relaxation times of the subthalamic nucleus, the red nucleus and the substantia nigra in Parkinsonian patients and control subjects

5.1 Patient Characteristics

The total number of subjects recruited for the study was 59, in the cross-sectional study 20 control, 19 PSP, 10 PD and 10 MSA. Patient characteristics are summarized in Table 5. There were no significant differences in age ($p=0.08$) or gender ($p=0.28$) among the four groups.

Among the disease groups there were significant differences in the H&Y ($p<0.01$), UPDRSII ($p<0.01$), UPDRSIII ($p<0.01$) and FAB scores ($p<0.01$). There was no difference in the UPDRSI ($p=0.40$), and significance trends recorded for disease duration ($p=0.06$) and MMSE ($p=0.07$).

Post-hoc (Games-Howell) tests (Table 5) showed significant differences between the PD group and the other disease groups, for the H&Y, UPDRS II and UPDRS III scores ($p<0.01$). For the UPDRS III scores there was a similar difference noted between the PSP and MSA groups ($p<0.01$, 95% CI, 2.99 to 21.85 ms).

		N	Mean	SD	95% CI	
					Lower	Upper
Age (Years)	Control	20	66.05	5.7	63.38	68.72
	PD	10	66.63	5.9	62.33	70.92
	PSP	19	69.79	6.7	66.53	73.05
	MSA	10	63.41	8.1	57.55	69.26
Dis Duration (Years)	PD	10	7.28	4.1	4.35	10.22
	PSP	19	4.40	2.8	3.04	5.76
	MSA	10	4.93	2.1	3.40	6.46
H&Y	PD	10	2.20	0.7	1.64	2.76
	PSP	19	3.84	0.7	3.47	4.21
	MSA	10	4.10	0.7	3.57	4.63
UPDRSI	PD	10	2.60	1.6	1.42	3.78
	PSP	19	3.53	1.8	2.63	4.43
	MSA	10	3.40	1.7	2.17	4.63
UPDRSII	PD	10	10.20	4.6	6.85	13.55
	PSP	19	20.89	6.9	17.53	24.26
	MSA	10	26.70	6.1	22.35	31.05
UPDRSIII	PD	10	23.90	9.2	17.28	30.52
	PSP	19	39.58	9.7	34.89	44.27
	MSA	10	52.00	9.3	45.29	58.71
MMSE	PD	10	28.90	1.2	28.04	29.76
	PSP	19	27.47	2.2	26.39	28.56
	MSA	10	28.80	1.0	28.06	29.54
FAB	PD	10	17.00	0.9	16.33	17.67
	PSP	19	12.68	3.8	10.84	14.52
	MSA	10	16.00	1.7	14.78	17.22

Table 5: Subjects' characteristics

For the longitudinal phase of the study, data from 27 subjects was available (8 control, 8 PD, 6 PSP, 5 MSA). The follow-up interval or duration between scan 1 to scan 2 was mean (SD) 11.04 (2.06) months, ranging from 5.6 to 15.7 months, 95% CI from 9.66 to 12.42 months, p-value=0.33 between groups of subjects that underwent a second scan.

There were significant differences between the UPDRS (I, II and III) scores at scan 1 and scan 2 with $p<0.01$, but no differences with other clinimetric scores. Considering the clinimetric scores at scan 2, there were significant differences in UPDRS scores and H&Y scores (p-value <0.01) in and between each of the disease groups. Post-hoc analysis revealed significant differences in the UPDRS (I, II and III) scores between the PD and the MSA groups (mean difference -33.45, SE 4.99, p= 0.00, 95% CI -49.02 to -17.69 ms).

5.2 Quality Control (QC)

QC of TSE-T2

During scan one or the first scan, two cases were excluded from analysis for degrading motion artifacts (n =20 control, n=10 PD, n=18 PSP, n=10 MSA). During scan 2, two cases were ruled out for similar reasons (8 control, 8 PD, 6 PSP, 5 MSA)

QC of Normalization

Initially during scan 1, 8 cases were identified with mis-registration, and re-orientation of the slices using SPM, so that they ran parallel to the AC-PC plane, corrected the error. Thus all scan 1 images were registered and included. During scan 2, 4 cases were excluded from analysis because re-orientation failed to sufficiently improve the quality of normalization as per the assessment of an experienced neurophysicist, Dr Enrico De Vita.

QC of Maps

The T2* maps that were calculated with 4 even TE points, and the T2 maps that were calculated with 31 TE points, were of greater quality than those that were calculated with 2 TE points: less noise and less artifacting were assessed by two experienced examiners. Thus 4 even TE T2* and 31-TE T2 maps were used to draw ROIs and extract values. 2-TE T2 time results are reported below for the STN only, whereas these were not analyzed for the RN and SN. This was done to give the reader an idea of STN T2 values calculated using only 2 TE points.

5.3 STN

T2* Times

T2* relaxation times of the STN ROI were extracted from 53 maps for 53 subjects (18 control, 9 PD, 16 PSP, 10 MSA) (Figure and Table 6).

T2* times were the lowest in the PSP and the PD groups, with a mean of 22.30 ms (95% CI 19.53 to 25.07 ms) for the PSP group and 21.60 ms (95% CI 19.42 to 23.77 ms) in the PD group. The highest values were seen in the STNs of the control group, with a mean of 26.48 ms (95% CI 24.21 to 28.75 ms).

In the control group, there was a trend toward correlation between age and the T2* taken as the mean of left and right ROI values, with a correlation coefficient of -0.44 and a p=0.06, when controlled for disease duration.

When controlled for both age and disease duration and within the PD group, a correlation was seen between T2* and UPDRS I scores (correlation coefficient 0.76, p=0.04). Controlling both age and disease duration within the PD group, there was also a strong negative correlation with the MMSE score, and a correlation coefficient of -0.88 and p=0.01.

One-way ANOVA among the groups revealed significant differences with a p-value 0.01 for the right STN and the mean of both nuclei—though it was only 0.08 for the left STN. Table 6 shows results of Games-Howell post-hoc test for the differences among the groups. The difference between the control group and the diseased groups was most marked in the right STN as well as the mean of both nuclei, and least on the left side. Differences were marked between the PD and the control groups, with a mean difference (effect size) of 4.88 ms (SD 1.4 ms) (95% CI 0.92 to 8.8 ms) and p= .12 for the mean of both nuclei.

Univariate ANOVA of the mean of both nuclei's ROIs, revealed significant correlations with age (years) by diagnosis, yielding adjusted R squared=0.21 and p-value=0.03 (Table 7).

Between the mean STN and the patient's age, there was a correlation coefficient of -0.3 and p=0.03 (right 0.01, left 0.23). Between the mean and the disease duration, controlled for age, there was a similar but negative correlation coefficient (-0.3) and p=0.04. Regression analysis with the mean as the dependent variable, against age and disease durations, demonstrated trends toward these being predictors (p=0.06).

Among the clinimetric scales, MMSE had relatively the highest correlation coefficient with a mean of -0.23, as well as the lowest p-value of 0.09, when controlled for age and disease duration.

Values were extracted from 24 cases in the follow-up study (8 control, 6 PD, 5 PSP, 5 MSA). Repeated measures of ANOVA using the Bonferroni correction did not show any significant differences of pair-wise comparison. Mean differences between the values of the right ROI at scan 1 and scan 2 were -0.234 ms (SD 0.636 ms) and p=0.72, 95% CI (-1.56 to 1.08 ms). On the left the mean difference (SD) was 1.13 ms (1.44 ms), p=0.44, 95% CI (-1.86 to 4.135 ms).

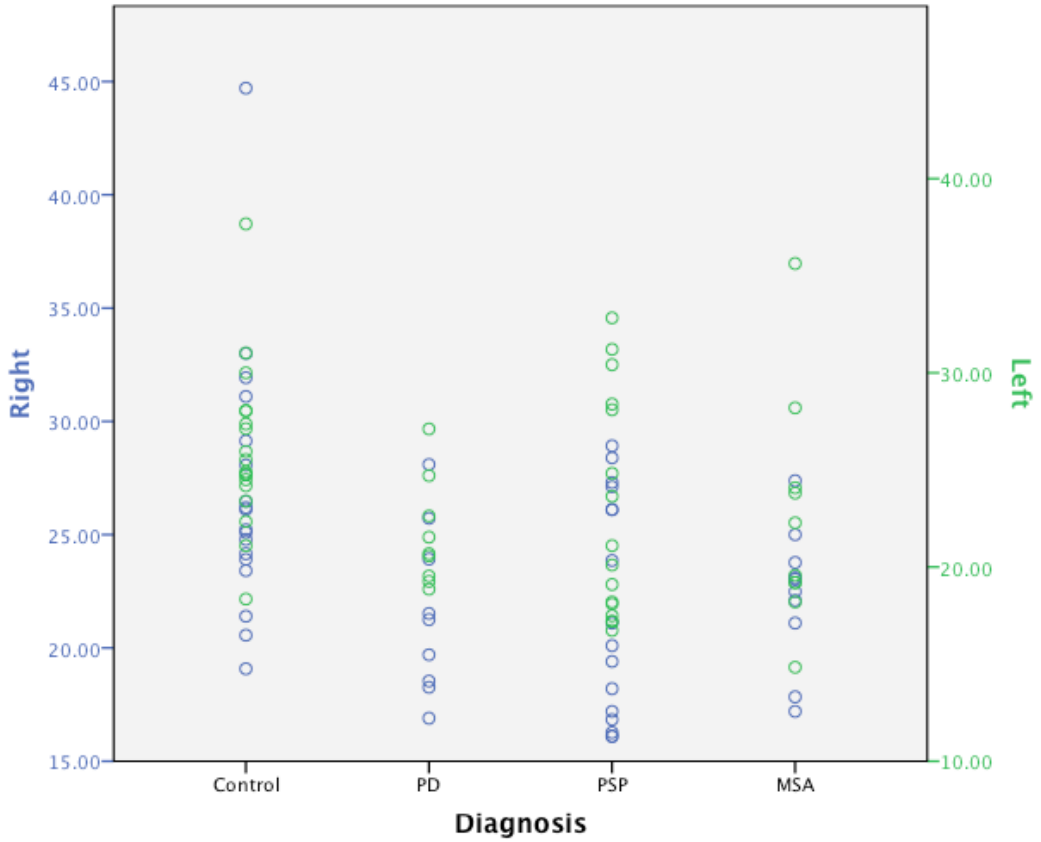

Figure 15: T2* times of the right and left STN ROIs (ms). The PD group had the lowest T2* times.

Diagnosis		Mean (ms)	95% Confidence Interval (ms)	
			Lower	Upper
Control	Right	26.90	24.01	29.80
	Left	26.05	23.96	28.15
	Mean	26.48	24.21	28.75
PD	Right	21.54	18.68	24.40
	Left	21.65	19.54	23.76
	Mean	21.60	19.42	23.77
PSP	Right	21.81	19.21	24.42
	Left	22.79	19.75	25.83
	Mean	22.30	19.53	25.07
MSA	Right	22.30	20.11	24.48
	Left	22.50	18.25	26.74
	Mean	22.40	20.08	24.72

Table 6: T2* relaxation times of the right, left and mean, of both STNs (ms)

Dependent Variable	(I) Diagnosis	(J) Diagnosis	Mean Difference (I-J)	Std. Error	Sig.	95% Confidence Interval	
						Lower Bound	Upper Bound
Right	Control	PD	5.36	1.84	**0.03**	0.24	10.47
		PSP	5.08	1.83	**0.04**	0.11	10.06
		MSA	4.60	1.67	0.05	0.00	9.20
	PD	Control	-5.36	1.84	**0.03**	-10.47	-0.24
		PSP	-0.27	1.74	0.99	-5.13	4.58
		MSA	-0.75	1.57	0.96	-5.26	3.75
	PSP	Control	-5.08	1.83	**0.04**	-10.06	-0.11
		PD	0.27	1.74	0.99	-4.58	5.13
		MSA	-.48	1.55	0.98	-4.77	3.81
	MSA	Control	-4.60	1.67	0.05	-9.20	-0.00
		PD	0.75	1.57	0.96	-3.75	5.26
		PSP	0.48	1.55	0.98	-3.81	4.77
Left	Control	PD	4.40	1.34	**0.01**	0.66	8.13
		PSP	3.26	1.73	0.26	-1.48	8.01
		MSA	3.55	2.12	0.37	-2.60	9.71
	PD	Control	-4.40	1.34	**0.01**	-8.13	-0.66
		PSP	-1.13	1.69	0.90	-5.82	3.55
		MSA	-0.84	2.08	0.97	-6.97	5.28
	PSP	Control	-3.26	1.73	0.26	-8.01	1.48
		PD	1.13	1.69	0.90	-3.55	5.82
		MSA	0.28	2.35	0.99	-6.34	6.92
	MSA	Control	-3.55	2.12	0.37	-9.71	2.60
		PD	0.84	2.08	0.97	-5.28	6.97
		PSP	-0.28	2.35	0.99	-6.92	6.34
Mean	Control	PD	4.88	1.43	**0.01**	0.92	8.83
		PSP	4.17	1.68	0.08	-0.40	8.76
		MSA	4.08	1.48	0.05	-0.016	8.18
	PD	Control	-4.88	1.43	**0.01**	-8.83	-0.92
		PSP	-0.70	1.60	0.97	-5.14	3.73
		MSA	-0.79	1.30	0.93	-4.76	3.16
	PSP	Control	-4.17	1.68	0.08	-8.76	0.40
		PD	0.70	1.60	0.97	-3.73	5.14
		MSA	-0.09	1.65	1.00	-4.65	4.46

MSA	Control	-4.08	1.48	0.05	-8.18	0.01
	PD	0.79	1.39	0.93	-3.16	4.76
	PSP	0.09	1.65	1.00	-4.46	4.65

Table 7: post hoc analysis for T2* times (ms) of the STN

2-TE-T2 Relaxation Times

T2 relaxation times of the STN ROI were extracted from 58 maps for 58 subjects (n=20 control, n=10 PD, n=18 PSP, n=10 MSA) (Table 8).

T2 times were the lowest in the PD and the PSP groups, with the mean of both sides at 67.6 ms (95% CI 63.41 to 71.78 ms) and 69.37 ms (95% CI 67.01 to 71.74 ms) respectively. The highest values were seen in the control group with a mean of 82.29 ms (95% CI 79.86 to 84.72 ms).

For the PSP group, there was a significant correlation between T2 and UPDRS III scores (correlation coefficient -0.50, p=0.03). Similarly, with UPDRS II (correlation coefficient -0.636, p=0.01) and UPDRS I (correlation coefficient -0.498, p=0.04). In the MSA group, there was significant correlation between FAB scores and the mean (correlation coefficient -0.661, p=0.037). These correlations faded and became non-significance when controlled for age and disease duration.

One-way ANOVA among the groups did not reveal significant differences for p-value >0.05 for the right, left or the mean of both STN ROIs.

Between the mean and the age there was a weak correlation coefficient of -0.24 and p-value of 0.04. Between the mean and the disease duration, there was a higher correlation coefficient (-0.618) and p-value 0.00. Regression analysis of the mean as a dependent variable, and age and disease duration as predictors, yielded $p<0.01$.

Among the clinimetric scores, UPDRS II had relatively the highest correlation coefficient with a mean of 0.29, as well as the lowest p-value of 0.04.

Values were extracted from 27 cases in the follow-up study (n=8 control, n=8 PD, n=6 PSP, n=5 MSA). Repeated measures via ANOVA using the Bonferroni correction did not show any significant differences for pair-wise comparison. The mean difference between the values of the right ROI at scan 1 and scan 2 were 0.61 ms (SE 1.18ms), p=0.61, 95% CI (-1.82 to 3.05 ms). On the left the mean difference was (SE) 1.312 (1.586) ms, p= 0.42, 95% CI (-1.948 to 4.571 ms).

Diagnosis		Mean (ms)	95% Confidence Interval (ms)	
			Lower	Upper
Ctrl	Right	82.67	80.05	85.29
	Left	81.90	78.27	85.54
	Mean	82.29	79.86	84.72
PD	Right	67.76	63.55	71.96
	Left	67.44	61.57	73.30
	Mean	67.60	63.41	71.78
PSP	Right	67.51	65.47	69.54
	Left	71.24	67.24	75.25
	Mean	69.37	67.00	71.74
MSA	Right	75.91	71.70	80.11
	Left	79.61	75.24	83.97
	Mean	77.76	74.97	80.54

Table 8: 2-TE-T2 relaxation times of the right, left and both STN

31-TE T2 Relaxation Times

T2 relaxation times of the STN ROI were extracted from 56 maps for 53 subjects (n=19 control, n=10 PD, n=17 PSP, n=10 MSA).

T2 times were the lowest in the PSP group, with a mean of 38.67 ms (95% CI 37.02 to 40.32 ms). The highest values were seen in the ROIs of the control and MSA groups with means of 47.03 ms, 95% CI 45.61 to 48.46 ms, and 46.36 ms, 95% CI 44.09 to 48.63 ms, respectively (Figure and Table 9).

For the MSA group, there was a significant correlation between the T2 and MMSE scores (correlation coefficient -0.771, p=0.01), when controlled for age and disease duration. This correlation became weaker when controlled for age and disease duration (correlation coefficient -0.71, p=0.05). With the PD group, it was the weakest (correlation coefficient 0.46, p=0.18). Otherwise, no significant correlations between clinimetric scores and T2 were demonstrated.

With the control group, correlations were noticed between age and T2 times averaged across both sides, with correlation coefficients equal to - 0.588 and p=0.01. No such correlations could be seen in the PD group (correlation coefficient -0.079) and the PSP group (correlation coefficient -0.097). Such correlations became stronger with the control group, when controlled for gender (correlation coefficient 0.635, p=0.01). These tended to be remain weak with the disease groups when controlled for gender, with a correlation coefficient of 0.006 for the PD group and 0.22 for the PSP group.

When controlling for age and disease duration within the PD group, strong correlations were noticed between T2 and UPDRS I scores (correlation coefficient 0.76, p-value=0.04). One-way ANOVA, among the groups, revealed significant differences, with a p-value<0.01 for the right, left and the mean of both STN ROIs.

Table 10 shows results of the Games-Howell post-hoc tests and the differences among the groups. The difference between the control group and the PSP group was most marked on the left nucleus, as well as on the mean of both nuclei, and less marked on the right side. The differences between the control group and the PD group had a large effect size of 2.91 ms, though this finding did not demonstrate statistical significance (p-value=0.128).

On regression analysis—between the mean of the T2 times against disease duration—there was an adjusted R-squared of -0.307 and a p-value of 0.011. Between the mean of T2 times and the age, there was no significant correlation. Regression analysis using the mean as a dependent variable, and using age and disease duration as predictors, yielded a p-value of 0.06. Regression analysis of the mean as dependent variable, and using disease duration alone as a predictor, yielded and adjusted R-squared of -0.31 (p=0.02).

T2 relaxation times of the STN were extracted from 21 cases in the follow-up study (n=8 control, n=7 PD, n=2 PSP, n=4 MSA). Repeated measures of the ANOVA using the Bonferroni correction did not show any significant difference for pair-wise comparison. Mean differences between the values of the right ROI at scan 1 and scan 2 were negligible: -0.048 ms (SD 0.454 ms), p-value=0.91, 95% CI (-0.995 to 0.899 ms). On the left, the difference was larger: mean difference (SD) -1.194 (0.899) ms, p-value=0.214, 95% CI (-3.03 to 0.72 ms).

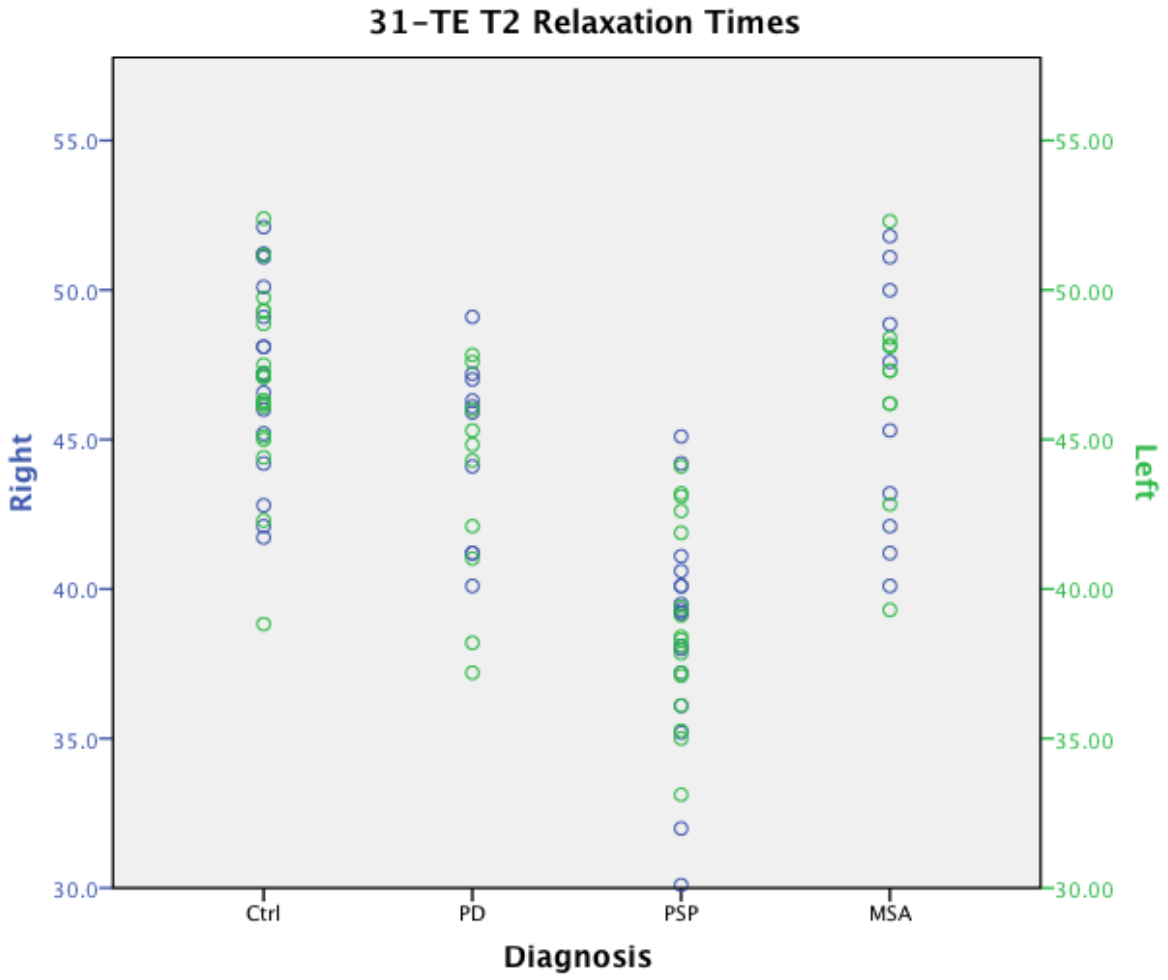

Figure 16: 31-TE T2 times of the right and left STN ROIs (ms). The PSP group had the lowest times.

Diagnosis				
		Mean (ms)	95% Confidence Interval (ms)	
			Lower	Upper
Ctrl	Right	47.22	45.71	48.73
	Left	46.85	45.35	48.34
	Mean	47.03	45.61	48.46
PD	Right	44.82	42.65	46.9
	Left	43.43	40.79	46.08
	Mean	44.12	41.77	46.48
PSP	Right	38.53	36.60	40.47
	Left	38.81	37.16	40.46
	Mean	38.67	37.02	40.32
MSA	Right	46.12	43.03	49.21
	Left	46.60	44.11	49.10
	Mean	46.36	44.09	48.63

Table 9: 31-TE T2 relaxation times (ms) for the right, left and mean STN

Dependent Variable	(I) Diagnosis	(J) Diagnosis	Mean Difference (I-J)	Std. Error	Sig.	95% Confidence Interval	
						Lower Bound	Upper Bound
Right	Ctrl	PD	2.40	1.19	0.22	-0.96	5.77
		PSP	8.69	1.16	**0.00**	5.54	11.84
		MSA	1.10	1.54	0.89	-3.37	5.57
	PD	Ctrl	-2.40	1.19	0.22	-5.77	0.96
		PSP	6.28	1.32	**0.00**	2.61	9.95
		MSA	-1.30	1.66	0.86	-6.07	3.46
	PSP	Ctrl	-8.69	1.16	**0.00**	-11.84	-5.54
		PD	-6.21	1.32	**0.00**	-9.95	-2.61
		MSA	-7.59	1.64	**0.00**	-12.25	-2.92
	MSA	Ctrl	-1.10	1.54	0.89	-5.57	3.37
		PD	1.30	1.66	0.86	-3.46	6.07
		PSP	7.59	1.64	**0.00**	2.92	12.25
Left	Ctrl	PD	3.41	1.36	0.10	-0.50	7.34
		PSP	8.03	1.05	**0.00**	5.18	10.88
		MSA	0.24	1.31	0.99	-3.49	3.98
	PD	Ctrl	-3.41	1.36	0.10	-7.34	0.50
		PSP	4.62	1.40	**0.02**	0.62	8.61
		MSA	-3.17	1.60	0.23	-7.71	1.37
	PSP	Ctrl	-8.03	1.05	**0.00**	-10.88	-5.18
		PD	-4.62	1.40	**0.02**	-8.61	-0.62
		MSA	-7.79	1.34	**0.00**	-11.61	-3.97
	MSA	Ctrl	-0.24	1.31	0.99	-3.98	3.44
		PD	3.17	1.60	0.23	-1.37	7.71
		PSP	7.79	1.34	**0.00**	3.97	11.61
Mean	Ctrl	PD	2.91	1.24	0.12	-0.62	6.44
		PSP	8.36	1.03	**0.00**	5.57	11.15
		MSA	0.67	1.21	0.94	-2.76	4.10
	PD	Ctrl	-2.91	1.24	0.12	-6.44	0.62
		PSP	5.45	1.29	**0.00**	1.79	9.11
		MSA	-2.23	1.44	0.43	-6.32	1.84
	PSP	Ctrl	-8.36	1.03	**0.00**	-11.15	-5.57
		PD	-5.45	1.29	**0.00**	-9.11	-1.79
		MSA	-7.69	1.26	**0.00**	-11.25	-4.12
	MSA	Ctrl	-0.62	1.21	0.94	-4.10	2.76
		PD	2.23	1.44	0.43	-1.84	6.32
		PSP	7.69	1.26	**0.00**	4.12	11.25

Table 10: post-hoc results for 31-TE STN T2 group differences (T2 values are in ms)

5.4 The Red Nucleus (RN)

T2* Relaxation Times

T2* relaxation times of the RN ROI were extracted from 53 maps for 53 subjects (n=18 control, n=9 PD, n=16 PSP, n=10 MSA).

Red nucleus T2* values were the lowest in the PD group, with a mean of 24.77 ms (95% CI 22.7 to 26.85 ms), and the highest in the controlled group with a mean of 30.69 ms (95% CI 28.29 to 33.09 ms) (Table 11 and Figure).

With the PD group, there was a significant correlation between the T2* and UPDRS III scores (correlation coefficient 0.773, p-value=0.015), when controlled for age and disease duration as confounding factors. Similarly, a significant correlation was seen in the same group with H&Y scores (correlation coefficient 0.704, p-value=0.034).

With the PD group, a correlation was observed between the age and the mean T2* with a correlation coefficient of -0.717 and p-value of 0.03. This significant correlation remained when controlling for disease duration (correlation coefficient -0.731, p=0.04).

One-way ANOVA analysis of the groups revealed significant differences for p-values for the right RN (0.002), for the left RN (0.016), and for the mean (L-R) T2 (0.004).

Table 12 shows results of Games-Howell post-hoc testing for inter-group differences. The differences between the control group and the disease groups was most marked for the right nucleus and the mean (L-R), and least marked for the left side. This differences were most marked between the PD group and the control group, with a mean difference (effect size) of 5.91 ms (SD 1.44 ms), 95% CI -1.92 to - 9.9 ms, and p=0.01 for mean (L-R).

Univariate ANOVA of the mean (L-R) revealed a significant correlation between genders, adjusting for diagnosis with an adjusted R-square of 0.253 and p-value=0.03.

Mean T2* and disease duration correlated significantly (correlation coefficient of -0.397, p-value of 0.03), when controlled for age. Regression with mean T2* as a dependent variable, using age and disease duration as predictors, trended toward significance (p=0.06). Among the clinimetric scales, UPDRS III correlated strongly with the mean of T2*, with a correlation coefficient of 0.28 and the lowest p-value of 0.103.

T2* time values were extracted from 24 cases in the follow-up study (n=8 control, n=6 PD, n=5 PSP, n=5 MSA). Repeated measures for ANOVA using the Bonferroni correction did not show any significant difference for pair-wise comparison. Mean differences between the values of the right ROI at scan 1 and scan 2 were: 0.106 ms (SD 0.361 ms), p=0.77, 95% CI (-0.642 to 0.853 ms); on the left the mean difference was (SD) 1.321 (0.844) ms, p=0.13, 95% CI (-0.425 to 3.067 ms).

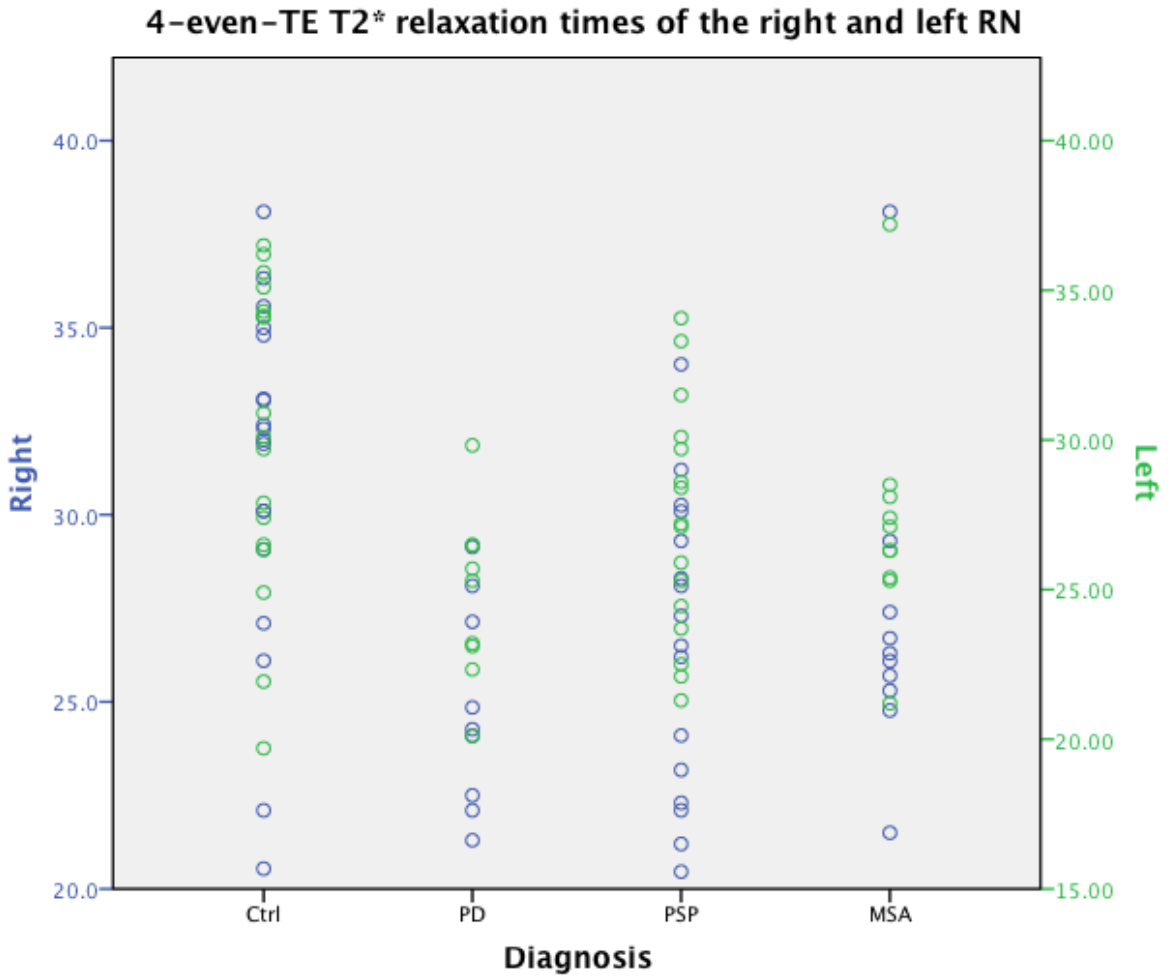

Figure 17: T2* relaxation times of the right and left RN ROI (ms). The PD and PSP groups had the lowest times.

Diagnosis		value (ms)	95% Confidence Interval (ms)	
			Lower	Upper
Ctrl	Right	31.09	28.75	33.43
	Left	30.30	27.76	32.83
	Mean	30.69	28.29	33.09
PD	Right	24.83	22.71	26.95
	Left	24.72	22.52	26.92
	Mean	24.77	22.70	26.85
PSP	Right	26.53	24.41	28.66
	Left	27.20	25.11	29.28
	Mean	26.86	24.89	28.84
MSA	Right	27.11	24.00	30.22
	Left	27.28	24.38	30.17
	Mean	27.19	24.39	30.00

Table 11: T2* relaxation times of the RN (ms)

Dependent Variable	(I) Diagnosis	(J) Diagnosis	Mean Difference (I-J)	Std. Error	Sig.	95% Confidence Interval	
						Lower Bound	Upper Bound
Right	Ctrl	PD	6.25	1.44	**0.00**	2.28	10.23
		PSP	4.55	1.49	**0.02**	0.51	8.59
		MSA	3.97	1.76	0.14	-.96	8.91
	PD	Ctrl	-6.25	1.44	**0.00**	-10.23	-2.28
		PSP	-1.70	1.35	0.59	-5.47	2.06
		MSA	-2.28	1.65	0.52	-7.03	2.46
	PSP	Ctrl	-4.55	1.49	**0.02**	-8.59	-0.51
		PD	1.70	1.35	0.59	-2.06	5.47
		MSA	-0.57	1.69	0.98	-5.37	4.21
	MSA	Ctrl	-3.97	1.76	0.14	-8.91	0.96
		PD	2.28	1.65	0.52	-2.46	7.03
		PSP	0.57	1.69	0.98	-4.21	5.37
Left	Ctrl	PD	5.57	1.53	**0.00**	1.35	9.79
		PSP	3.09	1.54	0.20	-1.09	7.29
		MSA	3.02	1.75	0.33	-1.83	7.87
	PD	Ctrl	-5.57	1.53	**0.00**	-9.79	-1.35
		PSP	-2.47	1.36	0.29	-6.27	1.32
		MSA	-2.55	1.59	0.40	-7.11	2.00
	PSP	Ctrl	-3.09	1.54	0.20	-7.29	1.09
		PD	2.47	1.36	0.29	-1.32	6.27
		MSA	-0.078	1.60	0.00	-4.60	4.44
	MSA	Ctrl	-3.02	1.75	0.33	-7.87	1.83
		PD	2.55	1.59	0.40	-2.00	7.11
		PSP	0.078	1.60	1.0	-4.44	4.60
Mean	Ctrl	PD	5.91	1.44	**0.00**	1.92	9.91
		PSP	3.82	1.46	0.06	-0.15	7.80
		MSA	3.49	1.68	0.19	-1.16	8.16
	PD	Ctrl	-5.91	1.44	**0.00**	-9.91	-1.92
		PSP	-2.09	1.29	0.39	-5.68	1.50
		MSA	-2.41	1.53	0.41	-6.80	1.96
	PSP	Ctrl	-3.82	1.46	0.06	-7.80	0.15
		PD	2.09	1.29	0.39	-1.50	5.68
		MSA	-0.32	1.54	0.99	-4.69	4.03
	MSA	Ctrl	-3.49	1.68	0.19	-8.16	1.16
		PD	2.41	1.53	0.41	-1.96	6.80

Table 12: Games-Howell post-hoc group-differences, testing for RN T2* (ms)

T2 Relaxation Times

T2 times were the lowest for the PD group, with a mean of 42.86 ms (95% CI 39.92 to 45.81 ms) and with the controlled group with a mean of 54.64 ms (95% CI 51.92 to 57.35 ms) (Table 12). With the PD group, there was a significant correlation between T2 and UPDRS III scores (correlation coefficient -0.707, p-value=0.02) when controlled for age and disease duration. Furthermore, there was a significant correlation with age (correlation coefficient -0.742, p-value=0.014) (Figure and Table 13).

With the MSA group, there was a significant correlation between the mean T2 and the MMSE scores (-0.636, p-value=0.048), when controlled for age. Similarly, there was strong correlation for disease duration when controlled for both age and gender (correlation coefficient -0.705, p=0.05).

One-way ANOVA among the groups revealed significant differences with a p-value <0.01 for the right, left and the mean of both RN ROIs.

Table 14 shows results of Games-Howell post-hoc testing for inter-group differences. The differences between the PD group and the other groups were significant. The differences between the controlled group and the PD group revealed a large and statistically significant effect size (11.72 ms, p<0.01, 95% CI, 6.344 to 17.01 ms).

Through regression analysis, and between the mean T2 and the disease duration, a correlation coefficient of -0.319 was seen (p=0.02), with no significant correlations between mean T2 and age. Regression analysis with mean T2 as a dependent variable, and using age and disease duration as predictors, yielded a p-value of 0.038. Regression with the mean T2 as the dependent variable, and using disease duration alone as a predictor, yielded an adjusted R-squared of -0.294 and p-value of 0.03.

Values were extracted from 21 cases during the follow-up study (n=8 control, n=7 PD, n=2 PSP, n=4 MSA). Repeated measures for ANOVA using the Bonferroni correction did not show any significant difference for pair-wise comparisons. The mean difference between the values of the left ROI at scan 1 and scan 2 were negligible: 0.626 ms (SD 1.282 ms), p=0.631, 95% CI (-2.048 to 3.300 ms). On the right, the difference was less: mean difference (SD) -0.212 (0.584) ms, p= 0.72, 95% CI (-1.429 to 1.006 ms).

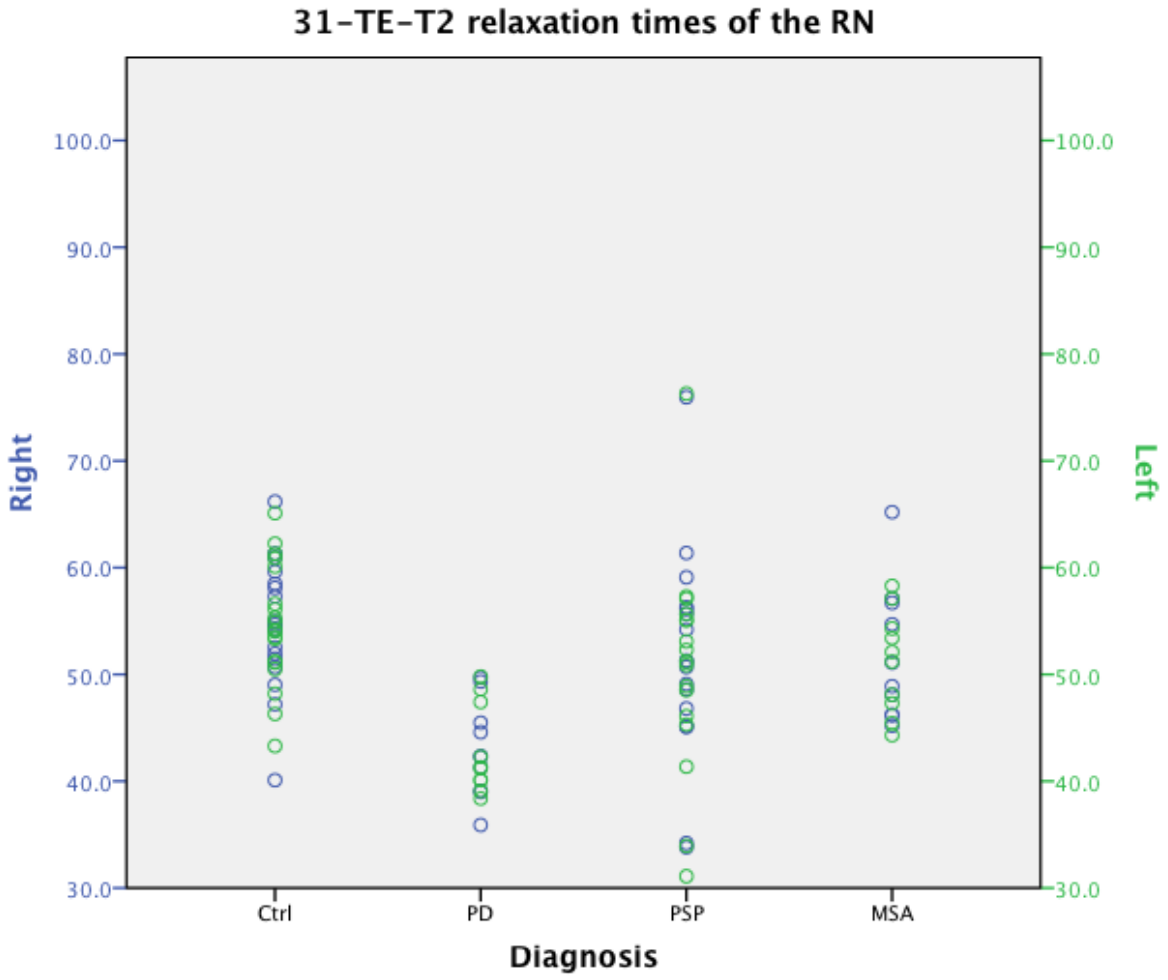

Figure 18: T2 relaxation times of the RN (ms). The PD group had the lowest T2 times.

		N	Mean	Std. Deviation	95% Confidence Interval for Mean		Minimum	Maximum
					Lower Bound	Upper Bound		
Right	Ctrl	19	54.62	5.83	51.81	57.44	40.1	66.2
	PD	10	42.90	4.46	39.71	46.09	35.9	49.7
	PSP	17	51.44	9.85	46.38	56.51	33.8	76.0
	MSA	10	51.94	6.40	47.36	56.51	45.2	65.2
Left	Ctrl	19	54.64	5.63	51.92	57.36	43.3	65.1
	PD	10	42.82	4.17	39.84	45.81	38.4	49.8
	PSP	17	50.54	10.06	45.36	55.71	31.1	76.3
	MSA	10	51.15	4.78	47.73	54.57	44.3	58.3
Mean	Ctrl	19	54.63	5.64	51.91	57.35	41.7	65.6
	PD	10	42.86	4.12	39.91	45.81	37.1	49.6
	PSP	17	50.99	9.78	45.96	56.02	32.5	76.1
	MSA	10	51.54	5.39	47.69	55.40	45.3	61.2

Table 13: 31-TE T2 relaxation times of the RN (ms), one-way ANOVA

Dependent Variable	(I) Diagnosis	(J) Diagnosis	Mean Difference (I-J)	Std. Error	Sig.	95% Confidence Interval	
						Lower Bound	Upper Bound
Right	**Ctrl**	**PD**	11.72	1.94	**0.00**	6.34	17.10
		PSP	3.17	2.73	0.65	-4.34	10.70
		MSA	2.68	2.42	0.69	-4.21	9.58
	PD	**Ctrl**	-11.72	1.94	**0.00**	-17.10	-6.34
		PSP	-8.54	2.77	**0.02**	-16.20	-0.88
		MSA	-9.03	2.46	**0.01**	-16.09	-1.98
	PSP	**Ctrl**	-3.17	2.73	0.65	-10.70	4.34
		PD	8.54	2.77	**0.02**	0.88	16.20
		MSA	-0.49	3.13	0.99	-9.11	8.13
	MSA	**Ctrl**	-2.68	2.42	0.69	-9.58	4.21
		PD	9.03	2.46	**0.01**	1.98	16.09
		PSP	0.49	3.13	0.99	-8.13	9.11
Left	**Ctrl**	**PD**	11.81	1.84	**0.00**	6.71	16.92
		PSP	4.10	2.7	0.46	-3.50	11.71
		MSA	3.48	1.99	0.32	-2.0	9.03
	PD	**Ctrl**	-11.81	1.84	**0.00**	-16.92	-6.71
		PSP	-7.71	2.77	0.04	-15.39	-0.03
		MSA	-8.32	2.0	**0.00**	-14.01	-2.63
	PSP	**Ctrl**	-4.10	2.76	0.46	-11.71	3.50
		PD	7.71	2.77	**0.04**	0.03	15.39
		MSA	-0.61	2.87	0.99	-8.53	7.30
	MSA	**Ctrl**	-3.48	1.99	0.32	-9.03	2.05
		PD	8.32	2.00	**0.00**	2.63	14.01
		PSP	0.61	2.87	0.99	-7.30	8.53
Mean	**Ctrl**	**PD**	11.76	1.83	**0.00**	6.70	16.83
		PSP	3.64	2.70	0.54	-3.79	11.07
		MSA	3.08	2.14	0.48	-2.92	9.10
	PD	**Ctrl**	-11.76	1.83	**0.00**	-16.83	-6.70
		PSP	-8.12	2.70	**0.03**	-15.61	-0.64
		MSA	-8.68	2.14	**0.00**	-14.78	-2.57
	PSP	**Ctrl**	-3.64	2.70	0.54	-11.07	3.79
		PD	8.12	2.70	**0.03**	0.64	15.61
		MSA	-0.55	2.92	0.99	-8.59	7.48
	MSA	**Ctrl**	-3.08	2.14	0.48	-9.10	2.92
		PD	8.68	2.14	**0.00**	2.57	14.78
		PSP	0.55	2.92	0.99	-7.48	8.59

Table 14: 31-TE T2 relaxation times of the RN (ms), post-hoc analysis

5.5 The Substantia Nigra

T2* Times

T2* times were the lowest for the PD group and the PSP group, with a mean of 30.47 ms (95% CI 26.04 to 34.9 ms) and 31.56 (95% CI 29.13 to 33.99) respectively, and the highest was with the controlled group with a mean of 36.87 ms (95% CI 34.58 to 39.15 ms). See Table 15.

With the control and PD groups, there was a noted tendency for values to increase between anterior and posterior ROIs. With the PSP and MSA groups, the opposite was seen and higher values were more frequently found anteriorly. There were no significant left-right difference between the two sides (p-value>0.05).

With the PD group, there was a correlation between T2* and H&Y scores (correlation coefficient -0.59, p-value=0.09) which weakened when controlled for age and disease duration (correlation coefficient -0.447, p-value=0.31). With the MSA group, there was a significant relationship between T2* and FAB scores (correlation coefficient -0.806, p-value=0.005) which strengthened when controlled for age and disease duration (correlation coefficient 0.943, p-value<0.01). No significant correlations were demonstrated between clinimetric scores and T2*; no correlations were demonstrated between T2* and age at scan, nor disease duration, with and without control for age and gender.

One-way ANOVA among the groups revealed significant group-mean SN T2* differences among the four groups (p=0.002). The highest differences were marked anteriorly on both sides with p-values<0.01, and least posteriorly with p=0.02 (Table 16).

Table 15 shows results for Games-Howell post-hoc testing for inter-group differences. The differences between the means of both sides were most marked between the control group and the PSP group (p-value=0.01, 95% CI 1.05 to 9.57 ms), with a similar difference between the control group and the PD group (p=0.05, 95% CI -0.057 to 12.85 ms). The mean values for the PD group and the PSP group were comparable (p= 0.961, 95% CI -7.59 to 5.42 ms).

The inter-group differences were more marked anteriorly and tended to decrease in the posterior ROIs. For instance, between the controlled group and the PD group the T2* difference was 9.61 ms (SE 1.62 ms, p <0.01, 95% CI 5.12 to 14.12 ms) in the right anterior ROIs and 4.42 ms (SE 3.76 ms, p-value 0.653, 95% CI -6.92 to 15.76 ms) in the right posterior ROI.

Between the all-ROI-mean T2* and the age correlation there were not any significant correlations (correlation coefficient -0.136, p-value=0.17), while correlations with disease duration were significant though yet weak (correlation coefficient -0.244 and p-value=0.039).

Among the clinimetric scales, UPDRS III had the highest correlation coefficient for regression against mean T2* was 0.337 (p=0.05), while for the H&Y the coefficient was 0.187 (p=0.28). When controlled for age and disease duration as confounding factors, no correlation was found.

Values were extracted from 24 cases in the follow-up study (n=8 control, n=6 PD, n=5 PSP, n=5 MSA). General Linear Model—repeated measures ANOVA—analysis yielded a p-value of 0.007. Post-hoc analysis (Games-Howell) showed significant differences between the T2* means of the PD group at scan 1 and scan 2, with a mean difference of 6.64 ms, SE 1.81 ms, p=0.02, 95% CI 1.22 to 12.07 ms).

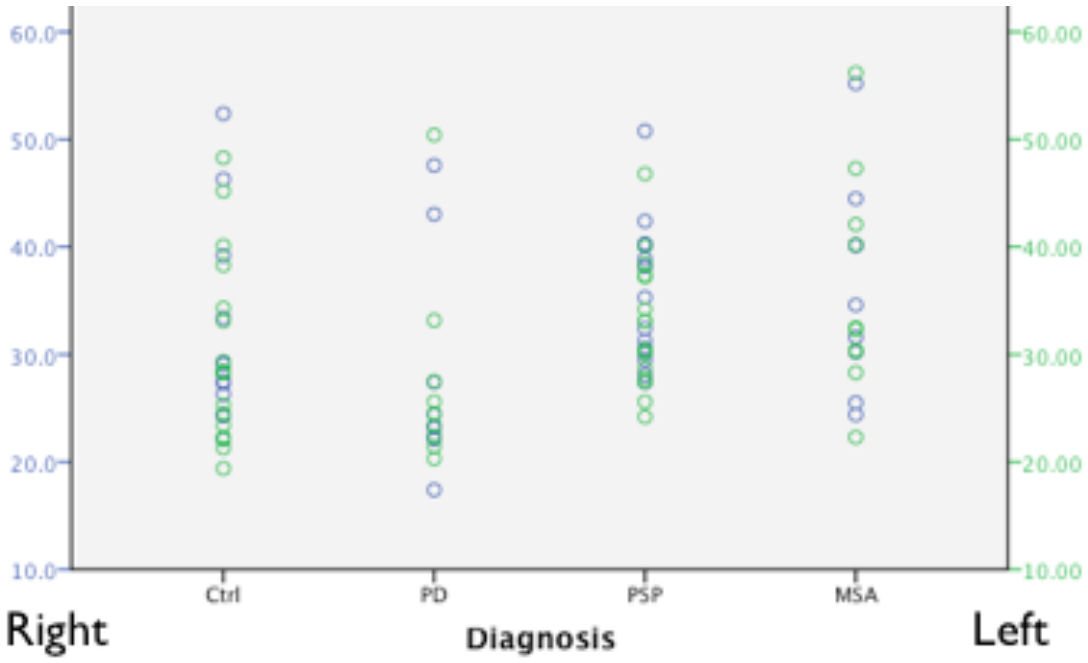

Figure 19 T2* relaxation times of the SN(ms). The PD group had the lowest times.

		N	Mean	Std. Deviation	95% Confidence Interval for Mean		Minimum	Maximum
					Lower Bound	Upper Bound		
RASN	Ctrl	18	35.15	4.74	32.79	37.51	28.10	44.30
	PD	9	25.53	3.50	22.84	28.23	20.10	30.10
	PSP	16	30.93	6.13	27.66	34.19	20.30	40.40
	MSA	10	39.39	7.95	33.69	45.08	23.40	48.40
RMSN	Ctrl	18	36.58	5.83	33.68	39.49	26.3	48.2
	PD	9	30.60	7.07	25.16	36.04	22.4	47.6
	PSP	16	29.83	5.43	26.93	32.72	19.5	38.4
	MSA	10	36.04	5.94	31.78	40.29	27.3	46.3
RPSN	Ctrl	18	38.99	6.149	35.93	42.05	23.5	47.5
	PD	9	34.57	10.41	26.56	42.57	28.2	58.1
	PSP	16	30.44	8.03	26.16	34.72	20.1	50.9
	MSA	10	34.73	6.34	30.19	39.26	22.2	43.3
LASN	Ctrl	18	35.36	7.19	31.78	38.94	22.3	47.5
	PD	9	25.52	2.82	23.35	27.70	21.2	28.4
	PSP	16	34.09	5.58	31.11	37.07	25.1	44.3
	MSA	10	38.67	5.80	34.52	42.8	24.6	45.4
LMSN	Ctrl	18	36.13	6.85	32.73	39.54	26.40	52.30
	PD	9	31.70	7.66	25.81	37.60	24.20	50.36
	PSP	16	31.71	3.83	29.67	33.76	20.10	36.50
	MSA	10	36.16	6.43	31.55	40.76	21.20	44.70
LPSN	Ctrl	18	38.99	4.83	36.58	41.39	29.40	45.30
	PD	9	34.89	10.56	26.77	43.01	26.30	57.25
	PSP	16	32.33	7.40	28.39	36.28	18.20	51.30
	MSA	10	31.93	5.03	28.32	35.53	22.60	42.90
Mean	Ctrl	18	36.87	4.58	34.58	39.15	27.76	45.68
	PD	9	30.47	5.76	26.04	34.90	26.03	43.91
	PSP	16	31.56	4.56	29.12	33.99	20.88	39.45
	MSA	10	36.15	5.36	32.31	39.99	23.55	41.11

Table 15: T2* relaxation times of the SN (ms), one-way ANOVA analysis

Dependent Variable	(I) Diagnosis	(J) Diagnosis	Mean Difference (I-J)	Std. Error	Sig.	95% Confidence Interval	
						Lower Bound	Upper Bound
RASN	Ctrl	PD	9.61	1.61	**0.00**	5.10	14.12
		PSP	4.22	1.89	0.14	-0.95	9.40
		MSA	-4.23	2.75	0.44	-12.34	3.87
	PD	Ctrl	-9.61	1.61	**0.00**	-14.12	-5.10
		PSP	-5.39	1.92	**0.04**	-10.72	-0.05
		MSA	-13.85	2.77	**0.00**	-22.02	-5.67
	PSP	Ctrl	-4.22	1.89	0.14	-9.40	0.95
		PD	5.39	1.92	**0.04**	0.05	10.72
		MSA	-8.45	2.94	0.05	-16.90	0.00
	MSA	Ctrl	4.23	2.75	0.44	-3.87	12.34
		PD	13.85	2.77	**0.00**	5.67	22.02
		PSP	8.45	2.94	0.05	0.008	16.90
RMSN	Ctrl	PD	5.98	2.73	0.17	-1.97	13.95
		PSP	6.75	1.93	**0.00**	1.51	11.99
		MSA	0.54	2.33	0.99	-6.02	7.12
	PD	Ctrl	-5.98	2.73	0.17	-13.95	1.97
		PSP	0.77	2.72	0.99	-7.18	8.72
		MSA	-5.43	3.01	0.30	-14.08	3.20
	PSP	Ctrl	-6.75*	1.93	**0.00**	-11.99	-1.51
		PD	-0.77	2.72	0.99	-8.72	7.12
		MSA	-6.20	2.31	0.06	-12.76	0.35
	MSA	Ctrl	-0.54	2.33	0.99	-7.12	6.02
		PD	5.43	3.01	0.30	-3.20	14.08
		PSP	6.20	2.31	0.06	-0.35	12.76
RPSN	Ctrl	PD	4.42	3.76	0.65	-6.92	15.76
		PSP	8.54	2.47	**0.00**	1.78	15.31
		MSA	4.26	2.47	0.34	-2.71	11.24
	PD	Ctrl	-4.42	3.76	0.65	-15.76	6.92
		PSP	4.12	4.01	0.73	-7.59	15.84
		MSA	-0.16	4.00	1.00	-11.93	11.61
	PSP	Ctrl	-8.54	2.47	**0.00**	-15.31	-1.78
		PD	-4.12	4.01	0.73	-15.84	7.59
		MSA	-4.28	2.83	0.44	-12.14	3.58
	MSA	Ctrl	-4.26	2.47	0.34	-11.24	2.71
		PD	0.16	4.00	1.00	-11.61	11.93
		PSP	4.28	2.83	0.44	-3.58	12.14
LASN	Ctrl	PD	9.83	1.94	**0.00**	4.48	15.18
		PSP	1.26	2.19	0.93	-4.69	7.22
		MSA	-3.30	2.49	0.55	-10.24	3.62
	PD	Ctrl	-9.83	1.94	**0.00**	-15.18	-4.48
		PSP	-8.56	1.68	**0.00**	-13.23	-3.90
		MSA	-13.14	2.06	**0.00**	-19.17	-7.11
	PSP	Ctrl	-1.26	2.19	0.93	-7.22	4.69
		PD	8.56	1.68	**0.00**	3.90	13.23
		MSA	-4.57	2.30	0.22	-11.06	1.91
	MSA	Ctrl	3.30	2.49	0.55	-3.62	10.24
		PD	13.14	2.06	**0.00**	7.11	19.17

		PSP	4.57	2.30	0.22	-1.91	11.06
LMSN	Ctrl	PD	4.43	3.02	0.48	-4.31	13.17
		PSP	4.41	1.87	0.11	-0.71	9.55
		MSA	-0.021	2.59	1.00	-7.29	7.25
	PD	Ctrl	-4.43	3.02	0.48	-13.17	4.31
		PSP	-0.01	2.73	1.00	-8.32	8.29
		MSA	-4.45	3.26	0.53	-13.81	4.91
	PSP	Ctrl	-4.41	1.87	0.11	-9.55	0.71
		PD	0.01	2.7	1.00	-8.29	8.32
		MSA	-4.44	2.24	0.24	-11.03	2.15
	MSA	Ctrl	0.02	2.59	1.00	-7.25	7.29
		PD	4.45	3.26	0.53	-4.91	13.81
		PSP	4.44	2.24	0.24	-2.15	11.03
LPSN	Ctrl	PD	4.09	3.70	0.69	-7.28	15.48
		PSP	6.65	2.17	**0.02**	0.68	12.62
		MSA	7.06	1.95	**0.01**	1.52	12.59
	PD	Ctrl	-4.09	3.70	0.69	-15.48	7.28
		PSP	2.55	3.97	0.91	-9.17	14.29
		MSA	2.96	3.86	0.86	-8.63	14.56
	PSP	Ctrl	-6.65	2.17	**0.02**	-12.62	-0.68
		PD	-2.55	3.97	0.91	-14.29	9.17
		MSA	0.45	2.44	0.99	-6.33	7.14
	MSA	Ctrl	-7.06	1.95	**0.01**	-12.59	-1.52
		PD	-2.96	3.86	0.86	-14.56	8.63
		PSP	-0.40	2.44	0.99	-7.14	6.33
Mean	Ctrl	PD	6.39	2.20	0.05	-0.05	12.85
		PSP	5.31	1.52	0.01	1.05	9.57
		MSA	0.71	2.01	0.98	-5.02	6.45
	PD	Ctrl	-6.39	2.20	0.05	-12.85	0.057
		PSP	-1.08	2.23	0.96	-7.59	5.42
		MSA	-5.68	2.56	0.16	-12.99	1.63
	PSP	Ctrl	-5.31	1.57	**0.01**	-9.57	-1.05
		PD	1.08	2.23	0.96	-5.42	7.59
		MSA	-4.59	2.04	0.15	-10.40	1.21
	MSA	Ctrl	-0.71	2.01	0.98	-6.45	5.02
		PD	5.68	2.56	0.16	-1.63	12.99
		PSP	4.59	2.04	0.15	-1.2	10.406

Table 16: T2* relaxation times of the SN (ms), post-hoc inter-group analysis

T2 Relaxation Times of the SN

T2 times were the lowest in the PD and PSP groups, with means of 46.66 ms (95% CI 42.48 to 50.84 ms) and 59.52 ms (95% CI 57.19 to 61.84) respectively, and highest ROIs were from the control group with a mean of 61.08 ms (95% CI 58.98 to 63.17 ms).

With the control, PD and MSA groups, there was a tendency for values to increase from anterior to posterior ROIs. With the PSP group, the opposite was observed, where higher values tended to be anterior. There were no significant differences between the two sides (p-value>0.05).

With the PSP group, there was a moderately negative correlation between T2 and UPDRS III scores (correlation coefficient -0.59, p-value=0.06), when controlled for age and disease duration. Otherwise, no correlations between clinimetric scores and T2 were observed.

There were no correlations between T2 and age at scanning or disease duration, both with and without control for age and gender.

One-way ANOVA among the groups revealed significant differences with a $p<0.01$ among all the ROIs values and their means when analysing between the groups (Table 17).

Table 18 shows results of Games-Howell post-hoc testing for inter-group differences. The differences between the all-ROI-mean T2 was most marked between the controlled and PD groups (mean difference 14.41 ms, $p<0.01$, 95% CI -8.34 to 20.49 ms). There were also marked and significant differences between the PD and PSP groups (mean difference -12.85 ms, $p< 0.01$, 95% CI -19.03 to -6.68 ms) and between the PD and MSA groups (-10.52 ms, $p< 0.01$, 95% CI -16.96 to -4.08 ms).

The inter-group ROI differences tended to be slightly more marked posteriorly and slightly smaller anteriorly. For instance, between the controlled group and the PD group, the differences were 12.08 ms (SE 1.97 ms, p-value=0.000, 95% CI 6.62 to 17.53 ms) for the right anterior ROI, compared with 17.35 ms (SE 3.92 ms, p-value=0.004, 95% CI 5.68 to 29.02 ms) for the right posterior ROI. These differences were not, however, evident on the left side.

Correlation between mean T2 and age was insignificant with a correlation coefficient of -0.114 and p-value of 0.166. Between mean T2 and disease duration controlled for age, a significant correlation was observed (coefficient -0.423, p-value=0.001). Regression analysis with the mean as a dependent variable, and using age and disease duration as predictors, yielded a p-value of 0.002.

Among the clinimetric scales, H&Y and UPDRS III yielded the highest correlations, controlled for age and disease duration, with means of 0.548 and 0.562 respectively, as well as the lowest p-value ($p < 0.01$)

Values were extracted from 21 cases during the follow-up study (n=8 control, n=7 PD, n=2 PSP, n=4 MSA). Repeated measures ANOVA and using the Bonferroni correction did not show any significant differences for pair-wise comparison. There were substantially no differences in the mean T2, between the values at scan 1 and scan 2, and the mean difference was 0.585 ms, SE 1.818 ms, 95% CI -3.207 to 4.376 ms (p=0.75).

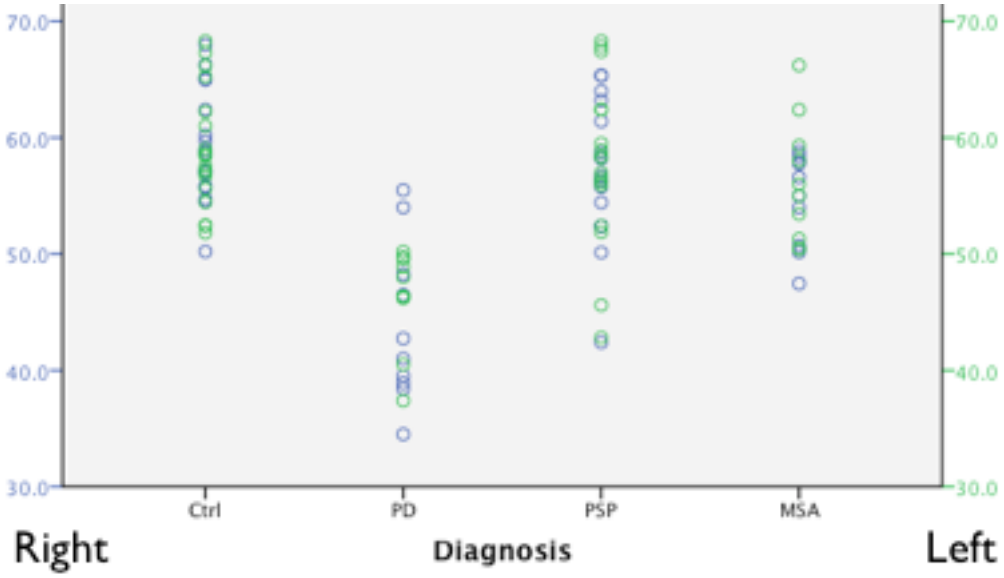

Figure 20 The T2 relaxation times of the SN(ms). The PD group had the lowest times.

		N	Mean	Std. Deviation	95% Confidence Interval for Mean		Minimum	Maximum
					Lower Bound	Upper Bound		
RASN	Ctrl	19	52.0	5.91	49.15	54.85	45.5	72.3
	PD	10	39.9	4.52	36.6	43.16	31.4	46.5
	PSP	17	66.2	8.78	61.70	70.73	42.3	73.9
	MSA	10	51.5	5.04	47.95	55.18	43.9	57.5
RMSN	Ctrl	19	58.9	4.97	56.55	61.34	51.8	68.3
	PD	10	46.3	4.21	43.30	49.34	37.4	50.2
	PSP	17	57.7	7.05	54.12	61.37	42.8	68.3
	MSA	10	56.25	5.27	52.47	60.02	50.4	66.2
		56	55.84	7.14	53.93	57.76	37.4	68.3
RPSN	Ctrl	19	71.38	6.23	68.38	74.38	51.8	79.0
	PD	10	54.03	11.54	45.77	62.29	35.2	66.9
	PSP	17	53.59	5.70	50.66	56.52	45.1	68.4
	MSA	10	65.99	6.27	61.50	70.49	56.0	74.0
LASN	Ctrl	19	55.10	5.99	52.22	57.99	45.2	68.3
	PD	10	40.98	4.23	37.95	44.01	31.4	47.4
	PSP	17	66.32	8.89	61.74	70.89	38.1	76.0
	MSA	10	49.46	3.54	46.92	52.00	44.5	54.0
LMSN	Ctrl	19	59.82	5.56	57.14	62.51	50.2	73.2
	PD	10	43.92	6.94	38.95	48.89	34.5	55.5
	PSP	17	58.44	8.25	54.20	62.68	42.4	80.7
	MSA	10	54.68	4.0	51.82	57.55	47.5	58.8
LPSN	Ctrl	19	69.21	4.18	67.19	71.23	61.6	77.4
	PD	10	54.78	10.43	47.31	62.24	40.3	69.8
	PSP	17	54.80	8.18	50.60	59.0	42.3	72.2
	MSA	10	65.12	4.70	61.75	68.4	57.1	72.8
Mean	Ctrl	19	61.08	4.34	58.98	63.17	52.80	69.28
	PD	10	46.66	5.84	42.48	50.84	37.12	54.10
	PSP	17	59.52	4.51	57.19	61.84	51.15	68.81
	MSA	10	57.18	4.07	54.26	60.09	50.92	62.10

Table 17: T2 relaxation times of the SN (ms): one-way ANOVA descriptives

Dependent Variable	(I) Diagnosis	(J) Diagnosis	Mean Difference (I-J)	Std. Error	Sig.	95% Confidence Interval	
						Lower	Upper
RASN	**Ctrl**	**PD**	12.07	1.97	**0.00**	6.62	17.53
		PSP	-14.21	2.5	**0.00**	-21.11	-7.30
		MSA	0.43	2.09	0.99	-5.40	6.27
	PD	**Ctrl**	-12.07	1.97	**0.00**	-17.53	-6.62
		PSP	-26.28	2.56	**0.00**	-33.34	-19.22
		MSA	-11.64	2.14	**0.00**	-17.70	-5.57
	PSP	**Ctrl**	14.21	2.52	**0.00**	7.30	21.11
		PD	26.28	2.56	**0.00**	19.22	33.34
		MSA	14.64	2.66	**0.00**	7.32	21.96
	MSA	**Ctrl**	-0.43	2.09	0.99	-6.27	5.40
		PD	11.64	2.14	**0.00**	5.57	17.70
		PSP	-14.64	2.66	**0.00**	-21.96	-7.32
RMSN	**Ctrl**	**PD**	12.62	1.75	**0.00**	7.73	17.51
		PSP	1.19	2.05	0.93	-4.41	6.80
		MSA	2.69	2.02	0.55	-3.03	8.43
	PD	**Ctrl**	-12.62	1.7	**0.00**	-17.51	-7.73
		PSP	-11.42	2.16	**0.00**	-17.39	-5.45
		MSA	-9.92	2.13	**0.00**	-15.99	-3.85
	PSP	**Ctrl**	-1.19	2.05	0.93	-6.80	4.41
		PD	11.42	2.16	**0.00**	5.45	17.39
		MSA	1.49	2.3	0.92	-5.10	8.10
	MSA	**Ctrl**	-2.69	2.02	0.55	-8.43	3.03
		PD	9.92	2.13	**0.00**	3.859	15.99
		PSP	-1.49	2.39	0.92	-8.10	5.10
RPSN	**Ctrl**	**PD**	17.35	3.92	**0.00**	5.68	29.02
		PSP	17.7	1.98	**0.00**	12.41	23.16
		MSA	5.38	2.44	0.160	-1.51	12.28
	PD	**Ctrl**	-17.35	3.9	**0.00**	-29.02	-5.68
		PSP	0.43	3.90	0.99	-11.21	12.08
		MSA	-11.96	4.15	0.05	-24.06	0.12
	PSP	**Ctrl**	-17.78	1.98	**0.00**	-23.16	-12.41
		PD	-0.43	3.90	0.99	-12.08	11.21
		MSA	-12.40	2.42	**0.00**	-19.26	-5.54
	MSA	**Ctrl**	-5.38	2.44	0.16	-12.28	1.51
		PD	11.96	4.15	0.05	-.12	24.06
		PSP	12.40	2.42	**0.00**	5.54	19.26
LASN	**Ctrl**	**PD**	14.12	1.92	**0.00**	8.83	19.41
		PSP	-11.21	2.55	**0.00**	-18.20	-4.21
		MSA	5.64	1.77	**0.01**	0.78	10.50
	PD	**Ctrl**	-14.12	1.92	**0.00**	-19.41	-8.83
		PSP	-25.33	2.54	**0.00**	-32.33	-18.33
		MSA	-8.48	1.74	**0.00**	-13.43	-3.52
	PSP	**Ctrl**	11.21	2.55	**0.00**	4.21	18.20
		PD	25.33	2.54	**0.00**	18.33	32.33
		MSA	16.85	2.43	**0.00**	10.12	23.59
	MSA	**Ctrl**	-5.64	1.77	**0.01**	-10.50	-0.78
		PD	8.48	1.74	**0.00**	3.52	13.43

		PSP	-16.85	2.43	**0.00**	-23.59	-10.12
LMSN	**Ctrl**	**PD**	15.89	2.54	**0.00**	8.58	23.21
		PSP	1.38	2.37	0.93	-5.10	7.87
		MSA	5.13	1.79	**0.04**	0.17	10.09
	PD	**Ctrl**	-15.89	2.54	**0.00**	-23.21	-8.58
		PSP	-14.51	2.97	**0.00**	-22.78	-6.25
		MSA	-10.76	2.53	**0.00**	-18.10	-3.41
	PSP	**Ctrl**	-1.38	2.37	0.93	-7.87	5.10
		PD	14.51	2.97	**0.00**	6.25	22.78
		MSA	3.75	2.36	0.40	-2.76	10.28
	MSA	**Ctrl**	-5.13	1.79	**0.040**	-10.09	-0.17
		PD	10.76	2.53	**0.00**	3.41	18.10
		PSP	-3.75	2.36	0.40	-10.28	2.76
LPSN	**Ctrl**	**PD**	14.43	3.43	**0.00**	4.01	24.84
		PSP	14.40	2.20	**0.00**	8.31	20.50
		MSA	4.09	1.77	0.13	-0.95	9.13
	PD	**Ctrl**	-14.43	3.43	**0.00**	-24.84	-4.01
		PSP	-0.02	3.85	1.00	-11.07	11.02
		MSA	-10.34	3.62	0.05	-21.02	0.34
	PSP	**Ctrl**	-14.40	2.20	**0.00**	-20.50	-8.31
		PD	.02	3.85	1.00	-11.02	11.07
		MSA	-10.31	2.48	**0.00**	-17.13	-3.49
	MSA	**Ctrl**	-4.09	1.77	0.13	-9.13	0.95
		PD	10.34	3.62	0.05	-0.34	21.02
		PSP	10.31	2.48	**0.00**	3.49	17.13
Mean	**Ctrl**	**PD**	14.41	2.09	**0.00**	8.33	20.49
		PSP	1.558	1.48	0.72	-2.4	5.56
		MSA	3.89	1.62	0.11	-0.66	8.46
	PD	**Ctrl**	-14.41	2.0	**0.00**	-20.49	-8.33
		PSP	-12.8	2.14	**0.00**	-19.0	-6.68
		MSA	-10.52	2.25	**0.00**	-16.96	-4.08
	PSP	**Ctrl**	-1.55	1.48	0.72	-5.56	2.44
		PD	12.85	2.14	**0.00**	6.68	19.03
		MSA	2.33	1.69	0.52	-2.38	7.05
	MSA	**Ctrl**	-3.89	1.62	0.11	-8.46	0.66
		PD	10.52	2.25	**0.00**	4.08	16.96
		PSP	-2.33	1.6	0.52	-7.05	2.38

Table 18: T2 relaxation times of the SN (ms): post hoc inter-group analysis

Summary

The total number of subjects recruited was 59 for the cross-sectional study (20 control, 19 PSP, 10 PD and 10 MSA), where 27 subjects were available (8 control, 8 PD, 6 PSP, 5 MSA). There were no significant differences in baseline characteristics among the four groups. The duration of follow-up intervals between scan 1 and scan 2 was a mean (SD) 11.04 (2.06) months.

After thorough quality control procedures, relaxation times were extracted from 53 maps during the cross-sectional study (scan 1), and from 24 cases during the follow-up study (scan 2).

T2* times of STN ROIs were the lowest with the PSP and PD groups, with a mean of both sides of 22.30 ms (95% CI 19.53 to 25.07 ms) for the PSP group, and 21.60 ms (95% CI 19.42 to 23.77 ms) for the PD group. When controlled for age and disease duration and with the PD group, a correlation was seen between T2* and UPDRS I scores (correlation coefficient 0.76, p=0.04). Repeated measures using ANOVA and the Bonferroni correction did not show any significant difference for pair-wise comparison. T2 times of STN ROIs were the lowest in the PSP group, with a mean of 38.67 ms (95% CI 37.02 to 40.32 ms). In the control group, correlations were noticed between age and T2 times, with a correlation coefficient of -0.588 and a p-value=0.01. Repeated measures using ANOVA and with the Bonferroni correction did not show significant differences for pair-wise comparison.

T2* times of the RN were the lowest with the PD group, which had a mean of 24.77 ms (95% CI 22.7 to 26.85 ms). The highest was the control group, with a mean of 30.69 ms (95% CI 28.29 to 33.09 ms). With the PD group, there was significant correlation between T2* and UPDRS III scores (correlation coefficient 0.773, p-value=0.015), when controlled for age and disease duration as confounding factors. With the PD group, a correlation was observed between age and mean T2*, with a correlation coefficient if -0.717 and a p-value of 0.03, even when controlled for disease duration. Repeated measures using ANOVA and the Bonferroni correction did not show any significant differences for pair-wise comparison. T2 times were the lowest in the PD group, with a mean of 42.86 ms (95% CI 39.92 to 45.81 ms) and in the control group with a mean of 54.64 ms (95% CI 51.92 to 57.35 ms). With the PD group, there was a significant correlation between T2 and UPDRS III scores (correlation coefficient -0.71, p-value=0.02) when controlled for age and disease duration.

T2* times of the SN were the lowest with the PD and PSP groups, with means of 30.47ms (95% CI 26.04 to 34.9 ms) and 31.56 ms (95% CI 29.13 to 33.99 ms) respectively. The highest

was the control group, with a mean of 36.87 ms (95% CI 34.58 to 39.15 ms). With the controlled and PD groups, there was a noted tendency for values to increase from anterior to posterior ROIs. Post-hoc analyses showed significant differences between the T2* means of the PD group at scan 1 and scan 2, with a mean difference of 6.64 ms, SE 1.81 ms, p= 0.02, 95% CI 1.22 to 12.07 ms. T2 times of the SN were the lowest with the PD and PSP groups, with means of 46.66 ms (95% CI 42.48 to 50.84 ms) and 59.52 ms (95% CI 57.19 to 61.84 ms) respectively. There was no difference in the mean T2 between the values at scan 1 and scan 2, with a mean difference of 0.585 ms, SE 1.818 ms, 95% CI -3.207 to 4.376 ms, p-value=0.75.

It should be noted that these results of differences between groups were for group-wide comparisons, and at an individual level there may be an overlap, which limits the use of these measures at the level of individual patients. In particular, that the different measures could not distinguish between controls and the three different conditions on an individual level because of the marked overlap but that a T2 relaxation time below 37ms in the STN would support a diagnosis of PSP.

CHAPTER SIX—Quantitative 3T MRI in Parkinsonism—Discussion—The implications of T2 and T2* measurements on the diagnosis of Parkinsonian disorders

6.1 STN

In this work I studied quantitative MRI indices of the STN from patients with Parkinsonian disorders and from control subjects.

T2* relaxation times of the STN tended to be reduced in patients with PD and PSP. There was no significant difference between T2* values obtained from 4-even or 4-odd TE points. However, 4-even-TE maps appeared less granular and had less artifacting and were therefore of better quality.

With the PD group there was a significant correlation between STN T2* and both the MMSE and UPDRS III scores, even when controlled for age and disease duration as confounding factors. However, correlations between relaxation times and clinimetric scores may have been affected by confounding factors like age and gender. There were significant correlations between T2* times and age, irrespective of diagnosis, and there were significant correlations between T2* times and disease duration, again regardless of clinical diagnosis.

STN T2 times tended to be lower in patients with PD and PSP. With the PSP group there were significant correlations between T2 and UPDRS (I, II &III) scores, even when controlled for age and disease. There were significant correlations between T2 times and age or disease duration irrespective of diagnosis, whereas with T2 times the correlations were significant with disease duration only. Age and disease duration, when used as predictors, versus the mean of both STN T2 times, and when used as dependent variables, were significant during regression analysis.

There is a paucity of published data comparing STN characteristics found by qMRI in Parkinsonian disorders against healthy subjects, despite evidence from histopathology that the nucleus suffers structural changes in PSP and PD.[4 8]

Kosta et al[4 21 69] evaluated STN T2, studying a cohort of 40 PD patients and using an 8 TE multi-echo sequence at 1.5T with manually drawn ROIs on 4 mm coronal slices. They found that STN T2s were shorter in PD patients with a disease duration longer than 5 years; STN T2s were also shorter in the PD group compared with the control group, though these differences were not statistically significant (p-value>0.05). The mean STN ROI T2 for the PD group was 73.1 ms v 74.8 ms in the controlled group.

The findings of the current study were similar to Kosta et al. STN T2 using both 2-TE and 31-TE multi-echo sequences are shorter with the PD group compared to the control group, though the difference is statistically insignificant. With the present study, significant correlations were found between T2 and disease duration, showing that the longer the disease the shorter the T2 relaxation time of the STN ROI.

Another study[17 112] investigated the correlation between T2 and clinimetric scale scores and found that STN T2 in groups with PD tended lower than control groups, though the differences was again statistically insignificant (p-value=0.11). In addition, this study found significant correlations between T2 and UPDRS I scores, but not between T2 and UPDRS II or III scores. In the present work, this previously described correlation was not found within the PD group, but rather within the PSP groups and including all UPDRS scales.

Both of the studies just mentioned identified the STN with coronal sections, rather than the axial sections that were used during this study. The advantages of our method of localizing the ROI include a series of well-defined and reproducible steps achieved by relating direct visualization to adjacent landmarks like the MTT and RN. However, disadvantages of our method might be expressed if the ROI is not considered as representative of the whole STN surface area for a given slice: the slice may correspond to the anteromedial portion of the STN, which is the associative and limbic portion of the STN (T2 hypointense) rather than the sensory-motor portion of the STN (T2 isointense).

Whereas the present study utilized 2- and 31- multi-echo sequences, further studies[19 49] have used 8- and 6-TE multi-echo sequences. This difference may be responsible for the large differences reported for STN T2 between the various studies: respectively, 67.6 ms, 52.9 ms, 73.1 ms, 44.13 ms, from 2-, 6-, 8- and 31-TE multi-echo sequences. Another explanation for the variances is the ROI methodology. For this study we relied on well-defined and fixed anatomical landmarks to place the ROIs, compared with other studies that replied on direct visualization of the nucleus.

No published studies have assessed T2* relaxation times, and indeed there are no studies that have assessed MRI metrics of the nucleus in PSP, despite pathological evidence that it is involved in disease processes.[8 19 86]

With PSP, histopathological evidence has suggested that the nucleus suffers 62% neuron loss, and a reduction in the percentage of its remaining neuron activity, leading to reduced output.[8 112] This provides strong evidence for the role of the nucleus in the natural history of the

disorder. Since initial descriptions of the disorder, in 1963 by Dr Clifford Richardson, and through subsequent publications made the following year,[72 112 113] the STN has been described as significantly involved in the disorder process, and likely responsible for some spectrum of the clinical phenotype.

The STN is involved in the pathophysiology and treatment of PD.[4 114 115] It is the surgical target of choice for medically refractory PD; it has been shown to improve the quality of life for select patients. No direct evidence from pathological studies has suggested that the STN undergoes structural changes in PD,[8 116 117] though some indirect evidence from imaging studies suggest otherwise. Both Kosta et al and Watanabe et al[4 19 118] concluded that iron deposition within the STN of patients with PD was relatively higher compared to their control groups, and that iron deposition within the STN was more pronounced in patients with a disease duration greater than five years.[4 119]

As reflected by the relative shortening of T2* and T2 relaxation times, the current study observed that iron deposition increases within the STN for patients with PSP and PD. Iron is paramagnetic and therefore reduces transverse relaxation times, and since the STN is composed of two parts—an anteromedial part that is T2 hypointense and a posterolateral part that is less hypointense—this difference in intensity was conjectured to be the result of iron deposition.[21 69 120]

Signal heterogeneity might come from the functional anatomy of the nucleus itself and its three territories—the limbic anteromedial part, the associative mid-part, and the sensorimotor posterolateral part—[121 122] and may provide an explanation for correlations found in this study, with different clinimetric scales reflecting the different clinical phenotype parts of the disorders.

In the STN and with the PD group, relationships were found between the T2* times and the UPDRS III and MMSE scores, reflecting the neuropsychological symptoms of MMSE and the cognitive status of the patients. These findings that may link the neurodegeneration of anteromedial STN with an increased iron deposition, which may contribute to the declined neuropsychological status of some patients. Similar findings have been reported by another study.[19 123]

In a meta-analysis of 20 studies, Daughtery et al[112] found a strongly positive correlation between a subject's age and their iron content—estimated from in vivo MRI, at different magnetic fields within the basal ganglia. Accumulation of non-haem iron within the brain has been proposed as a biomarker for progressive physiological and cognitive decline, as part of the

physiological ageing process.[4 112 113] In return, increased iron might suggest that MRI metrics could be used as surrogate markers for neurodegeneration in healthy (physiological ageing) and in diseased (degeneration is associated with increased iron) subjects.

In the present study, several MRI metrics of the STN were observed: T2* and T2 times showed significant correlations with disease duration—the time period between the clinical presentation and the first scan. Another study[4] has suggested that T2 might be related to the duration of symptoms, which might suggest that iron depositions increase as the disease progresses. Iron in the brain is known to increase in areas that undergo degeneration.[116 117]

The STN receives inhibitory projections from the globus pallidus and excitatory projections from the motor cortex.[118] With PD, the STN is imbalanced due to the lost inhibitory drive which causes overstimulation of the nucleus.[119] Additional evidence comes from animal studies where it has been demonstrated that iron injections into the SN results in degenerative changes.[120] Since there are direct connections between the SN and the STN,[123] excessive iron accumulations in Parkinsonian SN may be transported from the SN to the STN, suggesting that changes in iron deposition in the PD and the PSP do not take place solely within the SN but also within the STN.

Few published studies have investigated MRI metrics as they change over time,[123] yet good evidence exists that metrics reflecting iron concentrations within the deep nuclei do change with age.[112] In addition, Kosta et al[4] found that T2 times for the STN in patients with a PD disease duration of more that 5-years was significantly reduced; this may suggest that such metrics—primarily T2 and T2* relaxation times—might change over time. In the present study we found such changes. Despite the change in UPDRS scores for follow-up patients, and despite seeing scores that could be correlated to disease duration and age, we found significant differences between metrics form the first and the follow-up scans. These differences observed in the current study might be attributed to short follow-up durations, the wide variability in duration between scans (3 to 18 months), and the small size of the follow-up cohort as well as the lack of an actual differences between the subjects.

6.2 The Red Nucleus (RN)

T2* and T2 were reduced in the RN for the PD group. There were significant correlations between the TE T2* times of the RN for the PD group and their UPDRS III and H&Y scores. Significant correlations were revealed between T2* and T2 times and disease duration. There were correlations between T2* times and the age of patients within the PD group. T2 times

tended to be reduced with the RN for PD patients. A significant relationship was observed between T2 times of the RN within the PD group and their UPDRS II scores. There was also a significant relationship between the T2 times of the RN for the PD group and their UPDRS III scores.

In this study it has been found that the RN T2* was lower in patients with PD. Similar findings have been reported by other studies[33 73] despite different methodologies being used to define ROI and to map calculations. These lowered RN T2* times might suggest that higher iron contents coincide with Parkinsonian RN, regardless of demographics, disease duration, disease severity, treatment with Levodopa, or no treatment. In our study, the differences between the PD group and the other groups was statistically significant, which is contrary to other studies. The reasons for this difference might reside with the choice of TE points, where in the present study a 4-points selection was used, compared with a 6-echo-point selection reported by others.[33]

Other studies have shown that iron deposition increases with advanced age[112 124] and that T2* times are good indicators of iron concentrations within a living brain. This may explain the significant correlations between age and T2* times, even when controlled for disease duration.

There were significant correlations between T2 and motor scores (UPDRS II and III) within the PD group. Such findings have not been reported in the literature to date. However, one study[19] reported correlations between the STN T2—though not the RN T2—and their UPDRS I scores. That study hypothesized this was due to the increased iron content present as the diseases advances. Similarly with our study, T2 is known to be a good marker of iron content[69 125] and iron concentrations likely do increase as the disease progresses[126-129] causing declining motor performance. This might suggest that T2 times are a marker for disease progression,[130] and could be used to modify therapeutic strategies,[131] much like T2* times do already.[123]

MRI markers for iron have been shown to correlate with disease severity and duration in the SN, putamen and the STN of PD patients.[4 33 123] One study[73] investigated the relationship between the R2* (1/T2*) in RN and UPDRS scores, and concluded that there might be a relationship between dyskinesia and the iron content of the RN in PD patients. However, they did not report any relationships with disease duration. In our study, the T2* of the RN for the PD group showed a significant correlation with motor scores collected from UPDRS III and H&Y scales. This might suggest an association between higher RN iron content and the PD-related progression of motor disability.[73]

6.3 The Substantia Nigra

In this study, quantitative MRI metrics of the SN were assessed from patients with Parkinsonian disorders and from control subjects. T2* and T2 times were reduced in the SN of the PD and the PSP groups**.** T2* and T2 of the SN in the control and the PD groups were less in the anterior parts than they were in the posterior parts, in contrast to the PSP and the MSA groups. There were significant relationships between SN T2* in the MSA group and their FAB scores. There was a significant relationship between T2* times and disease duration regardless of diagnosis. The differences between groups were most marked anteriorly, tending to decrease posteriorly. UPDRS III scores showed good correlations with T2* times, regardless of diagnosis. Only longitudinal change with significant T2* times of the SN in PD patients tended to significantly decrease over time, probably due to aging or disease progression or both. T2* and T2 times of the anterior parts of the SN may differentiate between the PD and PSP groups and between the PD and MSA groups. There was significant correlation between 31-TE T2 times of the SN and disease duration regardless of diagnosis. Similarly, regressions of the T2* times based on age and disease durations were significant. There were significant correlations between T2 times and H&Y and UPDRS III scores.

The T2 relaxation time is a characteristic of tissue and it varies depending on the molecular structure and the reflecting interactions between protons. It is particularly sensitive to local magnetic field inhomogeneities. T2* time takes into account the contribution of magnetic field inhomogeneities.[5] Studies have shown that transverse relaxation time is non-invasive measure of tissue iron content.[15] However, the transverse relaxation times (T2 and T2*) are affected water binding as well as iron content.[7] Several studies have investigated transverse relaxation times in the substantia nigra in PD,[8 9 11-14 16-18] PSP[19] and MSA.[13] In this study transverse relaxation times were found to be lower in the SN for the PD and PSP groups, which is most likely secondary to increased iron content of the nucleus in those disorders.

Almost all groups have shown that relaxation times differs in the Parkinsonian SN compared to controls, though such differences may be reported as statistically significant[9 11] in some but not in other studies.[20] One possible reason for this diversity is the effect of ferritin on tissue used during T2, which is dependent on inter-echo times in a multi-echo sequence.[21] The reason for this may be that intracellular ferritin clusters are large, and that the time for water protons to diffuse can be comparable to the echo time.[13] This may provide an explanation for why the 31-TE T2 times showed better magnitude and statistical significance than then 2-TE T2 times, considering the disadvantages of prolonged scanning times, which in this study was overcome by scanning a block that includes mainly the midbrain rather the whole brain.

In this study, T2 and T2* times were reduced in the SN for the PD and PSP groups. The SN is known to be involved in the pathogenesis of PD and PSP.[22] However, involvement tends to effect different parts of the big nucleus: for example, with normal ageing the medial anterior and posterior tiers; with PD, the lateral anterior tiers;[23 24] with MSA, the posterior tier; with PSP, the posteromedial tier.[35-37]

These inhomogeneities and different involvements of the nucleus parts for the disorders may yield an explanation for our observation that the gradient of relaxation times from anterior to posterior parts of the nucleus were lower anteriorly and increased posteriorly in the controlled and PD groups. An opposite gradient was observed with the PSP and MSA groups, where it was observed that the anterior parts in the different groups tended be more marked between the posterior parts. Similar observations of regional selectivity have been reported in other ROI-based imaging studies of the SN.[9 38]

In the present study and when comparing the anterior parts of the SN between the different groups for their transverse relaxation times, the PD group could be differentiated from the PSP or MSA groups (p-value<0.05). This supports the evidence for regional selectivity of the SN's involvement in PD patients, first reported by Fearnley et al,[23] where they showed that the ventral or anterior tier "bearthe brunt of neuronal loss in PD suggesting that the cellular characters of the 'ventral' tier may be important in the pathogenesis of PD."[23]

Studies that have investigated the relationships between the severity of a disease—as assessed by clinimetric scores—and relaxation times are limited. Martin et al[9] noticed a correlation between the lateralised motor score from the most affected side of the SN and the R2* (1/T2*) from the opposite lateral SN, suggesting that it could be a potential biomarker for disease progression. In the present work, a significant correlation was found between T2* and T2 times and motor scores (UPDRS III) (p-value <0.05). An explanation for this finding is that higher clinimetric scores may reflect more and advanced neurodegeneration, which in turn is associated with increased iron deposition, leading to shortened transverse relaxation times as the disease worsens.[39-44] The sources for increased iron in the Parkinsonian SN are not clear.[45] However, another and less likely explanation for the correlation between transverse relaxation times and higher motor scores is advanced aging, because patients with higher motor scores tend to be older and their iron contents are known to increase as a part of the ageing process.[46 47]

Time is an important factor in the neurodegeneration of the SN, whereas in normal ageing the loss rate is 4.7% per decade compared to 45% pigmented neurons loss in the first decade of PD.[23] Moreover, there is a relationship between neuronal loss and disease severity, so that there

may be a relationship between disease duration and neuronal loss associated with increased iron content.[49] This might yield an explanation for the correlation between T2 times and disease duration in all disease groups, and the significant regression of the T2 times on age and disease duration (p-value<0.05). Similar findings have been reported in PD patients.[46]

There is a paucity of literature about longitudinal qMRI studies of the SN in Parkinsonian disorders. One study investigated R2* (1/T2*) using 14 patients with PD, at first scan and then a second scan 3-years later.[46] Additional qMRI studies have suggested that MRI metrics have a relationship with disease duration;[9] [38] they noticed that significant variations of R2* longitudinally were observed in the SN of patients with PD, that this evolved over the three-year period without similar changes in the control groups. In the present study, T2* times of the SN in the PD were similarly decreased in the follow-up scan of the longitudinal study. This is may be explained by increased age or increased iron content, or both.[46]

6.4 The STN, RN and SN

T2* (ms)	PD	PSP	MSA
STN	**21.60**	22.30	22.40
RN	**24.77**	26.86	27.19
SN	**30.47**	31.56	36.15

T2 (ms)	PD	PSP	MSA
STN	44.12	**38.67**	46.36
RN	**42.86**	50.99	51.54
SN	**46.66**	59.52	57.18

Table 19: Values of the T2* and T2 of the STN, RN, and the SN in the PD, PSP and MSA. T2* and T2 times tend to be lower in PD compared with PSP and MSA. The only exception is the STN in PSP where it undergoes volume loss, probably responsible for shorter T2 times. The lowest values are emphasized.

The findings of the present study suggest that MRI metrics of the SN, STN and RN add to the differential diagnosis of patients that present with Parkinsonian symptoms. qMRI may compensate for the lack of sensitivity and specificity offered by structural MRI when studying disorders, and may have the potential to provide insights into their pathophysiology. Table 19 summarizes the values of T2* and T2 of the studied structures in the three disease groups.

The RN metrics in PD were lower than in the other groups which suggests an involvement in the disease process Despite the fact that the RN is not the primary nucleus of Parkinsonian pathology (SN in PD, and multiple loci in PSP and MSA) its anatomical proximity and functional networking with other basal ganglia, and with the cerebellum and the cerebral cortex, may provide windows to new diagnostic and prognostic approaches for movement disorders.

In this work, anatomical localization of ROI placements relied on clearly defined and reproducible criteria, easily identified and minimally variable. Co-registration and spatial normalization of the acquired images, as well as maps, helped make the data representative of the population, especially for small sample imaging studies.[132] Wider variations makes it easier to see correlations between disease duration and severity and indices.

Limitations of this study include:

(1) The relatively small sample size may limit generalization of the findings, though many other similar studies have included similar sizes.[19 33 73 80 123 133] The sample size was limited by the availability of clinical meeting rooms, the availability of the scanner and its schedule, and by funding.

(2) The variability of disease duration and the severity among subjects could lead to an analogous variation in iron deposition and neuronal death, therefore reflecting wide variations in MRI metrics and less statistically robust results.[83]

(3) The varied duration of the follow-up, between 3 and 18 months, could have caused a similar variation in the metrics between the subjects.

(4) Furthermore, reliance on clinical diagnoses and clinical diagnostic criteria could have led to clinical misdiagnosis, and could have occurred in up to 1/5 of cases, especially during early staged diseases.[15 109 134 135]

(5) Finally, ROI-based methods could become time-consuming and operator dependent.

Additional larger-scale and prospective studies are genuinely warranted to identify which MRI metrics could provide robust diagnostic markers in the clinical workup of Parkinsonian patients, thus providing more a accurate diagnosis especially at the early stages of the disease.

Summary

In this work, I have studied T2* and T2 times of the STN, RN and SN in patients with Parkinsonian disorders and in control subjects.

Published data regarding qMRI characteristics of the STN in Parkinsonian disorders are limited, despite the evidence from histopathology suggesting that the nucleus suffers structural changes in PSP and PD.[4 8] In the present study, it was observed that T2* and T2 times showed significant correlation with disease duration. This may suggest that iron deposition increases as the disease progress.

In this study, it has been found that RN T2* times were lower in patients with PD. Similar findings have been reported by other studies[33 73] despite the use of different methodologies to define ROI and map calculations. This might suggest higher iron content in Parkinsonian RN. In our study, the differences between the PD group and the other groups was statistically significant, in contrast to other studies. Reasons for this may be due to TE point choices: the present study chose a 4-points selection, while 6-echo-point selections have been reported by others.[33] In our study, T2* times of the RN in the PD group was shown to have a significant correlation with motor scores from UPDRS III and H&Y scales. This might suggest an association between higher RN iron content and PD-related progression of motor disability.[73]

In this study, T2* and T2 times were reduced in the SN of the PD and the PSP groups**.** The SN is known to be involved in the pathogenesis of PD and PSP.[20]

The RN metrics in PD were lower than in other groups which suggests an involvement in the disease process. Despite the fact that the RN is not the primary nucleus of Parkinsonian pathology (SN in PD, and multiple loci in PSP and MSA), its anatomical proximity and functional networking with other basal ganglia, and with the cerebellum and the cerebral cortex, may provide windows to new diagnostic and prognostic approaches for movement disorders.

In this study, T2 and T2* times were lower in the STN, RN and SN for subjects with PD over other Parkinsonian disorders. This might suggest that measuring those metrics could help to differentiate PD from the other disorders. Furthermore, a short T2 of the STN in PSP might help to differentiate PSP from the other disorders.

The findings of the present studies suggest that MRI metrics of the SN, STN and RN add to the differential diagnosis in patients presenting with Parkinsonian symptoms. qMRI may compensate for the lack of sensitivity and specificity offered by structural MRI when studying disorders, and might have the potential to provide insights into their pathophysiology.

CHAPTER SEVEN—Conclusions and Future Directions

Parkinsonian disorders form a group of neurological diseases that share clinical signs and symptoms and yet manifest with large differences in their underlying pathogenesis, pathology, treatment and prognosis. Accurate diagnosis between Parkinsonian disorders is of paramount importance for the clinical management of patients that present with movement disorders.

Parkinsonian disorders can be divided into typical or idiopathic Parkinson's disease (PD) and atypical Parkinsonian disorders (APD), of which PSP and MSA are the most common. Post-mortem studies have shown that 20-25% of patients that were initially diagnosed with PD, would eventually have been diagnosed with APD.

Definite diagnoses are currently based on characteristic anatomical distributions of neuronal degenerations and subsequent glioses. Selective distributions of pathological changes mark any degenerative disorder and Parkinsonian disorders are not exempt. The anatomical accuracy of imaging is the key measure to provide insight into the chemical and pathological changes of the relatively small structures that are involved in the degenerative processes of Parkinsonian disorders.

Quantitative MR imaging or qMRI is a simple metric that can be used to measure the differences and changes resulting from pathological and physiological processes. T2 and T2* relaxation times are affected by iron concentrations, which in turn tend to increase during neurodegenerative processes.

The STN is a bilateral or almond-shaped piece of grey matter that is collected and located within the subthalamus and around the central area of the human brain. In PSP, the STN is about half the size as found in normal subjects, whereas in PD indirect evidence from MRI studies have suggested that iron deposition in the STN actually increases. Moreover, the STN is a key structure for the surgical treatment of PD and defining the STN's anatomy via MRI has proved challenging because of its small size and heterogeneity.

The RN is part of the extrapyramidal system and the human RN forms a pair of globular structures located in the midbrain. There is no direct evidence for RN involvement in Parkinsonian disorders, though indirect evidence suggests otherwise. R2* is an in vivo MRI marker of iron, and it has been shown to be lower in the RN of PD patients, where RN-R2* values are correlated with off-drug UPDRS-motor scores.[73 76]

The substantia nigra (SN) is the largest grey matter collection in the midbrain and it too can be affected in differently by varying pathological processes. Pathological studies have suggested that the SN is affected in PD and PSP. Defining its borders via MRI has proved challenging due its complexity and heterogeneity.

The purpose of this work was to determine the achievability of using T2 and T2* times, obtained at 3-Tesla, to discriminate among Parkinson's disease (PD), progressive supranuclear palsy (PSP), multi-system atrophy (MSA), and control subjects without neurological diseases. The main research question aimed to differentiate 3T MRI indices (T2, T2*) in key basal ganglia structures and thus enable improved differentiation between conditions presenting with Parkinsonian symptoms.

There is a scarcity of published data about how qMRIs characterize the STN in Parkinsonian disorders, despite evidence from histopathology suggesting that the nucleus suffers structural changes under PSP and PD.[4 8] In the present study it was observed that T2* and T2 times showed significant correlations with disease duration, which might suggest that iron deposition increase as the diseases progress.

In this study, it was found that RN T2* times were lower in patients with PD. Similar findings have been reported by other studies[33 73] despite different methodologies to define ROIs and to map calculations. These lowered times might suggest that there is higher iron content in Parkinsonian RN. With our study, the difference between the PD group and the other groups was statistically significant, in contrast to other studies. Reasons for this might be the choice of TE points, where the present used a 4-points selection and other studies used a 6-echo-point selection.[33] In the present study, T2* times of the RN in the PD group where shown to have significant correlations with motor scores acquired via UPDRS III and H&Y scales. This may suggest an association between of higher RN iron content and the PD-related progression of motor disability.[73]

With the present study, T2* and T2 times were reduced in the SN for the PD and PSP groups**.** The SN is known to be involved in the pathogenesis of PD and PSP.[22]

Longitudinal qMRI studies of the SN in Parkinsonian disorders are few. One study investigated R2* (1/T2*) in 14 patients with PD, an initial scan and then a second scan 3-years later.[46] Other qMRI studies have suggested that MRI metrics have a relationship with disease duration,[9 38] noting significant variations of R2* longitudinally in the SN of patients with PD evolving over three-year periods without similar change in control groups. With the present

study, T2* times of the SN in the PD group were similarly decreased in the follow-up scan of the longitudinal study. This is may be explained by increasing age or increasing iron content, or both.[46]

The RN metrics in PD were lower than the other groups, which suggests an involvement in the disease process. Despite the fact that the RN is not the primary nucleus of Parkinsonian pathology (SN in PD, and multiple loci in PSP and MSA), its anatomical proximity and functional networking with other basal ganglia, and with the cerebellum and the cerebral cortex, may provide windows to new diagnostic and prognostic approaches for movement disorders.

For this study, T2 and T2* times were lower in the STN, RN and SN for the PD group than they were for the other Parkinsonian disorders, which might suggest that measuring those metrics could help differentiate PD from the other disorders. Additionally, a short T2 time of the STN in PSP might help to differentiate PSP from the other disorders.

The findings of the present studies suggest that MRI metrics of the SN, STN and RN add to the differential diagnosis in patients that present with Parkinsonian symptoms. qMRIs may compensate for the lack of sensitivity and specificity offered by qualitative MRI when studying movement disorders, and might carry the potential to provide insights into their pathophysiology.

The aim of this thesis was to apply quantitative MRI metrics to patients with clinically diagnosed PD, PSP and MSA, in order to provide further insights into the biological behavior of these brain disorders and potentially influence clinical management.

After comprehensive work using the analysis of T2 and T2* times in a case-controlled study, these techniques were show to contribute to the understanding of the differential diagnosis of Parkinsonian disorders. Although T2* and T2 times of the STN, RN and SN are different among the different disorders and among healthy subjects, they were able to exhibit an association with clinical severity and disease duration. Further studies with larger cohorts are needed to verify the utility of T2 and T2* times as reliable biomarkers.

Previous chapters demonstrated the importance of MRI parameters to the understanding the differential diagnoses, the correlations with disease duration and severity, and the follow-up of patients with Parkinsonian disorders. There is much scope for further work, whereby T2 and T2* times could be used to improve the diagnoses and treatment of these patients.

The acquisition of T2 and T2* times using ROI-based, multi-echo qMRI remains somewhat subjective with inter- and intra-observer variability. This thesis has provided new and

reducible methods to help identify deep brain structures that might be poorly defined via conventional MRI. The use of ROI-based methods simplifies the analysis and allows inexperienced operators to obtain reproducible data. It would be interesting to implement this method for future acquisitions of MRI metrics.

Imaging markers are needed for the treatment response of patients with Parkinsonian disorders, and T2 and T2* times could be used as biomarkers for treatment response. Changes in treatments could be made if certain imaging markers have not changed over time, and it would be reassuring to know when effective treatments are mirrored by significant changes in MRI markers.

This work highlighted the importance of the red nucleus (RN) in Parkinsonian disorders. Despite being easily visualized on MRI, and despite being part of the extra-pyramidal motor system, there is a paucity of research into the RN's role when imaging Parkinsonian disorders. The findings of this thesis have provided indirect evidence for RN involvement in PD as well as its relationship with disease progression and severity. The RN acts as the elephant in the room and more research is needed to study its involvement in Parkinsonian disorders.

Longitudinal MRI studies are costly and time-consuming which are probably why there are limited studies in the literature. Published findings of shortened T2 and T2* times of the SN, in repeat scans of same patients, suggests that MRI metrics may have the ability to act as biomarkers for monitor disease progression. The marked reduction of T2* and T2 times within the STN, RN and SN for PD patients helps answer the primary research question. Low T2* and T2 times of the STN, RN and SN differentiates PD from atypical Parkinsonian disorders.

This work has highlighted the importance of qMRI metrics in the differentiating process of Parkinsonian disorders. Recruiting more patients and having the follow up scans at longer interval periods could take this work forward, and ultimately helping patients suffering with those disorders to improve their symptoms and quality of life.

References

1. Frith CD, Friston KJ, Dolan RJ. *Human Brain Function*: Academic Press, 2004.
2. Brooks DJ. Assessment of Parkinson's Disease with Imaging. *Parkinsonism & Related Disorders* 2007;**13**:S268-S75.
3. Ashburner J, Neelin P, Collins DL, et al. Incorporating Prior Knowledge into Image Registration. *NeuroImage* 1997;**6**(4):344-52.
4. Kosta P, Argyropoulou MI, Markoula S, et al. Mri Evaluation of the Basal Ganglia Size and Iron Content in Patients with Parkinson's Disease. *Journal of Neurology* 2005;**253**(1):26-32.
5. Barsottini OGP, Ferraz HB, Maia ACM, et al. Differentiation of Parkinson's Disease and Progressive Supranuclear Palsy with Magnetic Resonance Imaging: The First Brazilian Experience. *Parkinsonism & Related Disorders* 2007;**13**(7):389-93.
6. Hughes AJ, Daniel SE, Kilford L, et al. Accuracy of Clinical Diagnosis of Idiopathic Parkinson's Disease: A Clinico-Pathological Study of 100 Cases. *Journal of Neurology, Neurosurgery & Psychiatry* 1992;**55**(3):181-84.
7. Wenning GK, Ben-Shlomo Y, Hughes AJ. What Clinical Features Are Most Useful to Distinguish Definite Multiple System Atrophy from Parkinson's Disease? *Journal of Neurology, Neurosurgery & Psychiatry* 2000;**68**(4):434-40.
8. Hardman CD, Halliday GM, McRitchie DA, et al. The Subthalamic Nucleus in Parkinson′s Disease and Progressive Supranuclear Palsy. *Journal of Neuropathology and Experimental Neurology* 1997;**56**(2):132-42.
9. Lees AJ, Hardy J, Revesz T. Parkinson's Disease. *The Lancet* 2009;**373**(9680):2055-66.
10. Brooks DJ. Diagnosis and Management of Atypical Parkinsonian Syndromes. *Neurology* 2002.
11. Alvarez L, Macias R, Guridi J, et al. Dorsal Subthalamotomy for Parkinson's Disease. *Movement Disorders* 2001;**16**(1):72-78.
12. Wenning GK, Odin P, Morrish P, et al. Short- and Long-Term Survival and Function of Unilateral Intrastriatal Dopaminergic Grafts in Parkinson's Disease. *Annals of Neurology* 1997;**42**(1):95-107.
13. Wenning GK, Tison F, ben Shlomo Y, et al. Multiple System Atrophy: A Review of 203 Pathologically Proven Cases. *Movement Disorders* 1997;**12**(2):133-47.
14. Diamond SG, Marchkham CH, Hoehn MM, et al. Multi-Center Study of Parkinson Mortality with Early Versus Later Dopa Treatment. *Annals of Neurology* 1987;**22**(1):8-12.
15. Hughes AJ, Daniel SE, Ben-Shlomo Y, et al. The Accuracy of Diagnosis of Parkinsonian Syndromes in a Specialist Movement Disorder Service. *Brain* 2002;**125**(4):861-70.
16. Limousin P, Pollak P, Benazzouz A, et al. Bilateral Subthalamic Nucleus Stimulation for Severe Parkinson's Disease. *Movement Disorders* 1995;**10**(5):672-74.
17. Williams DR, de Silva R, Paviour DC. Characteristics of Two Distinct Clinical Phenotypes in Pathologically Proven Progressive Supranuclear Palsy: Richardson's Syndrome and Psp-Parkinsonism. *Brain* 2005;**128**(6):1247-58.
18. Litvan I, Agid Y, Calne D, et al. Clinical Research Criteria for the Diagnosis of Progressive Supranuclear Palsy (Steele-Richardson-Olszewski Syndrome): Report of the Ninds-Spsp International Workshop. *Neurology* 1996;**47**(1):1-9.
19. Watanabe S, Suenaga K, Yamamoto A, et al. Correlation of Subthalamic Nuclei T2 Relaxation Times with Neuropsychological Symptoms in Patients with Parkinson's Disease. *Journal of the Neurological Sciences* 2012;**315**(1-2):96-99.
20. Paviour DC, Price SL, Jahanshahi M, et al. Regional Brain Volumes Distinguish Psp, Msa-P, and Pd: Mri-Based Clinico-Radiological Correlations. *Movement Disorders* 2006;**21**(7):989-96.
21. Massey L, Miranda M, Zrinzo L, et al. High Resolution Mr Anatomy of the Subthalamic Nucleus: Imaging at 9.4t with Histological Validation. *NeuroImage* 2012;**59**(3):2035-44.
22. Martínez-Martín P, Gil-Nagel A, Gracia LM, et al. Unified Parkinson's Disease Rating Scale Characteristics and Structure. *Mov Disord* 1994;**9**(1):76-83.
23. Litvan I, Agid Y, Jankovic J, et al. Accuracy of Clinical Criteria for the Diagnosis of Progressive Supranuclear Palsy (Steele-Richardson-Olszewski Syndrome). *Neurology* 1996;**46**(4):922-30.
24. Massey LA, Micallef C, Paviour DC, et al. Conventional Magnetic Resonance Imaging in Confirmed Progressive Supranuclear Palsy and Multiple System Atrophy. *Mov Disord* 2012;**27**(14):1754-62.
25. Rossi M, Ruottinen H, Elovaara I, et al. Brain Iron Deposition and Sequence Characteristics in Parkinsonism : Comparison of Swi, T2* Maps, T2-Weighted-, and Flair-Space. *Investigative Radiology* 2010;**45**(12):795-802.
26. del Tredici K, Rub U, de Vos R, et al. Where Does Parkinson Disease Pathology Begin in the Brain? *Journal of Neuropathology and Experimental Neurology* 2002;**61**(5):413-26.

27. Papapetropoulos S, Gonzales J, Mash D. Natural History of Progressive Supranuclear Palsy : A Clinicopathologic Study from a Population of Brain Donors. *European Neurology* 2005;**54**(1):1-9.
28. Oyanagi K, Tsuchiya K, Yamazaki M, et al. Substantia Nigra in Progressive Supranuclear Palsy, Corticobasal Degeneration, and Parkinsonism-Dementia Complex of Guam : Specific Pathological Features. *Journal of Neuropathology and Experimental Neurology* 2001;**60**(4):393-402.
29. Gibb W. Neuropathology in Movement Disorders. *Journal of Neurology, Neurosurgery, and Psychiatry* 1989;**52**(Special Suppliment):55-67.
30. Fearnley JM, Lees AJ. Ageing and Parkinson's Disease: Substantia Nigra Regional Selectivity. *Brain* 1991;**114**(5):2283-301.
31. Dickson DW. Parkinson's Disease and Parkinsonism: Neuropathology. *Cold Spring Harbor Perspectives in Medicine* 2012;**2**(8):a009258-a58.
32. Brar S, Henderson D, Schenck J, et al. Iron Accumulation in the Substantia Nigra of Patients with Alzheimer Disease and Parkinsonism. *JAMA Neurology* 2009;**66**(3):371-74.
33. Martin WRW, Wieler M, Gee M. Midbrain Iron Content in Early Parkinson Disease: A Potential Biomarker of Disease Status. *Neurology* 2008;**70**(Issue 16, Part 2):1411-17.
34. Braffman B, Grossman R, Goldberg H, et al. Mr Imaging of Parkinson Disease with Spin-Echo and Gradient-Echo Sequences. *American Journal of Roentgenology* 1989;**152**(1):159-65.
35. Tofts P. *Quantitative Mri of the Brain : Measuring Changes Caused by Disease*. Ann Arbor, MI: University of Michigan, 2003.
36. Schäfer A, Forstmann BU, Neumann J, et al. Direct Visualization of the Subthalamic Nucleus and Its Iron Distribution Using High-Resolution Susceptibility Mapping. *Human Brain Mapping* 2011;**33**(12):2831-42.
37. Yelnik J, Percheron G. Subthalamic Neurons in Primates: A Quantitative and Comparative Analysis. *Neuroscience* 1979;**4**(11):1717-43.
38. Kitajima M, Korogi Y, Kakeda S, et al. Human Subthalamic Nucleus: Evaluation with High-Resolution Mr Imaging at 3.0 t. *Neuroradiology* 2008;**50**(8):675-81.
39. Taoka T, Hirabayashi H, Nakagawa H, et al. "Sukeroku Sign" and "Dent Internal-Capsule Sign"—Identification Guide for Targeting the Subthalamic Nucleus for Placement of Deep Brain Stimulation Electrodes. *Neuroradiology* 2008;**51**(1):11-16.
40. Richter EO, Hoque T, Halliday W, et al. Determining the Position and Size of the Subthalamic Nucleus Based on Magnetic Resonance Imaging Results in Patients with Advanced Parkinson Disease. *Journal of Neurosurgery* 2004;**100**(3):541-46.
41. Coenen VA, Prescher A, Schmidt T, et al. What Is Dorso-Lateral in the Subthalamic Nucleus (Stn)?—a Topographic and Anatomical Consideration on the Ambiguous Description of Today's Primary Target for Deep Brain Stimulation (Dbs) Surgery. *Acta Neurochir (Wien)* 2008;**150**(11):1163-65.
42. Dormont D, Ricciardi KG, Tardé D. Is the Subthalamic Nucleus Hypointense on T2-Weighted Images? A Correlation Study Using Mr Imaging and Stereotactic Atlas Data. *American Journal of Neuroradiology* 2004;**25**(1):1516-23.
43. Ashkan K, Blomstedt P, Zrinzo L, et al. Variability of the Subthalamic Nucleus: The Case for Direct Mri Guided Targeting. *British Journal of Neurosurgery* 2007;**21**(2):197-200.
44. Patel NK, Khan S, Gill SS. Comparison of Atlas- and Magnetic-Resonance-Imaging-Based Stereotactic Targeting of the Subthalamic Nucleus in the Surgical Treatment of Parkinson&Rsquo;S Disease. *Stereotactic and Functional Neurosurgery* 2008;**86**(3):153-61.
45. den Dunnen WFA, Staal MJ. Anatomical Alterations of the Subthalamic Nucleus in Relation to Age: A Postmortem Study. *Movement Disorders* 2005;**20**(7):893-98.
46. Ardekani BA, Bachman AH. Model-Based Automatic Detection of the Anterior and Posterior Commissures on Mri Scans. *NeuroImage* 2009;**46**(3):677-82.
47. Pallavaram S, Dawant BM, Koyama T, et al. Validation of a Fully Automatic Method for the Routine Selection of the Anterior and Posterior Commissures in Magnetic Resonance Images. *Stereotactic and Functional Neurosurgery* 2009;**87**(3):148-54.
48. Schaltenbrand G, Waldemar W. *Atlas for Stereotaxy of the Human Brain*. New York, NY: Thieme, 1977.
49. Yelnik J, Damier P, Demeret S, et al. Localization of Stimulating Electrodes in Patients with Parkinson Disease by Using a Three-Dimensional Atlas—Magnetic Resonance Imaging Coregistration Method. *Journal of Neurosurgery* 2003;**99**(1):89-99.
50. Danish SF, Jaggi JL, Moyer JT, et al. Conventional Mri Is Inadequate to Delineate the Relationship between the Red Nucleus and Subthalamic Nucleus in Parkinson's Disease. *Stereotactic and Functional Neurosurgery* 2006;**84**(1):12-18.
51. Caire F, Maubon A, Moreau J-J, et al. The Mamillothalamic Tract Is a Good Landmark for the Anterior Border of the Subthalamic Nucleus on Axial Mr Images. *Stereotactic and Functional Neurosurgery* 2011;**89**(5):286-90.

52. Toda H, Sawamoto N, Hanakawa T, et al. A Novel Composite Targeting Method Using High-Field Magnetic Resonance Imaging for Subthalamic Nucleus Deep Brain Stimulation. *Journal of Neurosurgery* 2009;**111**(4):737-45.
53. Lee C, Young B, Sanders MF. The Role of the Supramammillary Commissure in Mr Localization of the Subthalamic Nucleus. *Stereotactic and Functional Neurosurgery* 2006;**84**(5-6):193-204.
54. Rijkers K, Temel Y, Visser-Vandewalle V, et al. The Microanatomical Environment of the Subthalamic Nucleus. *Journal of Neurosurgery* 2007;**107**(1):198-201.
55. Andrade-Souza YM, Schwalb JM, Hamani C, et al. Comparison of Three Methods of Targeting the Subthalamic Nucleus for Chronic Stimulation in Parkinson's Disease. *Operative Neurosurgery* 2005;**56**:360-68.
56. Talairach J, Tournoux P. *Co-Planar Stereotaxic Atlas of the Human Brain*. New York, NY: Thieme, 1998.
57. Brunenberg EJL, Platel B, Hofman PAM, et al. Magnetic Resonance Imaging Techniques for Visualization of the Subthalamic Nucleus. *Journal of Neurosurgery* 2011;**115**(5):971-84.
58. King JS, Schwyn RC, Fox CA. The Red Nucleus in the Monkey (Macaca Mulatta): A Golgi and an Electron Microscopic Study. *The Journal of Comparative Neurology* 1971;**142**(1):75-107.
59. Bebin J. The Central Tegmental Bundle. An Anatomical and Experimental Study in the Monkey. *The Journal of Comparative Neurology* 1956;**105**(2):287-332.
60. Ermolaeva VY, Chernigovskii VN. Evoked Potentials in the Red Nucleus and Central Tegmental Tract of the Cat During Stimulation of the Splanchnic Nerve. *Bulletin of Experimental Biology and Medicine* 1965;**60**(1):723-26.
61. Massion J. Red Nucleus: Past and Future. *Behavioural Brain Research* 1988;**28**(1-2):1-8.
62. Nathan PW, Smith MC. The Rubrospinal and Central Tegmental Tracts in Man. *Brain* 1982;**105**(2):223-69.
63. Pu Y, Hou J. Demonstration of the Medullary Lamellae of the Human Red Nucleus with High-Resolution Gradient-Echo Mr Imaging. *American Journal of Neuroradiology* 2000;**21**(1):1243-7.
64. Gruber P, Gould DJ. The Red Nucleus: Past, Present, and Future. *Neuroanatomy* 2001;**9**:1-3.
65. Liu Y, Pu Y, Gao J-H, et al. The Human Red Nucleus and Lateral Cerebellum in Supporting Roles for Sensory Information Processing. *Human Brain Mapping* 2000;**10**(4):147-59.
66. Olszewski J, Baxter D, P.I.Y. Cytoarchitecture of the Human Brain Stem. *Neurology* 1954;**4**(11):881-81.
67. Wells J, Carpenter WB, Sutin J, et al. *Human Neuroanatomy*. 8th ed. Baltimore, MD: Williams & Wilkins, 1983.
68. Habas C, Cabanis EA. Cortical Projection to the Human Red Nucleus: Complementary Results with Probabilistic Tractography at 3 T. *Neuroradiology* 2007;**49**(9):777-84.
69. Rutledge JN, Hilal SK, Silver AJ, et al. Study of Movement Disorders and Brain Iron by Mr. *American Journal of Roentgenology* 1987;**149**(2):365-79.
70. Seab JA. Anatomy and Pathology of Extrapyramidal Diseases. *Brain Research Bulletin* 1983;**11**(2):135-41.
71. Dickson DW, Rademakers R, Hutton ML. Progressive Supranuclear Palsy: Pathology and Genetics. *Brain Pathology* 2007;**17**(1):74-82.
72. Steele JC. Progressive Supranuclear Palsy. *Arch Neurol* 1964;**10**(4):333.
73. Lewis MM, Du G, Kidacki M, et al. Higher Iron in the Red Nucleus Marks Parkinson's Dyskinesia. *Neurobiology of Aging* 2013;**34**(5):1497-503.
74. Foroutan P, Murray ME, Fujioka S, et al. Progressive Supranuclear Palsy: High-Field-Strength Mr Microscopy in the Human Substantia Nigra and Globus Pallidus. *Radiology* 2013;**266**(1):280-88.
75. Braak H, Tredici KD, Rüb U, et al. Staging of Brain Pathology Related to Sporadic Parkinson's Disease. *Neurobiology of Aging* 2003;**24**(2):197-211.
76. Standring S. *Gray's Anatomy: The Anatomical Basis of Clinical Practice*. 40th ed. Chicago, IL: Churchill Livingstone Elsevier, 2008.
77. Massey LA, Yousry TA. Anatomy of the Substantia Nigra and Subthalamic Nucleus on Mr Imaging. *Neuroimaging Clinics of North America* 2010;**20**(1):7-27.
78. Oikawa H, Sasaki M, Tamakawa Y. The Substantia Nigra in Parkinson Disease: Proton Density-Weighted Spin-Echo and Fast Short Inversion Time Inversion-Recovery Mr Findings. *American Journal of Neuroradiology* 2002;**23**(1):1747-56.
79. Cordato NJ, Halliday GM, Harding AJ, et al. Regional Brain Atrophy in Progressive Supranuclear Palsy and Lewy Body Disease. *Annals of Neurology* 2000;**47**(6):718-28.
80. Eckert T, Sailer M, Kaufmann J, et al. Differentiation of Idiopathic Parkinson's Disease, Multiple System Atrophy, Progressive Supranuclear Palsy, and Healthy Controls Using Magnetization Transfer Imaging. *NeuroImage* 2004;**21**(1):229-35.
81. Adachi M, Hosoya T, Haku T. Evaluation of the Substantia Nigra in Patients with Parkinsonian Syndrome Accomplished Using Multishot Diffusion-Weighted Mr Imaging. *American Journal of Neuroradiology* 1999;**20**(1):1500-6.

82. Martin WRW. Quantitative Estimation of Regional Brain Iron with Magnetic Resonance Imaging. *Parkinsonism & Related Disorders* 2009;**15**:S215-S18.
83. Mahlknecht P, Hotter A, Hussl A, et al. Significance of Mri in Diagnosis and Differential Diagnosis of Parkinson's Disease. *Neurodegenerative Diseases* 2010;**7**(5):300-18.
84. Nieuwenhuys R, Voogd J, van Huijzen C. The Human Central Nervous System: Springer Science + Business Media, 2008.
85. Foltynie T, Zrinzo L, Martinez-Torres I, et al. Mri-Guided Stn Dbs in Parkinson's Disease without Microelectrode Recording: Efficacy and Safety. *Journal of Neurology, Neurosurgery & Psychiatry* 2010;**82**(4):358-63.
86. Hardman CD, Halliday GM, McRitchie DA, et al. Progressive Supranuclear Palsy Affects Both the Substantia Nigra Pars Compacta and Reticulata. *Experimental Neurology* 1997;**144**(1):183-92.
87. Compston A. Hemichorea Resulting from a Local Lesion of the Brain. (the Syndrome of the Body of Luys.) by James Purdon Martin, Md (London). Brain 1927: 50; 637-651; Hemichorea Associated with a Lesion of the Corpus Luysii. By James Purdon Martin and N.S. Alcock. Brain 1934: 57; 504-516; and Hemichorea (Hemiballismus) without Lesions in the Corpus Luysii. By J. Purdon Martin (from the National Hospital, Queen Square, W.C.1) Brain 1957: 80; 1-10. *Brain* 2006;**129**(7):1633-36.
88. Hariz MI, Krack P, Melvill R, et al. A Quick and Universal Method for Stereotactic Visualization of the Subthalamic Nucleus before and after Implantation of Deep Brain Stimulation Electrodes. *Stereotactic and Functional Neurosurgery* 2004;**80**(1-4):96-101.
89. Yamada NK, Cross DT, Pilgram TK, et al. Effect of Antiplatelet Therapy on Thromboembolic Complications of Elective Coil Embolization of Cerebral Aneurysms. *American Journal of Neuroradiology* 2007;**28**(9):1778-82.
90. Counelis GJ, Simuni T, Forman MS, et al. Bilateral Subthalamic Nucleus Deep Brain Stimulation for Advanced Pd: Correlation of Intraoperative Mer and Postoperative Mri with Neuropathological Findings. *Movement Disorders* 2003;**18**(9):1062-65.
91. Haberler C, Alesch F, Mazal PR, et al. No Tissue Damage by Chronic Deep Brain Stimulation in Parkinson's Disease. *Annals of Neurology* 2000;**48**(3):372-76.
92. Henderson JM, Pell M, O'Sullivan DJ, et al. Postmortem Analysis of Bilateral Subthalamic Electrode Implants in Parkinson's Disease. *Movement Disorders* 2002;**17**(1):133-37.
93. Jarraya B, Bonnet A-M, Duyckaerts C, et al. Parkinson's Disease, Subthalamic Stimulation, and Selection of Candidates: A Pathological Study. *Movement Disorders* 2003;**18**(12):1517-20.
94. Nielsen MS, Bjarkam CR, Sørensen JC, et al. Chronic Subthalamic High-Frequency Deep Brain Stimulation in Parkinson's Disease ? A Histopathological Study. *Eur J Neurol* 2007;**14**(2):132-38.
95. Sun DA, Yu H, Spooner J, et al. Postmortem Analysis Following 71 Months of Deep Brain Stimulation of the Subthalamic Nucleus for Parkinson Disease. *Journal of Neurosurgery* 2008;**109**(2):325-29.
96. Guehl D, Vital A, Cuny E, et al. Postmortem Proof of Effectiveness of Zona Incerta Stimulation in Parkinson Disease. *Neurology* 2008;**70**(Issue 16, Part 2):1489-90.
97. Plaha P. Stimulation of the Caudal Zona Incerta Is Superior to Stimulation of the Subthalamic Nucleus in Improving Contralateral Parkinsonism. *Brain* 2006;**129**(7):1732-47.
98. McClelland S, Vonsattel JP, Garcia RE, et al. Relationship of Clinical Efficacy to Postmortem-Determined Anatomic Subthalamic Stimulation in Parkinson Syndrome. *NP* 2007;**26**(11):267-75.
99. Starr PA, Christine CW, Theodosopoulos PV, et al. Implantation of Deep Brain Stimulators into Subthalmic Nucleus: Technical Approach and Magnetic Imaging—Verified Electrode Locations. *Journal of Neurosurgery* 2002;**97**(2):370-87.
100. Vedam-Mai V, Yachnis A, Ullman M, et al. Postmortem Observation of Collagenous Lead Tip Region Fibrosis as a Rare Complication of Dbs. *Mov Disord* 2012;**27**(4):565-69.
101. McKeith IG, Dickson DW, Lowe J, et al. Diagnosis and Management of Dementia with Lewy Bodies: Third Report of the Dlb Consortium. *Neurology* 2005;**65**(1):1863-72.
102. De La Garza BH, Muir ER, Shih Y-YI, et al. 3d Magnetic Resonance Microscopy of the Ex Vivo Retina. *Magnetic Resonance in Medicine* 2011;**67**(4):1154-58.
103. Fatterpekar GM, Naidich TP, Delman BN. Cytoarchitecture of the Human Cerebral Cortex: Mr Microscopy of Excised Specimens at 9.4 Tesla. *American Journal of Neuroradiology* 2002;**23**(1):1313-21.
104. Fahn S. Description of Parkinson's Disease as a Clinical Syndrome. *Annals of the New York Academy of Sciences* 2006;**991**(1):1-14.
105. Hoehn MM, Yahr MD. Parkinsonism: Onset, Progression, and Mortality. *Neurology* 1998;**50**(2):318-18.
106. Paviour DC, Price SL, Stevens JM, et al. Quantitative Mri Measurement of Superior Cerebellar Peduncle in Progressive Supranuclear Palsy. *Neurology* 2005;**64**(4):675-79.
107. Kerl HU, Gerigk L, Pechlivanis I, et al. The Subthalamic Nucleus at 7.0 Tesla: Evaluation of Sequence and Orientation for Deep-Brain Stimulation. *Acta Neurochir* 2012;**154**(11):2051-62.

108. Bejjani B-P, Dormont D, Pidoux B, et al. Bilateral Subthalamic Stimulation for Parkinson's Disease by Using Three-Dimensional Stereotactic Magnetic Resonance Imaging and Electrophysiological Guidance. *Journal of Neurosurgery* 2000;**92**(4):615-25.
109. Litvan I, Bhatia KP, Burn DJ, et al. Sic Task Force Appraisal of Clinical Diagnostic Criteria for Parkinsonian Disorders. *Movement Disorders* 2003;**18**(5):467-86.
110. Wenning GK, Gilman S, Seppi K. Second Consensus Statement on the Diagnosis of Multiple System Atrophy. *Akt Neurol* 2008;**35**(S 01).
111. McRobbie D, Moore E, Graves M, et al. *Mri from Picture to Proton*. 2nd ed. Cambridge: Cambridge University Press, 2007.
112. Daugherty A, Raz N. Age-Related Differences in Iron Content of Subcortical Nuclei Observed in Vivo: A Meta-Analysis. *NeuroImage* 2013;**70**:113-21.
113. Kennedy KM, Raz N. Aging White Matter and Cognition: Differential Effects of Regional Variations in Diffusion Properties on Memory, Executive Functions, and Speed. *Neuropsychologia* 2009;**47**(3):916-27.
114. Gan J, Xie-Brustolin J, Mertens P, et al. Bilateral Subthalamic Nucleus Stimulation in Advanced Parkinson's Disease. *Journal of Neurology* 2007;**254**(1):99-106.
115. Obeso J, Olanow C, Rodriguez-Oroz M. Deep-Brain Stimulation of the Subthalamic Nucleus or the Pars Interna of the Globus Pallidus in Parkinson's Disease. *New England Journal of Medicine* 2001;**345**(13):956-63.
116. Dexter DT, Jenner P, Schapira AHV, et al. Alterations in Levels of Iron, Ferritin, and Other Trace Metals in Neurodegenerative Diseases Affecting the Basal Ganglia. *Annals of Neurology* 1992;**32**(S1):S94-S100.
117. Vymazal J, Brooks RA, Patronas N, et al. Magnetic Resonance Imaging of Brain Iron in Health and Disease. *Journal of the Neurological Sciences* 1995;**134**:19-26.
118. Rodriguez-Oroz MC, Rodriguez M, Guridi J. The Subthalamic Nucleus in Parkinson's Disease: Somatotopic Organization and Physiological Characteristics. *Brain* 2001;**124**(9):1777-90.
119. Levy R, Hazrati LN, Herrero MT, et al. Re-Evaluation of the Functional Anatomy of the Basal Ganglia in Normal and Parkinsonian States. *Neuroscience* 1997;**76**(2):335-43.
120. Hironishi M, Ueyama E, Senba E. Systematic Expression of Immediate Early Genes and Intensive Astrocyte Activation Induced by Intrastriatal Ferrous Iron Injection. *Brain Research* 1999;**828**(1-2):145-53.
121. Prensa La, Cossette M, Parent A. Dopaminergic Innervation of Human Basal Ganglia. *Journal of Chemical Neuroanatomy* 2000;**20**(3-4):207-13.
122. Yelnik J, Bardinet E, Dormont D, et al. A Three-Dimensional, Histological and Deformable Atlas of the Human Basal Ganglia. I. Atlas Construction Based on Immunohistochemical and Mri Data. *NeuroImage* 2007;**34**(2):618-38.
123. Ulla M, Bonny JM, Ouchchane L, et al. Is R2* a New Mri Biomarker for the Progression of Parkinson's Disease? A Longitudinal Follow-Up. *PLoS ONE* 2013;**8**(3):e57904.
124. Martin WRW, Ye FQ, Allen PS. Increasing Striatal Iron Content Associated with Normal Aging. *Movement Disorders* 1998;**13**(2):281-86.
125. Bartzokis G, Cummings JL, Markham CH, et al. Mri Evaluation of Brain Iron in Earlier- and Later-Onset Parkinson's Disease and Normal Subjects. *Magnetic Resonance Imaging* 1999;**17**(2):213-22.
126. Berg D, Hochstrasser H. Iron Metabolism in Parkinsonian Syndromes. *Movement Disorders* 2006;**21**(9):1299-310.
127. Cass WA, Grondin R, Andersen AH, et al. Iron Accumulation in the Striatum Predicts Aging-Related Decline in Motor Function in Rhesus Monkeys. *Neurobiology of Aging* 2007;**28**(2):258-71.
128. Griffiths PD, Dobson B, Jones G. Iron in the Basal Ganglia in Parkinson's Disease: An in Vitro Study Using Extended X-Ray Absorption Fine Structure and Cryo-Electron Microscopy. *Brain* 1999;**122**(4):667-73.
129. Wallis LI, Paley MNJ, Graham JM, et al. Mri Assessment of Basal Ganglia Iron Deposition in Parkinson's Disease. *J Magn Reson Imaging* 2008;**28**(5):1061-67.
130. Planetta PJ, Prodoehl J, Corcos DM, et al. Use of Mri to Monitor Parkinson's Disease. *Neurodegenerative Disease Management* 2011;**1**(1):67-77.
131. Gassen M, Youdim MBH. The Potential Role of Iron Chelators in the Treatment of Parkinson's Disease and Related Neurological Disorders. *Pharmacology & Toxicology* 1997;**80**(4):159-66.
132. Bardinet E, Bhattacharjee M, Dormont D, et al. A Three-Dimensional Histological Atlas of the Human Basal Ganglia. Ii. Atlas Deformation Strategy and Evaluation in Deep Brain Stimulation for Parkinson Disease. *Journal of Neurosurgery* 2009;**110**(2):208-19.
133. Vaillancourt DE, Spraker MB, Prodoehl J, et al. High-Resolution Diffusion Tensor Imaging in the Substantia Nigra of De Novo Parkinson Disease. *Neurology* 2009;**72**(16):1378-84.

134. Litvan I, Agid Y, Goetz C, et al. Accuracy of the Clinical Diagnosis of Corticobasal Degeneration: A Clinicopathologic Study. *Neurology* 1997;**48**(1):119-25.
135. Tolosa E, Wenning G, Poewe W. The Diagnosis of Parkinson's Disease. *The Lancet Neurology* 2006;**5**(1):75-86.